A CALCIUM IMAGING APPROACH TO INVESTIGATE TYPE II COCHLEAR AFFERENT ACTIVITY AFTER TRAUMA

by

Nathaniel James Nowak

A dissertation submitted to Johns Hopkins University in conformity with the requirements for degree of the Doctor of Philosophy

Baltimore, Maryland

November 2020

Abstract

Auditory information is sent to the central nervous system from the cochlea through type I and type II cochlear afferents. While the function of the type I afferents is relatively well understood, definitive proof for the role of type II afferents lags far behind. Limited recordings from type II afferents suggest they are activated by near maximal outer hair cell stimulation, ATP, and by rupture of nearby outer hair cells. Taken together, these lines of evidence suggest that type II afferents sense damaging levels of sound. Recordings of type II afferents have been confined to the low-frequency regions of excised organs of Corti in pre-hearing animals due to the intractable nature of these methods. TH^{CreER}:GCaMP6f, $DrD2^{Cre}$:GCaMP6f, and $Tac1^{Cre}$:GCaMP6f mice were used to overcome some of these limitations by introducing a genetically encoded fluorescent calcium indicator in type II afferents spanning the range of the organ of Corti. In concordance with direct recordings, most type II afferents are inactive without external stimuli but become more and more responsive after depolarization with increasing levels of external potassium. Moreover, pre-hearing type II afferents in both the apex and the base reliably experience calcium transients following hair cell ablation, recapitulating previous electrophysiological recordings. Additionally, both indirect and direct methods of measuring epithelial cell activity suggest that these cell types also strongly respond to ablation. The combination of calcium imaging and innovative dissection techniques allowed for reliable recording of type II afferent activity in

response to ablation in mature and noise-exposed animals. While the response is changed and less likely to occur, mature type II afferents can still experience calcium transients to focal ablation. Type II afferents in noise-exposed animals appear to become sensitized both through an increase in the number of presynaptic ribbons and by shifting their response to focal ablation. Overall, calcium imaging is capable of capturing type II afferent responses to damage even in mature and noise-exposed animals, further supporting their role as putative auditory nociceptors.

Primary reader and advisor: Paul Fuchs, Ph.D.

Secondary reader: Elisabeth Glowatzki, Ph.D.

Acknowledgments

First and foremost, I must thank my advisors Paul Fuchs and Elisabeth Glowatzki for their wonderful guidance and for establishing a great environment to learn and collaborate. The free flow of ideas and resources between the two labs enriched my studies and elevated my research to heights I would not have been able to achieve alone. This thesis would be entirely different without the input and dedication of every member of the lab though there is one person that was especially influential: Megan Beers Wood. From dissecting cochleae in parallel to teaching me about the immune system, Megan constantly supported me and pushed me to do better and learn more. Our frictionless partnership has set the bar high for all future collaborations I may have. I also appreciate the help of Phillipe Vincent for performing the TTX experiments and Keira Mull and Anda Nyati for performing some of the data analysis. I thank Fatima Chakir for maintaining and ordering mouse lines, genotyping, and always helping me out when locating items around the lab, Hakim Hiel for teaching me dissection techniques and dealing with protocols, and Mohamed Lehar for his skill at electron microscopy. To Adam Goldring, Daniël Reijntjes, Marco Manca, YuanYuan Zhang, Ye-Hyun Kim, Kevin Rohmann, Steven Zachary: I would like to thank them all for their advice, support, and for making my time in the lab over the years fun and exciting. Additionally, I wish to express my gratitude to the graduate students and postdoc who paved the way for my research: Cat Weisz, Chang Liu, Sherry Wu, and Pankhuri Vyas. The trailblazing work of Cat Weisz

inspired my interest in type II afferents, and I owe so much to the time, detail, and effort she put into this project. Chang Liu recruited me to this project and personally demonstrated how to push this project into new territories. The entire basis of the calcium imaging work depends on the careful characterization of genetic lines done by Sherry Wu and Pankhuri Vyas. I would not be in the place I am now without the contributions of all four of these amazing women.

I am also incredibly lucky to have a supportive and knowledgeable thesis committee that helped shape the course of my studies. My rotation with Chris Potter made me realize my passion for sensory biology and he has been a constant presence in my training ever since. Amanda Lauer has been incredibly generous with her wisdom and technical expertise and has helped to ensure that all my experiments are well thought out. Although a late addition, Dwight Bergles has been instrumental in getting my project off the ground and has provided insightful commentary. A good deal of my time performing experiments through grad school has been in the labs of Chris (for my rotation), Amanda (for ABRs), and Dwight (for calcium imaging experiments). Just as in my own lab the collaborations with these labs and their students has been so vital to accomplishing my goals. I want to highlight the efforts of Travis Babola in Dwight's lab who inspired the idea for tackling this project with calcium imaging and even spent a great deal of time teaching us how to run these experiments. Mark Lay from Xinzhong Dong's lab was another student that assisted this project. He generously donated his time and mouse lines so we could find and characterize a new genetic line for type II afferents.

So many other people and organizations here at Hopkins have helped in some way that I cannot possibly list them all here. Shortly, Michele Pucak and the two-photon imaging core has been extremely helpful for our microscopy needs, the Center for Hearing and Balance and the Center for Sensory Biology for resources and seminars, the Neuroscience program directors and Beth Wood-Roig and Rita Ragan for keeping us on track and supported.

On the personal side, I would not even be here in the first place without the love and support of my entire family. I owe them everything and I know they are all very proud of me. Here in Baltimore, my friends and fellow students have helped me settle into Baltimore with activities like attending Baltimore Symphony Orchestra performances. And lastly to my partner, Rosty, I am so happy that I met you during my time here. You have made me feel so loved and supported, especially in these current uncertain times. It has been great to have you constantly by my side.

Table of Contents

List of Tables

Materials and Methods

Results

List of Figures

Background

1. Sound Transduction in the Cochlea

1.1 Overview

The sense of hearing, or audition, is an important sense that allows for various critical behaviors, such as detection of the footsteps of a predator as well as long range communication between conspecifics. In mammals, the sense of hearing is exquisitely sensitive and expansive, spanning multiple orders of magnitude in terms of frequencies and sound intensity. Mammalian hearing functions by converting compressions and rarefactions of air molecules into electrical signals. This transduction of sound waves into neuronal activity depends on the intricate organization of several cell types housed within the bony, snail-shaped structure within the inner ear, termed the cochlea. To even reach the cochlea, sound must be funneled by the external pinnae on the sides of the head and progress through the external auditory meatus to the tympanic membrane. Once there, the vibrations drive the movement of three ossicles whose lever action pistons the energy to the oval window which connects to one of the three fluid filled chambers that span the spiral organization of cochlea. Depending on the frequency of the ossicle motion pumping the oval window, a wave of fluid propagates up from the base to the apical tip of the cochlea and back down to exert pressure on the round window. The exact distance at which this motion

forms a standing wave is reliant on properties of the basilar membrane that sits

on the bottom of one of the fluid-filled chambers (Bekesy, 1960, Reichenbach

and Hudspeth, 2014) (see Figure B1). The basilar membrane is stiff and narrow

at the basal pole and progressively widens and becomes less stiff towards the

apical pole (Richter et al., 2000; Emadi et al., 2004). Combined, these physical

attributes of the basilar membrane create a gradient of possible standing wave

locations across the length of the cochlea such that high frequency vibrations

resonate at the base and low frequency vibrations at the apex. While these

physical processes are much more complex, they can be more simply analogized

by imagining the basilar membrane as a series of springs that vary both in their

stiffness and the weight of their material with equal mass weights attached to

them. Once the weights drop, each spring will oscillate at differing frequencies

depending on their respective material properties in a relationship described by

the equation $f = \frac{1}{2\pi}\sqrt{\frac{k}{m}}$, where f is frequency, m is mass, and k is the spring

constant. Therefore, frequency is maximized with low mass and high stiffness

like seen in the basal basilar membrane.
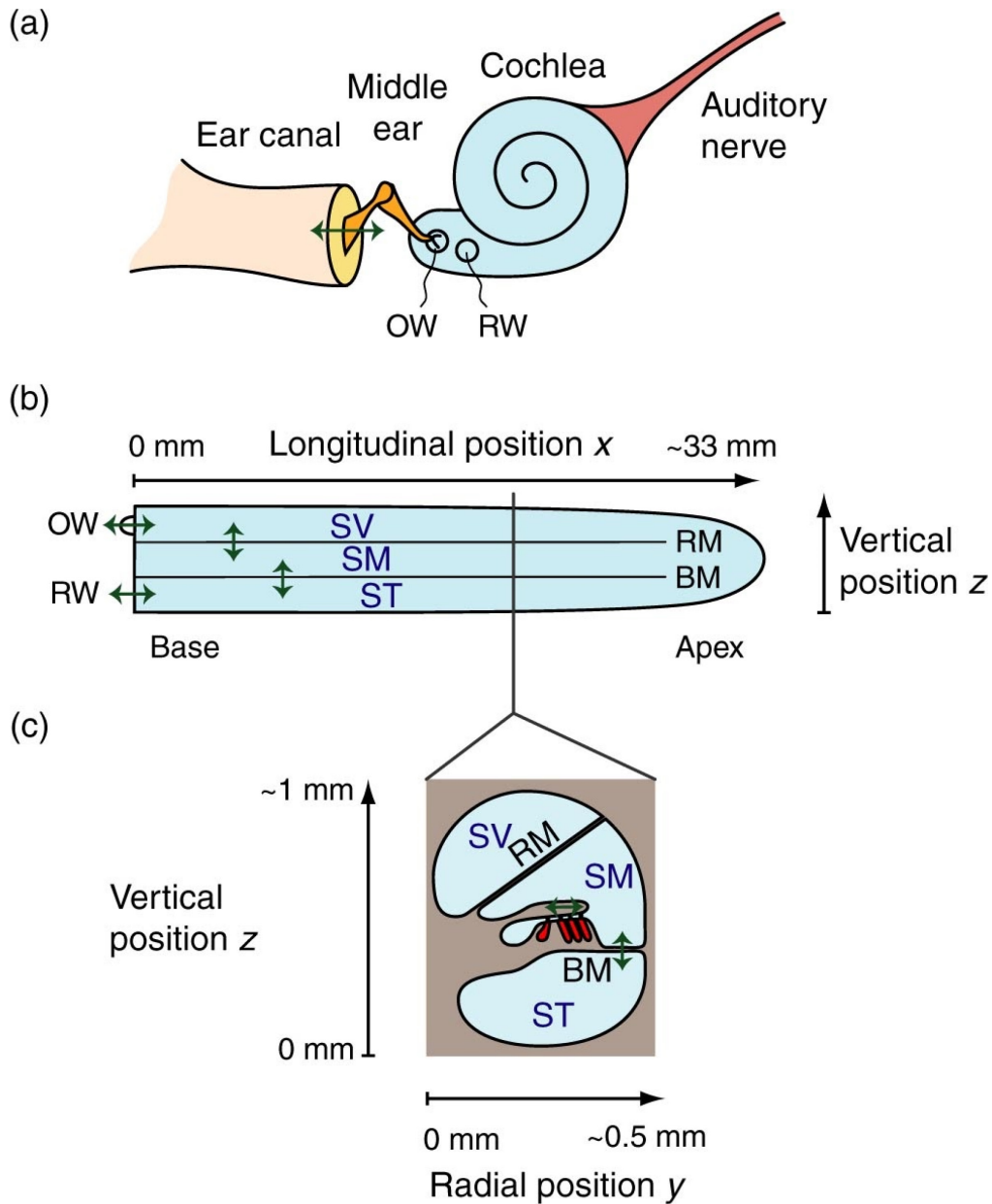
Figure B1: Structure of the ear. (*a*) Sound propagating through air as a compressive wave is funneled onto the eardrum by the external ear and the ear canal. The middle ear conveys the eardrum's resulting vibration (green arrow) to the inner ear, or cochlea, where it oscillates the elastic oval window (OW). A second elastic membrane, the round window (RW), can also oscillate to compensate for the resulting fluid displacement inside the cochlea. (*b*) A longitudinal and (*c*) a transverse section of the uncoiled cochlea show its interior structure. Two elastic membranes, the basilar membrane (BM) and Reissner's membrane (RM), delineate three liquid-filled chambers: the scala vestibuli (SV), scala media (SM), and scala tympani (ST). The mechanosensitive hair cells (red)

are embedded in the organ of Corti on the basilar membrane. Adapted from Reichenbach and Hudspeth, 2014.
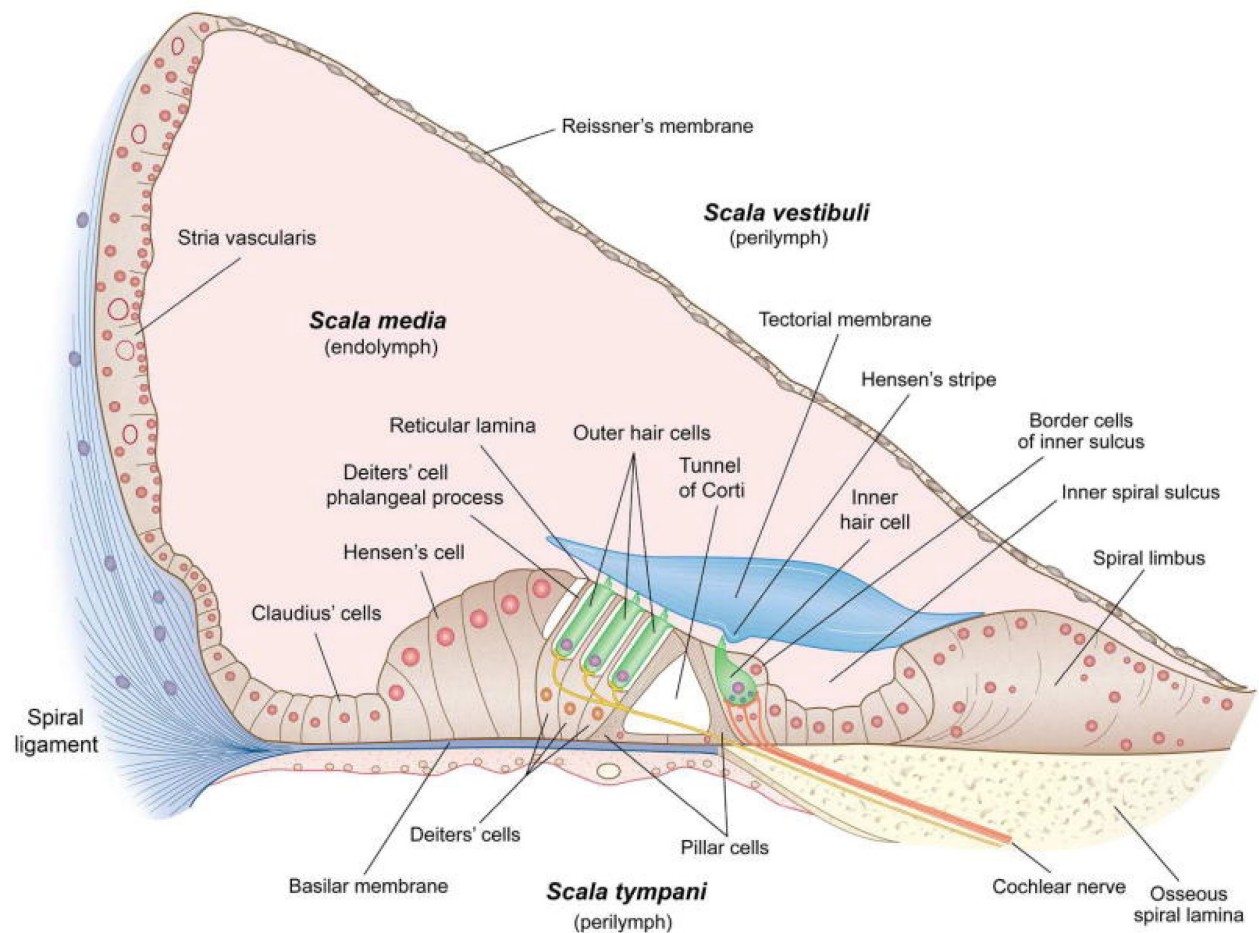
Figure B2: Cross section though the cochlear duct showing the cellular structure. The scala media is delimited by Reissner's membrane, the spiral ligament and the basilar membrane which is surmounted by the organ of Corti. The width of the basilar membrane ranges from approximately 100 to 500 µm in humans. The scala media is filled with a K^+-based endolymph, here colored pink. The organ of Corti contains the sensory hair cells embedded in assorted supporting cells of distinct shape. The hair-cell stereociliary bundles are covered in an acellular tectorial sheet and the cells are innervated by the cochlear branch of the VIIIth cranial nerve. Inner hair cells are contacted by afferents (orange) whereas outer hair cells are innervated mainly by efferent fibers (yellow). The stria vascularis is an epithelial strip on the lateral wall that is specialized for secreting endolymph. Adapted from Fettiplace, 2017.

On top of the basilar membrane sits the cochlear sensory epithelium, called the organ of Corti, which is responsible for transducing the vibration of the basilar membrane into an electrical signal (diagrammed in Figure B2). The organ of Corti is highly structured. Radially out from the center of the cochlea, the modiolus, to the lateral edge there are four rows of specialized cells called hair cells that contain mechanosensitive ion channels, mechanoelectrical transduction or MET channels, in their rigid, actin filled hair-like organelles called stereocilia (Flock et al., 1982). Deflections of the stereocilia in their preferred direction opens the channel allowing cations to enter the hair cell whereas deflections in the opposite direction close the MET channels that are constitutively open (Shotwell et al., 1981). This arrangement allows for bidirectional control of the hair cell's membrane potential that can mirror the sinusoidal nature of sound signals. Activation of the hair cells in the three rows furthest away from the modiolus, termed outer hair cells, has an additional function. These cells have a protein called Prestin (Zhang et al., 2000) packed tightly into their cell membranes that when depolarized causes physical movement of the cell by the combined motion of the confirmational changes of the protein (Brownell et al., 1985; Ashmore, 1987&2008; Zhang et al., 2006). The elongation and contraction of the OHCs amplify the vibrations of the basilar membrane (Meaud and Grosh, 2011; Ó Maoiléidigh and Hudspeth, 2011) and through their connection to the overlying tectorial membrane causes an increased shearing force that deflects the stereocilia of the remaining row of hair cells called the inner hair cells (IHCs).

Depolarizations of the hair cells through the MET channels also causes voltage-gated Ca^{2+} channels to open. The subsequent Ca^{2+} entry allows for vesicle release at the specialized presynaptic structure called the ribbon. Inner hair cell vesicles are loaded with glutamate by the vesicular glutamate transporter 3, Vglut3 (Seal et al., 2008; Ruel et al., 2008) and are capable of driving action potentials in their postsynaptic neuronal partners, the type I spiral ganglion neurons (Glowatzki and Fuchs, 2002). Spiral ganglion neurons, henceforth referred to as cochlear afferents, have their cell bodies situated in the portion of the cochlea named the spiral ganglion and have axons that travel centrally to the brainstem as a portion of the eighth cranial nerve along with the vestibular afferent neurons. With that final step, sound processing is completed in the cochlea and is transmitted to the central nervous system for further processing and action.

1.2 Tonotopic organization

An important organizational strategy within the cochlea and the rest of the auditory pathway is representation of frequency by position, called tonotopy (reviewed in Kandler et al., 2009, Fettiplace and Nam 2019). As described previously, the physical properties of the basilar membrane have multiple dimensions that all vary from the base to the apex such that high frequency vibrations primarily oscillate in the base and low frequencies in the apex (Figure B3). The preferential vibration of the basilar membrane triggers the amplifying

effects of OHCs in the same location. In turn IHCs in that same area are activated and release glutamate to their respective type I cochlear afferents (Glowatzki and Fuchs, 2002). In this way, a pure tone at the minimum detection threshold should exclusively stimulate activity of a narrow band of cochlear afferents (Galambos and Davis, 1943).
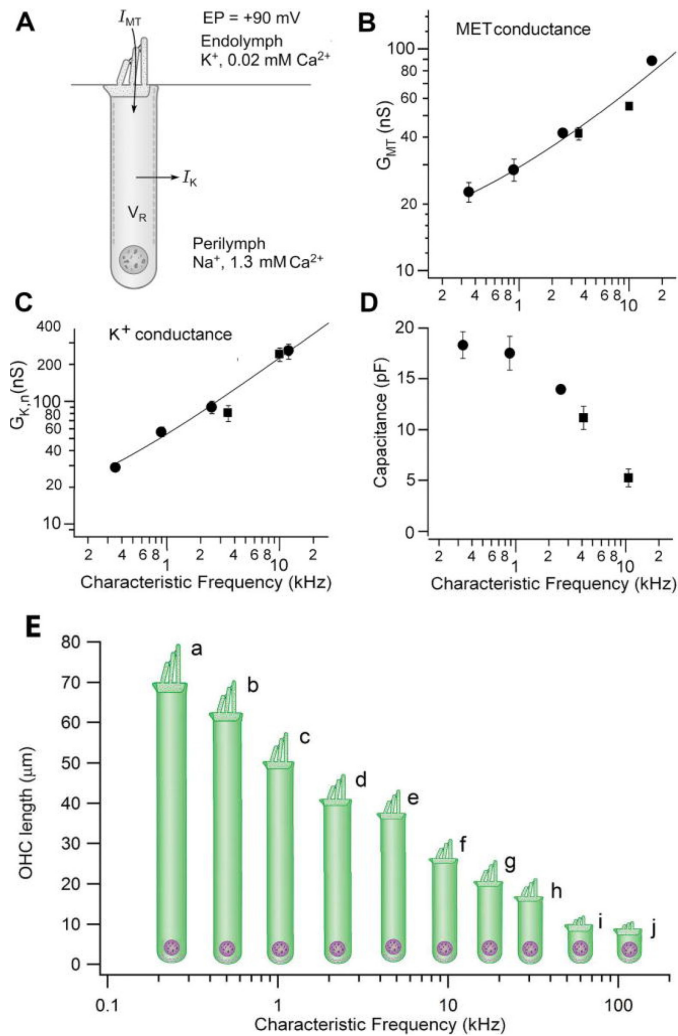
Figure B3: Tonotopic variations in membrane properties of rodent outer hair cells. (A) Principal membrane currents determining potential of outer hair cell. MET current, IMT, carried mainly by K+ ions, flows in through MET channels down a potential gradient determined by the positive endolymphatic potential (EP, 90 mV) and the resting potential (VR, ~ −50 mV); the K+ current exits mainly via

GK,n channels in lateral wall, down a K+ concentration gradient into the perilymph. (B) MET conductance, GMT, increases with the characteristic frequency at the location of the hair cell. (C) Voltage-dependent K+ conductance, GK,n, increases with hair-cell characteristic frequency. (D) Membrane capacitance decreases with hair-cell characteristic frequency, signifying a progressive decrease in the size, mainly the length, of the outer hair cell. Combining results in B, C, and D, implies a significant reduction in the membrane time constant determined by C/(GMET + GKn). Results are combined measurements from gerbils (filled circles) and rats (filled squares) and were taken, with permission, from (Johnson et al., 2011). (E) OHC length (and hence membrane area and electrical capacitance) decreases with increase in characteristic frequency in different mammals: (a) chinchilla, human; (b) guinea pig; (c) chinchilla, gerbil; (d) guinea pig, chinchilla; (e) gerbil, rat; (f) chinchilla, mouse, rat; (g) guinea pig, rat, human; (h) rat, bat; (i) mouse; (j) bat; rat, bat, guinea pig, and gerbil, chinchilla, human, and rat, mouse, and gerbil. Adapted from Fettiplace, 2017.

These neurons then travel together and innervate similar portions of the cochlear nucleus (Bourk et al., 1981; Ehret and Fischer, 1991). Throughout the auditory pathway from the cochlea to the auditory cortex this spatial relationship between neurons carrying similar frequency sound information is preserved (Middlebrooks et al., 1980; Hackett et al., 2011). Thus, the frequency of the sound stimulus can be decoded from knowing which neuron is conveying the information. Similar relationships are established in other sensory systems where similar stimuli project to nearby areas. For example, the visual system has a retinotopic map where information from neurons that receive information from nearby parts of the retina project to similar areas (Scalia and Arango, 1979; Brown et al., 2000).

Just as representation of frequency gradually changes along the basal to apical axis of the cochlea, many dimensions of cell physiology and anatomy vary gradually depending on their location. These properties are established by

gradients of soluble factors, such as sonic hedgehog and activin A, during development (Driver et al., 2008; Benito-Gonzalez and Doetzlhofer, 2014; Son et al., 2015; Prajapati-DiNubila et al., 2019). These gradients also influence the timing of the hair cell development. In wave-like fashion from the apex to base hair cells exit the cell cycle. Then the wave propagates back from the base to apex for the differentiation into functional hair cells (Ruben, 1967; Sher, 1971, Lee et al., 2006; Bok et al., 2013). Two major anatomical differences along the tonotopic axis are the size of hair cells and their stereocilia. Hair cells of the base are smaller (Dannhof et al., 1991) with shorter stereocilia (Roth and Bruns, 1992; Fettiplace and Nam, 2019) whereas hair cells of the apex are larger on both accounts. These anatomical differences contribute to differences in how these cells respond to their preferred frequencies. However, these variations also play a significant role in the susceptibility of hair cells to insults (Fettiplace and Nam, 2019). The smaller basal hair cells are more prone to cell death from senescence and after traumatic levels of noise exposure. One theory is that with smaller volumes, these hair cells are less able to buffer free Ca^{2+} in the cytosol which can lead to initiation of apoptotic mechanisms. Therefore, when large and prolonged influxes of Ca^{2+} occur from persistent, loud sounds, OHCs of the base may die. Over the years damage in OHCs appears to build up leading to age-related OHC death starting in the base causing progressive high frequency hearing loss in older individuals (Wu et al., 2019).

1.3 K$^+$ recycling and the stria vascularis

Within the cochlea, homeostasis must be maintained to allow for continuous sound transduction. On the lateral edge of the cochlea sits the stria vascularis, a highly vascularized, layered tissue that is responsible for ion balance between the three scalae (Hibino et al., 2009; Mistrik and Ashmore, 2009). The scala vestibuli and tympani contain a fluid called perilymph that is similar in composition to cerebrospinal fluid. Conversely, within the central scala media there is a unique fluid called endolymph that bathes the apical portion of all the hair cells. Unlike perilymph and cerebrospinal fluid, endolymph has a high concentration of K^+ and is deficient in Ca^{2+}. This unusual arrangement is the work of Na^+K^+-ATPases and $Na^+K^+2Cl^-$ cotransporters on type II and IV fibrocytes and marginal cells that shuttle K^+ into the intrastrial space and scala media, respectively (Offner et al., 1987; Schulte and Adams, 1989; Schulte and Steel, 1994). Fibrocytes lie outside in the perilymph and pump K^+ ions into a large syncytium that is formed together with the basal and intermediate cells of the stria vascularis (Cohen-Salmon et al., 2007). The intrastrial space is a small, tight, fluid compartment delineated by the basal and intermediate cells on one side and marginal cells on the other side near the endolymph-filled scala media (Spicer and Schulte, 2005). Intermediate cells express an inwardly rectifying K^+ channel, Kir4.1, that allows the K^+ ions to flow into the K^+-poor but high potential intrastrial space (Salt et al., 1987; Marcus et al., 2002; Nin et al., 2008). Marginal cells then pump in K^+ ions from the intrastrial space to create a high concentration of K^+ ions within the cell. Marginal cells typically have a potential difference of about 10 mV over the endolymph solution allowing K^+ ions to flux

into the scala media (Offner et al., 1987) through KCNQ1/KCNE1 channels on their apical surface (Sakagami et al., 1991; Casimiro et al., 2001). Overall, the stria vascularis establishes the endolymph through a repeated two step mechanism where K^+ ions are pumped across its electrochemical gradient on the basolateral surface and then allowed to flow down the gradient on the apical surface to create a fluid with high potential and a high concentration of K^+ ions (Nin et al., 2008) (Figure B4).

Because the endolymph has such a large positive driving force over the hair cells, there is a large inward cationic current when the MET channels open. If the hair cells were surrounded by endolymph, they would need taxing ATP-dependent ion pumps to maintain their resting potential. Fortunately, the majority of the volume of hair cells is bathed by perilymph that has a low concentration of K^+ making the loss of K^+ through KCNQ4 (Kubisch et al., 1999; Beisel, 2005) and Ca^{2+}-activated K^+ channels (Dulon et al., 1995; Oliver et al., 2000; Rohmann et al., 2015) into the perilymph energetically favorable. In essence, this establishes the stria vascularis as a battery by creating a potential difference of about 80mV between the compartments of the cochlear spiral that flows through the hair cells when motion of the basilar membrane opens the MET channels (Hibino et al., 2009; Reichenbach and Hudspeth, 2014). This arrangement switches the energetic demands of re-establishing ion balance from the post-mitotic hair cells to the replaceable cells of the stria vascularis. Supporting cells of the organ of Corti also contribute by sponging up K^+ ions that build up in the perilymph and funneling it back to the stria vascularis (Boettger et al., 2002; Boettger et al.,

2003; Kikuchi et al., 2000; Mammano et al., 2007; Eckhard et al., 2012). Genetic

mutations in one of the connexins, connexin 26 (Kelsell et al., 1997; Cohen-

Salmon et al., 2002; Hilgert et al., 2009) that constitute the gap junctions

between the supporting cells that allow for the passage of ions, are the most

common genetic cause of deafness globally (Kemperman et al., 2002).

Connexins also are expressed in the cells of the stria vascularis and are

important for the flow of ions across the syncytium formed from the fibrocytes,

basal cells, and intermediate cells (Cohen-Salmon et al., 2007). The overall

effect is that K^+ ions cannot properly be recycled and extruded into the

endolymph leading to an eventual disappearance of the potential difference

between the scalae. Without the higher relative K^+ in the endolymph, less current

enters through the MET channels. In the absence of this increased voltage

change in hair cells, the cochlear gain from the OHCs is not sufficient and leads

to deafness.
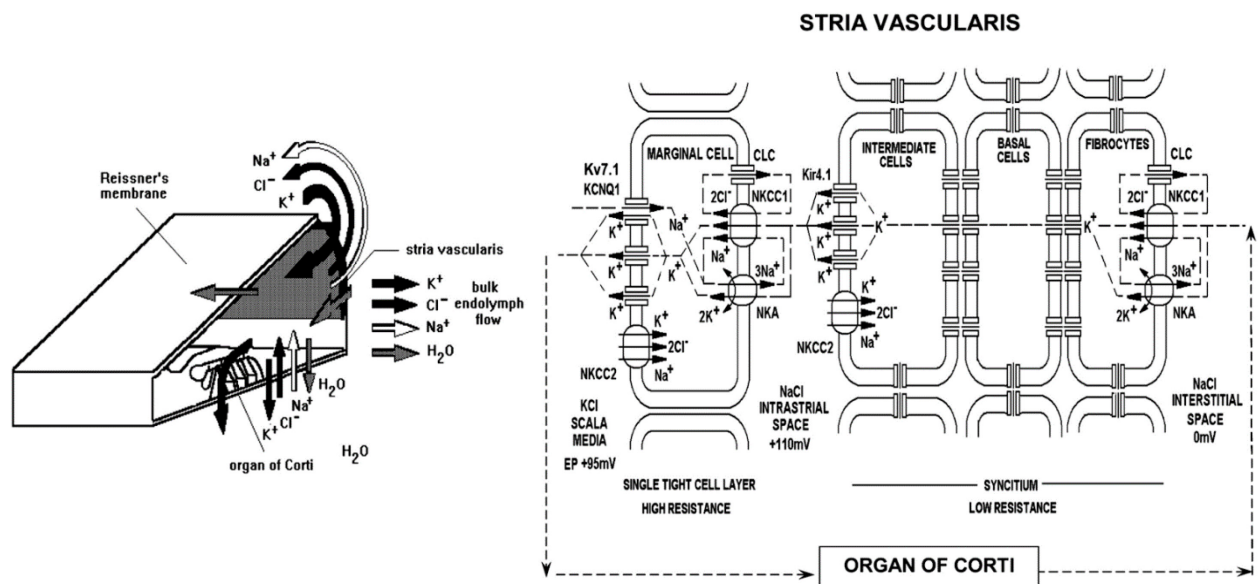
Figure B4: The main ion transporters of stria vascularis. A single layer of marginal cells (MCs) that extrude K+ into the endolymph of scala media, producing the positive +95 mV endocochlear potential (EP). The source of this K+ is the underlying syncitial cell layers, comprised of intermediate cells (ICs), basal cells (BCs) and fibrocytes (FCs), which form one giant pseudo-cell due to the high density of gap junctions between them. Transport through the pseudo-cell seems dominated by the apical membranes of the ICs (separated from MCs by the interstrial space), and by the basolateral membranes of the FCs (that appear to obtain K+ from the perilymph of the spiral ligament, rather than from blood). The capillary layer between the MCs and ICs supplies oxygen and nutrients to these cells, and is permeable to some drugs, but it seems to offer a high resistance to current flow, as indicated by the high positive potential in the intrastrial space (the intrastrial potential or ISP). Adapted from Patuzzi, 2011.

1.4 The hair cell mechanotransduction machinery

For many decades, the identity of the MET channel was elusive (Fettiplace 2016, Corey et al., 2019). Recent work has demonstrated the role of TMC1 as a component of the MET channel pore complex in mice (Pan et al., 2018). Pan and colleagues provide two separate but complementary arguments for TMC1 as the pore-forming protein of the MET channel complex. First, they presented a model for the structure of TMC1 that shows it can fold into a channel-like dimer similar to TMEM16 (also modeled in Ballesteros et al., 2018). Secondly and more definitively, Pan and colleagues introduced cysteine substitutions into the amino acid structure of the TMC1 protein and injected a viral construct to force expression in TMC double knockout mice. 16 out of the 17 cysteine substitutions were still functional, 11 caused changes to Ca^{2+} selectivity, 5 caused whole cell current decreases, and 3 caused lower single channel currents after chemical alteration of these cysteine inclusions. These changes to the currents only occurred when the channel was open (not closed due to

inhibitory deflections or channel blockers) suggesting that the changed amino

acids resided within the pore region (Figure B5).
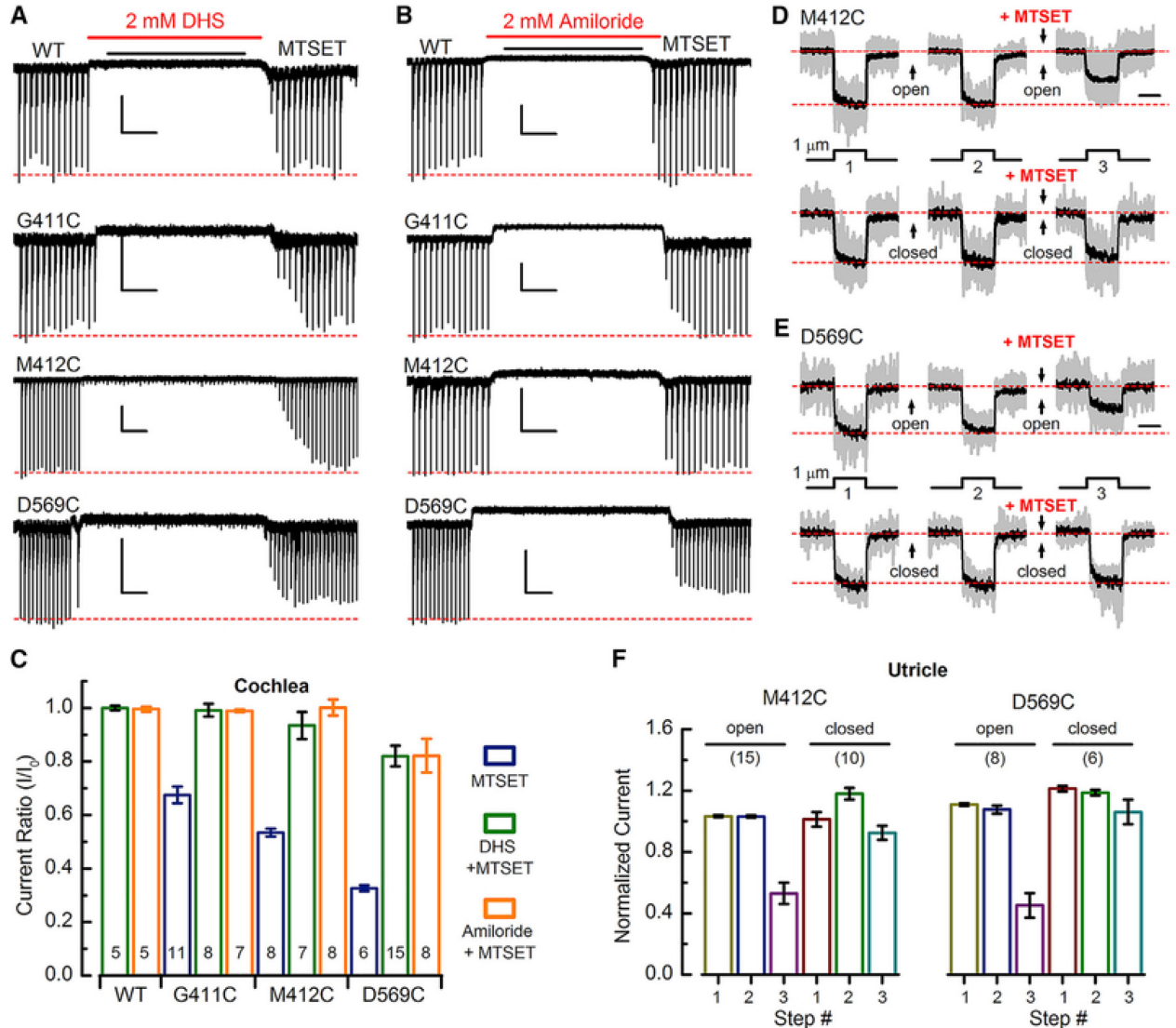
Figure B5: Pore Blockers and Closed Channels Impede Access to Cysteine Mutations (A) Representative IHC sensory transduction currents for WT, G411C, M412C, and D569C in response to dual application of 2 mM dihydrostreptomycin (DHS) and MTSET as indicated above. MTSET was applied at 2 mM for G411C, 10 mM for M412C, and 0.2 mM for D569C, selected as the minimal concentration required to achieve the maximal response during the 8-s application. The scale bars represent 2 s (horizontal) and 100 pA (vertical). (B) IHC responses for dual application of 2 mM amiloride and MTSET. Scale bars indicate 2 s (horizontal) and 100 pA (vertical). (C) Mean (±SEM) current ratios for WT, G411C, M412C, and D569C in response to MTSET alone, DHS + MTSET, or amiloride + MTSET. Number of cells, from 2–5 mice/condition, is shown at the bottom of each bar. (D)

Mean sensory transduction current traces (black) superimposed on 10–15 normalized individual traces (gray) recorded from utricle type II hair cells expressing M412C. Deflection protocol is shown below. Between each step, the bundle was deflected 1.7 µm (top row) or −0.5 µm (bottom row) for 6 s to open or close channels, respectively. 2 mM MTSET was applied between the 2nd and 3rd steps as indicated. The scale bar represents 25 ms. (E) Mean sensory transduction traces (black) superimposed on 6–8 normalized individual traces (gray) recorded from utricle type II hair cells expressing D569C.The same stimulation protocol was used to evoke the responses shown in (D) and (E) except the bundle was deflected for 2 s and the MTSET concentration was 0.5 mM. (F) Mean (±SEM) normalized M412C and D569C currents for each step (1–3) shown in (D) and (E) for bundles held in the open and closed positions. Number of cells, from 2–5 mice/condition, is shown above the bars. Adapted from Pan et al., 2018.

TMC1 alone does not appear to be sufficient for mechanosensation however. Expression in heterologous systems has been unsuccessful, suggesting that the mechanosensory properties of the MET channel arise from the coordination of several proteins. LHFPL5 is a protein that is necessary for mechanotransduction (Zhao et al., 2014) and is localized to the tips of the stereocilia (Mahendrasingam et al., 2017). While the protein seems too small to form the pore region of the MET channel, it may be required to localize TMC1 to the tips of the stereocilia as well (Xiong et al., 2012). TMIE is another integral protein for transduction to occur which is known to interact with LHFPL5 and protocadherin 15 (Zhao et al., 2014). CIB2 (Giese et al., 2017) and mTOMT (Cunningham et al., 2017) are two other proteins that appear to interact with TMC1 and 2 and contribute to audition. The identity of many of these proteins, including TMC1, were discovered by characterization of several deafness genes (Deol and Robins, 1962; Kurima et al., 2002; Longo-Guess et al., 2005; Xiong et al., 2012). The *Beethoven* mutation caused genetically dominant defects in the

TMC1 gene (Vreugde et al., 2002) and causes progressive hearing loss and decrease in the Ca^{2+} selectivity of the MET current (Pan et al., 2013; Beurg et al., 2015; Corns et al., 2016). As a dominant, single gene mutation *Beethoven* has been targeted with viral genetic therapeutics to restore hearing in mice (Askew et al., 2015).

Mechanotransduction also depends on the combined protein complex's interactions with the cell membrane, the actin filaments that form stereocilia, and the tip links (Kachar et al., 2000) (Figure B6). Tip links are structures made up of protocadherin 15 and cadherin 23 that connect the tip of one stereocilia to the side of its neighboring taller stereocilia (Pickles et al., 1984; Kazmierczak et al., 2007). As the stereocilia are deflected towards the tallest one, tension in the tip links increases and opens the 2 estimated MET channels where the tip links connect to the top of each stereocilium (Beurg et al., 2009). Conversely, movement away from the tallest stereocilium releases some of the baseline tension that keeps some of the channels partially open and thus decreases the current flowing through the MET channels. This intrinsic tension has been implicated in the slow (tens of milliseconds) adaptation process that keeps MET channels from saturating from static or prolonged deflections (Kros et al., 1992; Kennedy et al., 2003). A myosin motor (Kros et al., 2002; Marcotti et al., 2016) acting on the actin in the stereocilia is thought to maintain the tension contributing to the open probability of the MET channels and through an ATP and Ca^{2+}-dependent (Jia et al., 2007; Corns et al., 2014) process relieves the tension during prolonged bouts of stimulation. There is also a second faster adaptation

that occurs (Kennedy et al., 2005; Beurg et al., 2006; Stauffer and Holt, 2007). In mammals this fast adaptation may not require Ca^{2+} (Peng et al., 2013; Caprara et al., 2019; but see Corns et al., 2014) but may be sensitive to PIP_2 (Effertz et al., 2017) and therefore may relate to the properties of the channel and/or the cell membrane.
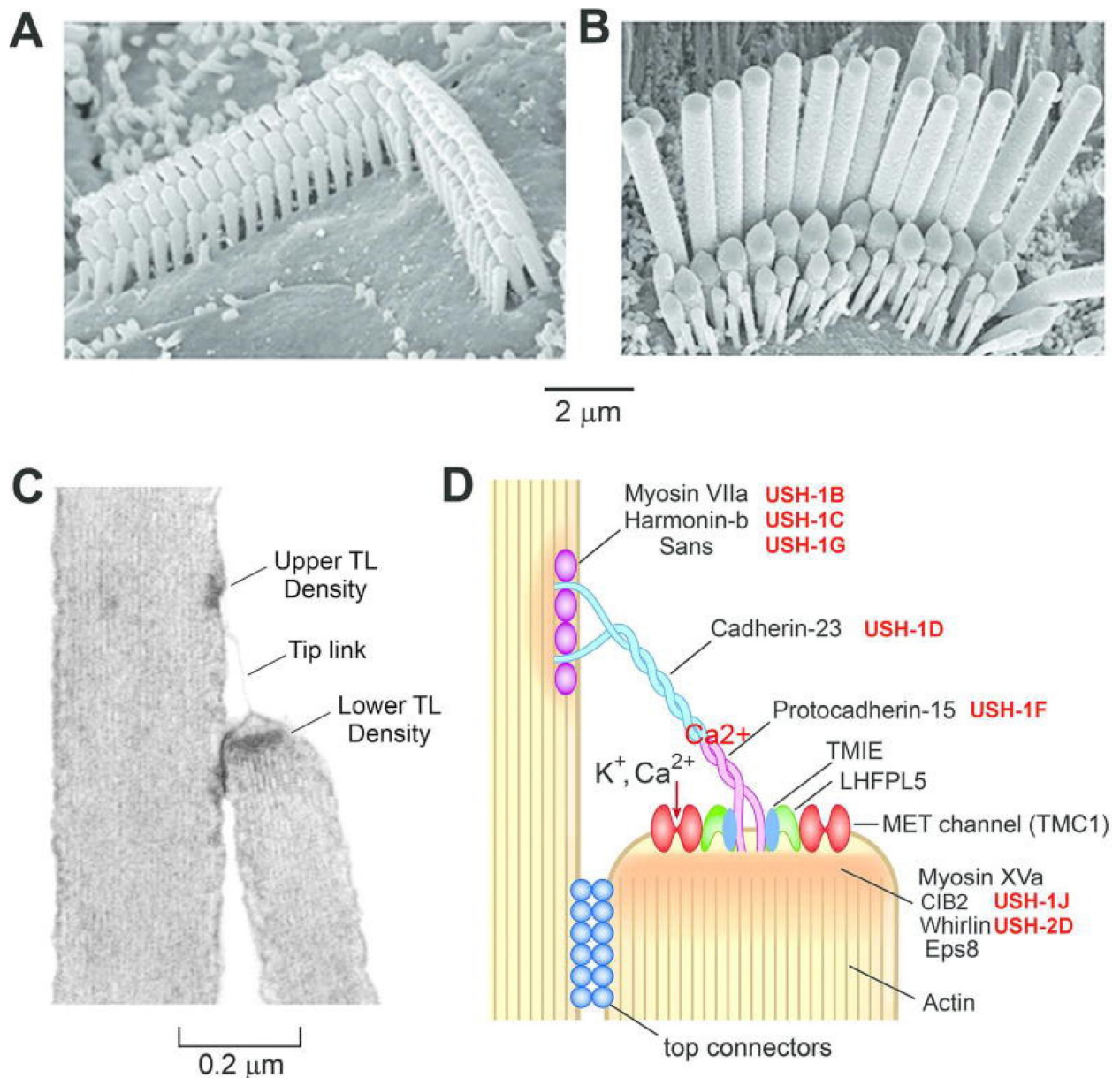
Figure B6: Stereociliary bundles and the transduction apparatus. Scanning electron micrographs of stereocilary bundles of A, an outer hair cell and B, an

inner hair cell, showing the staircase in heights of the rows. C. Transmission electron micrograph of an outer hair cell showing a tip link connecting two stereocilia; the insertion sites of the tip link (TL) are heavily electron dense suggesting dense protein densities. D. Schematic of the molecular structure of the tip link apparatus deduced from various mutations. USH-1 and USH-2 denote different Usher type 1 and type 2 mutations. The association between the N-termini of protocadherin-15 and cadherin-23 is Ca2+ dependent. Two MET channels (red) are situated at the lower end of the tip link and are present as complexes with TMIE, LHFPL5, TMC1 and possibly other proteins. Adapted from Fettiplace, 2017 and Fettiplace and Kim, 2014.

1.5 The hair cell synaptic machinery

In IHCs, depolarization from MET channel activation causes opening of CaV1.3 voltage-gated Ca^{2+} channels (Platzer et al., 2000). OHCs also express CaV1.3 (Knirsch et al., 2007) but in smaller numbers than the IHCs correlating with their reduced synaptic efficiency (Weisz et al., 2012). In mature IHCs these channels cluster near the synaptic release machinery, ribbons (Brandt et al., 2005; Wong et al., 2014; Vincent et al., 2014) and are responsible for the majority of the Ca^{2+} entry required for vesicle release (Michna et al., 2003; Brandt et al., 2003; Dou et al., 2004; Nemzou et al., 2006). Ribbons are dense proteinaceous structures seen at presynaptic release sites in auditory and vestibular hair cells as well as in photoreceptors and bipolar cells of the retina (Sterling and Matthews, 2005). They are mainly composed of Ribeye, which has two parts, an A domain and a B domain similar to the transcriptional repressor CtBP2; and typically have a halo of tethered synaptic vesicles (Schmitz et al., 2000). While not exactly worked out, it is thought that ribbons are important for continuous release from the hair cell synapse. However, in ribeye knockout

experiments, despite the lack of the physical ribbon structure, synaptic vesicles still cluster near active zones and only minor hearing defects occur (Becker et al., 2018; Jean et al., 2018). The main deficits were that exocytosis of synaptic vesicles was reduced during low intensity stimulation but not with prolonged stimulation and the rate of replenishment was slower in the knockout mice. Bassoon is another protein integral to the formation of the synaptic ribbon. Genetic manipulations of bassoon lower the amount of the readily releasable pool of vesicles leading to decreased frequency and amplitude of EPSCs in the postsynaptic type I afferents (Khimich et al., 2005; Jing et al., 2013). Overall, it appears that the ribbon is important for the coordination and availability of vesicles for release.

Glutamate release as measured by the AMPA currents from the postsynaptic type I afferent bouton reveals that glutamate is not released neatly in a single, monotonically decreasing bolus (Glowatzki and Fuchs, 2002). Glutamate release events can have multiple peaks, typically over a longer timeframe than the monotonic events. Interestingly, multiphasic release is peculiar to IHCs and glutamate release from OHCs and vestibular hair cells are small and monophasic. Some have argued that these events reflect the flickering of single vesicle release events where the pore formed from the fusion of the vesicle opens and shuts repeatedly before releasing its contents (Chapochnikov et al., 2014). Others have argued that these separate peaks in the AMPA currents reflect individual vesicles (Goutman and Glowatzki, 2007; Li et al., 2009; Grant et al., 2010; Graydon et al., 2011; Johnson et al., 2017b) (overviewed in

Figure B7). Regardless of the number of vesicles released per event, vesicle release does not depend on the typical suite of SNARE proteins such as SNAP-25, syntaxin-1, synaptobrevin-1 or 2 (Nouvian et al., 2011). Instead both the docking, calcium dependent fusion, and replenishment of synaptic vesicles appear to depend on the protein otoferlin (Roux et al., 2006; Vogl et al., 2015). Though, in the first postnatal days, synaptotagmin-1 is expressed and can cause vesicle release (Beurg et al., 2010). In an otoferlin knockout, occasional vesicles can be released spontaneously but there is no coordinated release of vesicles in response to depolarizations as would occur with MET channel activity or other increases in internal Ca^{2+} (Takago et al., 2018). As such, the otoferlin knockout mice are totally deaf (Roux et al., 2006).
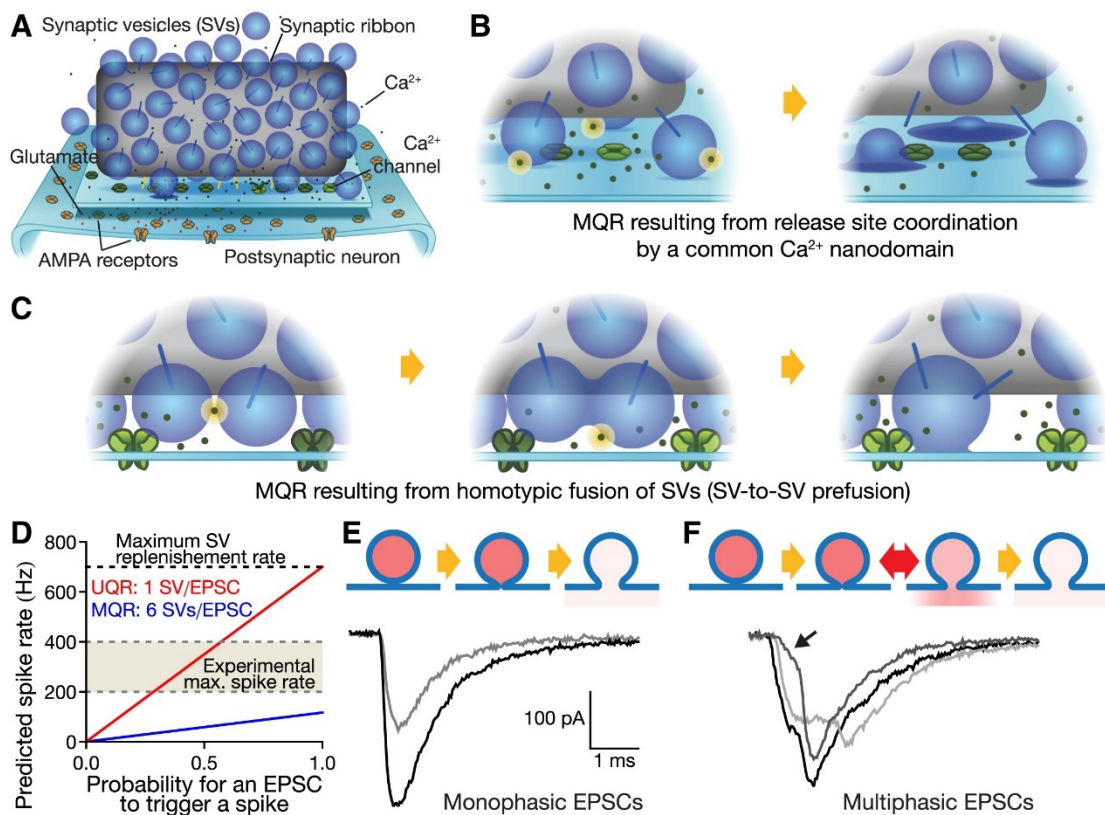
Figure B7: MQR and UQR Hypotheses at the IHC Ribbon Synapse (A) Schematic of an IHC synapse. The ribbon (gray) tethers (blue sticks) SVs (blue spheres). Ca^{2+} ions (green dots) enter through Ca^{2+} channels (green pores) and trigger the exocytosis of docked SVs via activation of the Ca^{2+} sensor(s) of fusion. Open Ca^{2+} channels are depicted in light green, closed ones in dark green. Fusing SVs release their glutamate content (red dots) into the synaptic cleft. Glutamate binding to AMPARs (orange pores) on the SGN elicits their opening and EPSC generation. Ca^{2+} ions and channels are not drawn to scale. (B) Scheme of the "Ca^{2+}-synchronized MQR" scenario. Left: Ca^{2+} channel opening elicits the entry of Ca^{2+} ions. Ca^{2+} binding to the Ca^{2+} sensors (yellow) triggers the release of three nearby docked SVs. Right: SVs exocytose at slightly different times. Such a multiquantal release would trigger an EPSC about three times the amplitude of a uniquantal EPSC. (C) Scheme of the homotypic fusion scenario of MQR. The homotypic fusion of two SVs (left) creates a larger compound (middle), which then fuses with the plasma membrane (right). This event would generate an EPSC about twice the amplitude of a uniquantal EPSC. (D) Predicted steady-state spike rate in MQR (blue) and UQR (red) scenarios as a function of the probability for an EPSC to trigger a spike. The SV replenishment rate was 700 Hz. The experimental steady-state spike rate was set to 200–400 Hz. (E) UQR scenario: monophasic EPSCs result from the exocytosis of single SVs, with the whole glutamate content released at once. (F) UQR scenario: multiphasic EPSCs result from the exocytosis of single SVs, occurring with subsequent fusion pore openings and closings, and/or variations in pore diameter. Some multiphasic EPSCs were reminiscent of "foot events" (black arrow). Adapted from Chapochnikov et al., 2014

2. Supporting Cell Organization and Function

"Supporting cell" is a general term for a myriad of cell types within the organ of Corti that are not directly part of the chain of signaling from transduction of sound stimuli to the central nervous system, but instead indirectly support their function (as reviewed in Monzack and Cunningham, 2013). One primary function of supporting cells is the literal support they provide by establishing the physical environment surrounding the sensory cell types. Pillar cells form a sturdy physical barrier between the IHCs and the OHCs creating the tunnel of Corti. Deiters' cells connect to the basilar membrane and provide the substrate to transmit the vibrations of the basilar membrane to the OHCs (as reviewed in Raphael and Altshuler, 2003).

More recently, supporting cells, as well as glia in the central nervous system, have been revealed to have many roles besides structural and trophic support (Hansen et al., 2001; Stankovic et al., 2004). For example, supporting cells around the IHCs express GLAST (now called EAAT1), making them capable of clearing synaptic clefts of excess glutamate after IHC activity (Furness and Lehre, 1997; Glowatzki et al., 2006). Many supporting cell types also are capable of internalizing excess K^+ ions following intense hair cell activation (Boettger et al., 2002; Boettger et al., 2003; Kikuchi et al., 2000; Mammano et al., 2007; Eckhard et al., 2012). Through the syncytium of supporting cells connected by gap junctions formed from connexin 26 and 30, K^+ ions are transported to the stria vascularis for pumping into the endolymph (as discussed in a previous

section, stria vascularis). Supporting cells have also been observed extruding

and phagocytosing nearby dying tissue to clear the organ of Corti after damage

(Forge, 1985; Raphael and Altschuler, 1991; Anttonen et al., 2014; Monzack et

al., 2015; Hirose et al., 2017) (see section on damage and repair mechanisms for

more details).

In the developing cochlea of altricial animals such as mice, supporting

cells of the greater epithelial ridge play an important role in establishing neural

activity before the animal is capable of hearing. The Tecta expressing cells of

Kölliker's organ spontaneously undergo transient calcium signaling that

propagates as a wave through nearby supporting cells. This mechanism depends

upon ATP-induced ATP release and results in the release of K^+, Cl^-, and water

causing shrinkage of the supporting cell and activation of local inner hair cells.

The shrinkage of multiple, contiguous supporting cells causes an obvious

wrinkling of the tissue visible with differential interference contrast (DIC) imaging,

termed a crenation (Tritsch et al., 2007; Tritsch et al., 2010; Wang et al., 2015)

(Figure B8). The random activation of groups of neighboring inner hair cells in the

pre-hearing cochlea can cause coordinated activity in the central nervous system

(Babola et al., 2018) and is thought to establish and refine synapse formation

between the type I afferent and their central targets (Zhang and Poo, 2001;

Clause et al., 2014). Sufficiently widespread crenation activity in the greater

epithelial ridge region has been observed to cross the tunnel of Corti and

coordinate the activity of the present Deiters' cells and OHCs (Ceriani et al.,

2019). Elimination of this large synchronous activity has been found to disrupt the

characteristic pathfinding of type II afferent dendrites underneath the OHCs. It

remains to be seen whether crenations are also important for the

electrophysiological maturation of type II afferents or for refining their central

projections.
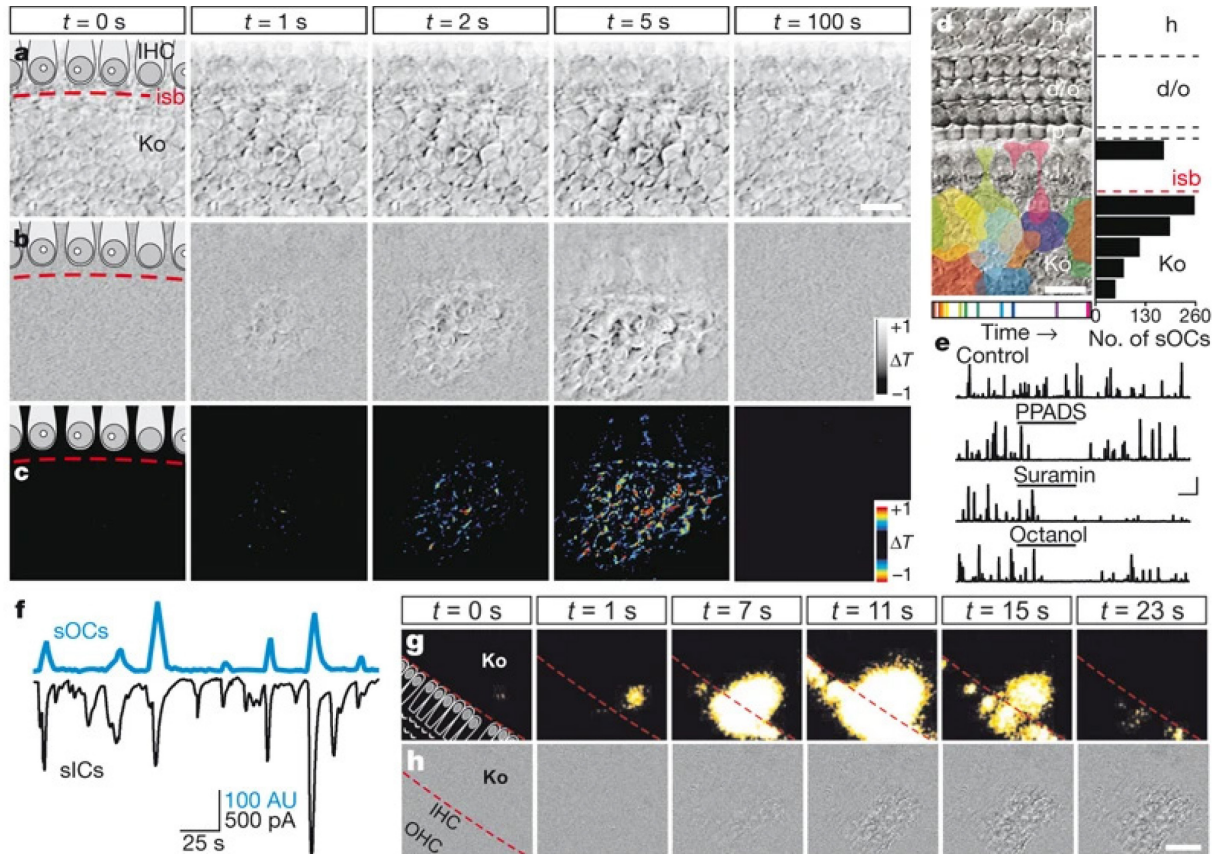
Figure B8: Spontaneous optical changes within Kölliker's organ. a, Sequence of DIC images at indicated times (*t*). Dashed line demarcates the inner spiral bundle. b, Difference images after subtraction (see Methods). c, Pseudocoloured difference images after thresholding. d, Left: location and furthest extent of spontaneous optical changes (sOCs) during 300 s (time of occurrence is shown at the bottom). Right: distribution of origins of spontaneous optical changes in 10 µm bins (*n* = 879 events in 21 preparations). e, Plots of normalized transmittance changes (Δ*T*) over time; spontaneous optical changes are shown as upward deflections. Scale: 400 AU (arbitrary units), 200 s. f, Simultaneous recording of supporting cell spontaneous inward currents (black) and spontaneous optical changes (blue) from Kölliker's organ. sICs, spontaneous inward currents. g, h, Simultaneous time-lapse imaging of [Ca2+]i (g) and

intrinsic optical changes (difference images, h). d/o, Deiters' and outer hair cells; h, Hensen cells; i/IHC, inner hair cells; isb, inner spiral bundle; Ko, Kölliker's organ; OHC, outer hair cells; p, pillar cells. Scale bars for a–c, 15 µm; d, 20 µm, g, h, 30 µm. Adapted from Tritsch et al., 2007.

2.1 Purinergic receptors

ATP is sensed by two flavors of purinergic receptors: ligand-gated

ionotropic P2X receptors and metabotropic P2Y receptors that can sense ATP,

ADP, or UTP depending on the receptor subtype composition (reviewed in

Burnstock and Kennedy, 1985). Many of the subtypes of purinergic receptors are

expressed throughout the cochlea though the expression profile does change at

developmental time points (full details of expression reviewed in Köles et al.,

2019). Of particular interest, cochlear afferents have been observed to express

several P2 receptor subunits: P2X1,2,3,4, and 7 (Nikolic et al., 2001; Housley et

al., 1998; Brändle et al., 1999; Huang et al., 2006) and P2Y4,6,12, and 14

(Huang et al., 2010; O'Keeffe et al., 2010); which supports the findings that type

II afferents respond to ATP and UTP (Weisz et al., 2009; Liu et al., 2015). Hair

cells and supporting cells also express various P2 receptors. The purinergic

receptor subunit with the most impact on cochlear function is the P2X2 subunit.

P2X2 expression is upregulated following loud noise exposure (Wang et al.,

2003) and has a protective role for noise-induced and age-related hearing loss

(Housley et al., 2013; Yan et al., 2013). ATP is also important for the paracrine

and autocrine signaling of the supporting cells as well as the functioning of K^+ ion

shunting through gap junctions (Zhu and Zhao et al., 2012) (See sections on

supporting cells and stria vascularis for more details). Additionally, ATP is also a potent chemoattractant signal for immune cells (Chen et al., 2006) (see response to damage section for more details). Overall, ATP is a critical signal for many processes in the cochlea.

3. Differences Between Type I and Type II Cochlear Afferents

3.1 Anatomical differences

Early anatomical studies of the mammalian cochlea revealed two distinct

populations of cochlear afferents based on their morphology and divergent

innervation patterns within the organ of Corti (Spoendlin, 1971; Spoendlin, 1974;

Kiang et al., 1982) (Figure B9). The vast majority of cochlear afferents send out a

single, unbranched process to a single inner hair cell, i.e. type I cochlear

afferents (Spoendlin 1971). Type II cochlear afferents project past IHCs making a

characteristic near-right angle turn to the base of the cochlea to contact an

average of 24 OHCs each with some reports of upwards of 100 OHCs contacted

(Smith, 1975, Kiang et al., 1982, Berglund and Ryugo, 1987, Weisz et al., 2012;

Martinez-Monedero et al., 2016; Ghimire and Deans, 2019). This difference was

revealed when investigators transected the auditory nerve in cats and observed

the degeneration of the spiral ganglion neurons. After transections type I

cochlear afferents preferentially died, leaving just a small minority of afferent

neurons that projected to the OHCs. This was the first evidence that the

unmyelinated spiral ganglion neurons formed a distinct population of neurons

and did not just have some defect in myelination (Spoendlin, 1971).

One of the other most striking differences between the two populations of

neurons is that type I afferents are thick and myelinated and that type II afferents

are thin and have no myelin (Thomsen, 1966, Spoendlin, 1971; Spoendlin, 1973;

Romand and Romand, 1987). Morphologically, these neurons have been

differentiated in anatomic studies by taking the ratio of the peripheral going and the central travelling processes in these mostly bipolar neurons (Kiang et al., 1982; Brown, 1987; Berglund and Ryugo, 1987). In type II afferents the pseudounipolar shape and lack of myelin means both processes are approximately equally thin whereas the ratio is larger because of the myelin on the central going process of type I afferents. With this metric, researchers were able to classify these neurons and then follow their projections to the cochlear nucleus after horseradish peroxidase staining. Like the type I cochlear afferents, type II afferents travel along the eighth nerve to the cochlear nucleus and tend to form an ascending and descending branch at different locations in the cochlear nucleus depending on the tonotopic origin of the fiber (Brown, 1987; Brown and Ledwith, 1990; Berglund and Brown, 1994; Morgan et al., 1994). One of the major differences however is that type II afferents were likely to terminate near the granule cell layer of the marginal zone in the cochlear nucleus (Brown et al., 1988; Brown and Ledwith, 1990, Berglund and Brown, 1994; Berglund et al., 1996; Benson and Brown, 2004). This area receives a wide array of sensory information especially somatosensory information (Young et al., 1995; Oertel and Young, 2004; Haenggeli et al., 2005). Staining and electron microscopy has been used to try to identify the postsynaptic targets of type II afferents but has been somewhat limited and unclear especially because many of the putative synapses were *en passant* and not from terminal endings (Brown and Ledwith, 1990; Ryugo et al., 1991; Berglund and Brown, 1994; Morgan et al., 1994). Rarely, putative type II afferents synapse onto principal neurons that also receive type I

afferent or medial olivocochlear (MOC) innervation, but they were also seen

synapsing onto a variety of cell types (Berglund et al., 1996; Benson and Brown,

2004).
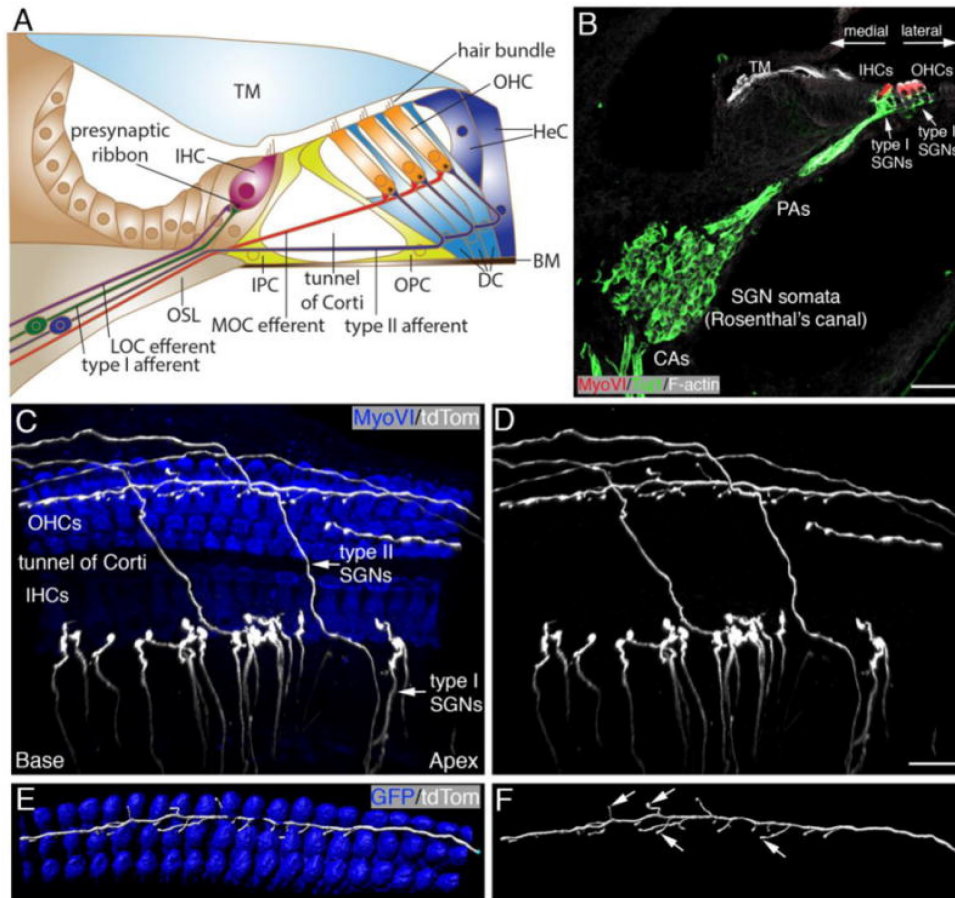
Figure B9: Innervation of the organ of Corti. (A) A cartoon of the mature organ of Corti. There is one row of IHCs and three rows of OHCs separated by the tunnel of Corti. The organ of Corti is innervated by two types of afferents (type I and type II) and two types of efferents (MOC and LOC). OSL: osseous spiral lamina. LOC: lateral olivocochlear neuron. MOC: medial olivocochlear neuron. IPC: inner pillar cell. OPC: outer pillar cell. DC: Deiters' cell. BM: basilar membrane. HeC: Hensen's cell. TM: tectorial membrane. (B) A cross-sectional image of a P0 mouse cochlea at the base. The SGNs are labeled with an antibody against Tuj1 (green), a class III β-tubulin, and hair cells are labeled with an antibody against Myosin VI (red). Phallodin labeling of F-Actin (white) marks hair cell bundles, SGNs and TM. The majority of SGNs are type I SGNs innervating IHCs, while the rest SGNs are type II SGNs making connections with OHCs. PAs: peripheral axons. CAs: central axons. Scale bar: 50 μm. (C and D) A whole-mount image of a P8 cochlea from a mouse carrying *Neurog1-CreERT2*, *R26R-tdTomato* and

Atoh1-GFP. Sparse numbers of labeled SGNs are detected using an anti-dsRED antibody that binds to tdTomato (white). Hair cells are labeled with Myosin VI (blue). Each type I SGN has an unbranched peripheral axon contacting a single IHC. Type II SGN processes pass through the tunnel of Corti, turn towards the base and form *en passant* contacts with OHCs. (E and F) 3D reconstruction of a type II SGN process (white) and OHCs (blue) in B. OHCs are reconstructed with GFP expressed by *Atoh1-GFP* (psuedocolored blue). Arrows point to a few examples of *en passant* contacts between the type II SGN and OHCs. Scale bar in C–F: 15 μm. Adapted from Zhang and Coate, 2017.

3.2 Electrophysiological differences

In vivo sharp electrode recordings from the auditory nerve revealed that type I cochlear afferents encode important parameters of sounds such as intensity, frequency, and timing (Galambos and Davis, 1943, Robertson 1984). Such recordings from type II cochlear afferents have been rare but suggest that these neurons are unresponsive to all but the loudest of sounds (Robertson 1984, Brown, 1994; Robertson et al., 1999; Flores et al., 2015). In fact, out of all the neurons recorded from the auditory nerve in this manner only one neuron has been verified to be a putative type II afferent based on horseradish peroxidase staining and on the speed of the retrograde action potential - unmyelinated fibers should have a much slower action potential conduction velocity. All other attempted cells either did not fill properly or could not be induced to fire action potentials at all (Brown, 1994; Robertson et al., 1999). Though finding any number of putative type II afferents considering how intractable the recordings are to begin with, let alone for small, unmyelinated fibers with minimal to no baseline firing rate, is impressive.

One hypothesis is that type II cochlear afferents signal damaging levels of sound, acting as the equivalent of a nociceptor for the auditory system (Tonndorf, 1987; Simmons and Liberman, 1988; Brown et al., 1988, Flores et al., 2015, Liu et al., 2015). There have been several studies that support this hypothesis. One study observed immediate early gene expression in the cochlear nucleus after loud noises in Vglut3 KO mice (Flores et al., 2015) (Figure B10). In these mutants, glutamate cannot be transferred into vesicles of the IHCs and therefore when depolarized by sound cannot activate the AMPA receptors on the postsynaptic type I afferent boutons. Therefore, the researchers argued that any Fos activity in the cochlear nucleus could not have come from type I afferent synaptic activity and thus could represent the activity of the remaining type II afferents. If the observed Fos activity is truly reflective of type II afferent activity, then their work suggests that loud sounds can activate type II afferents. While this a distinct possibility, there are a few alternative explanations especially considering the mutation is present from birth and thus there could be compensating mechanisms employed by the system. A separate study that used the same Vglut3 KO observed widespread spontaneous activity in pre-hearing mice (Babola et al., 2018). The origin of these spontaneous waves of activity is well worked out in the wild type condition with activity coming from wave-like ATP release from transient inner supporting cells which ultimately causes type I afferent activation through depolarization of the IHCs (See section on supporting cells for more information of the role of supporting cells in development). In the Vglut3 KO mutant, even though IHC to type I synaptic activity is abrogated, type I

activation continues because of the direct action of supporting cells onto the type I afferent. There is a possibility, especially because IHCs cannot directly activate type I afferents, that this supporting cell-type I afferent relationship could persist in adult animals and cause activation of some type I afferents. Another possibility is that with a sufficiently loud stimulus like these researchers used it could cause vibrations that could be transduced by somatosensory neurons. Some somatosensory information is transmitted to the granule cell layer of the marginal zone in the cochlear nucleus. Because type II afferents tend to synapse in this area, Fos activity from somatosensory neuron synapses could be easily confused with the expected pattern from type II stimulation. These are unlikely scenarios but considering the indirectness of how they measured type II activity, they cast doubt on the findings. In the same study they also tested whether loud sounds in Vglut3 KO mice caused nocifensive behavior, e.g. avoiding the room with loud sounds. Despite presumed type II afferent activity, these mice did not change their behavior in the presence of extremely loud sounds suggesting that type II afferent activity does not convey negative or positive affective qualities and may need to be combined with type I activity to drive behavior.
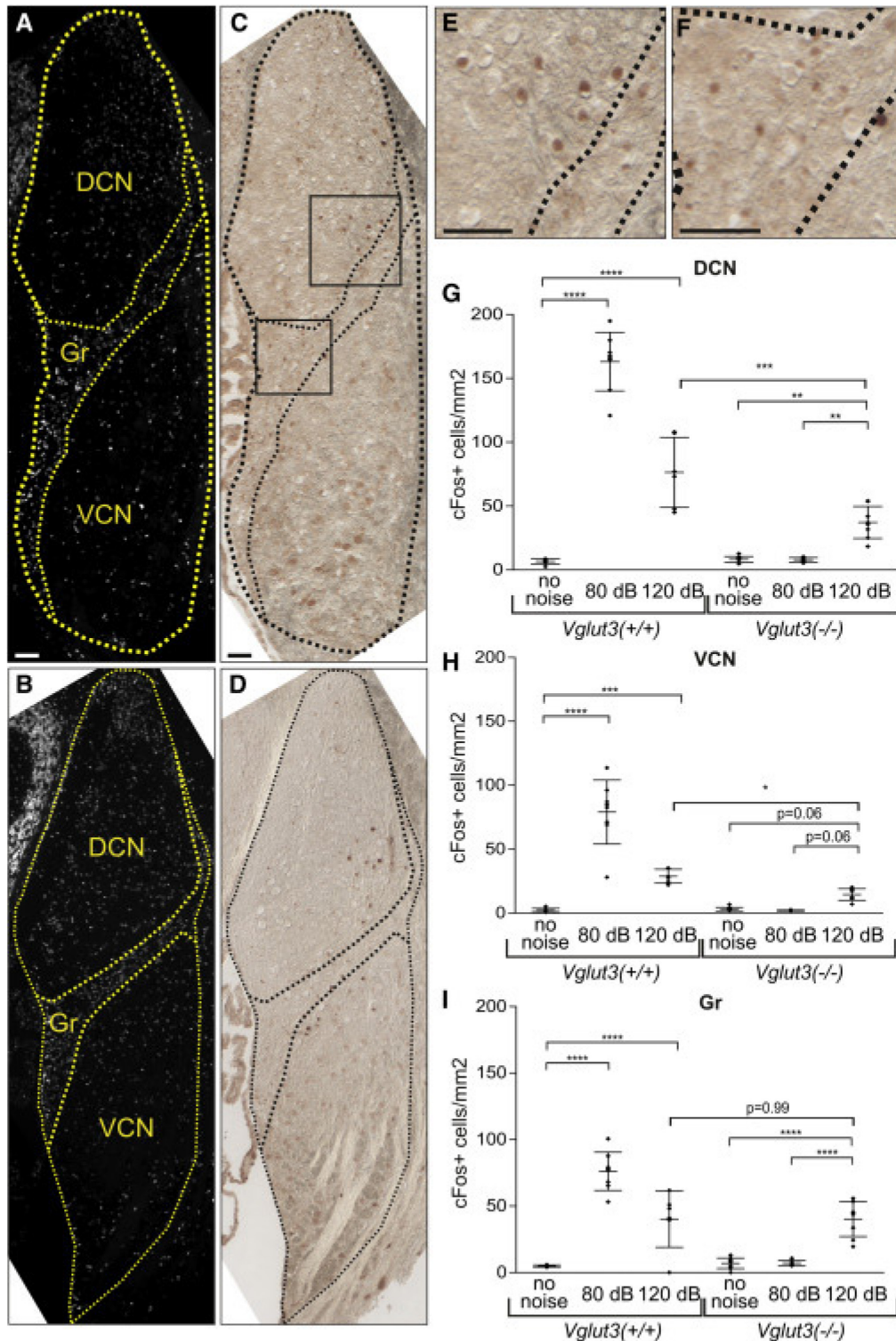
Figure B10: Tissue-Damaging Noise Activates Neurons in CN Gr Primarily through a VGLUT3-Independent Pathway (A and B) DAPI fluorescence of coronal sections of *Vglut3−/−* CN (A) and *Vglut3+/+*CN (B) exposed to 120 dB SPL reveals its three subdivisions: dorsal cochlear nucleus (DCN), ventral cochlear nucleus (VCN), and granule cell region (Gr). (C–F) c-Fos

immunoreactivity within the same coronal section reveals positive cells throughout the three CN subdivisions (C and D). The areas of (C) magnified in (E) and (F) demonstrate positive neurons within the DCN and Gr areas of *Vglut3−/−* CN. (G–I) Densities of c-Fos-expressing neurons in each CN subdivision: DCN (G), VCN (H), and Gr (I). Wild-type mice display significant increases of neuronal activity in all three subdivisions after exposure to 80 dB SPL and 120 dB SPL. *Vglut3−/−* mice display significant increases of neuronal activity following exposure to 120 dB SPL in the DCN (G) and Gr (I), whereas increases in VCN approached significance ($p = 0.06$; H). However, in the Gr, which is not innervated by type-I afferents, neuronal activity induced by noxious (120 dB SPL) noise is VGLUT3 independent (indistinguishable between wild-type and *Vglut3−/−* mice). Error bars represent the SD. Pairwise comparisons were calculated for each CN area with the type III F test (DCN, $F_{(2, 22)} = 76.95$; VCN, $F_{(2, 22)} = 40.01$; Gr, $F_{(2, 22)} = 44.85$). p values are <0.0001 (∗∗∗∗), <0.001 (∗∗∗), <0.01 (∗∗), and <0.05 (∗). Scale bars represent 50 μm. Adapted from Flores et al., 2015.

Few studies have been able to perform electrophysiological recordings from type II afferents. Two studies have recorded from neurons in the spiral ganglion and looked at the biophysical differences between type I and type II afferents after identifying the cell type with biocytin fills (Jagger and Housley, 2003; Markowitz and Kalluri, 2020). Both studies revealed that type II afferents were more likely to have small K^+ currents that inactivated rapidly. Other work performed whole-cell patch clamp recordings on the dendrites of type II cochlear afferents underneath the outer hair cells and found that they were moderately unresponsive to outer hair cell stimulation. By systematically activating OHCs with a water jet, a map of presynaptic OHCs was able to be generated for each recorded type II afferent. Activation of OHCs could cause monotonic excitatory postsynaptic potentials that could be blocked by AMPA receptor blockers (Weisz et al., 2012, Martinez-Monedero et al., 2016). Evidence of glutamatergic transmission is also bolstered by the presence of immunostaining for GluR2

34

subunit-containing AMPA receptors on type II afferents opposite OHC ribbons,

although many of the synapses (immunolabeled for postsynaptic density

proteins) are silent, i.e. they have no ribbons and no corresponding AMPA

receptors (Martinez-Monedero et al., 2016). There were no strict rules for which

OHCs were presynaptic to type IIs, but many tended to be from the same row of

OHCs and overall, there were on average 9 functionally coupled OHCs but that

could range from 1-31. This work also was able to estimate the quantum content.

Each connected OHC had about a 26% chance of releasing a single vesicle

(equivalent to a quantum content, m, of 0.34) which tended to depolarize the type

II afferent by about 4mV, about 1/7th the amount needed to reach the threshold

for firing an action potential, 26mV. Taking all these factors together suggests

that action potentials derived purely from glutamate release are rare and would

require essentially the activation of every single presynaptic OHC. Instead, type II

afferents in these studies could be activated by ATP, considering the large

currents after puffing on ATP (Weisz et al., 2009). An interesting wrinkle in the

ATP response is that in the few experiments that took place past the onset of

hearing the currents from exogenous ATP were greatly reduced and sometimes

did not occur at all. In a similar paradigm, type II cochlear afferents were reliably

activated by rupture of nearby outer hair cells and this effect was greatly

diminished by the purinergic receptor blocker, PPADS. This damage response

also was reduced in the presence of KCNQ channel openers (Liu et al., 2015)

(Figure B11). Overall, these findings suggest that type II cochlear afferents

respond directly to tissue damage through ATP signaling and can be activated by

damaging levels of sound, analogous to somatic nociceptors (Cook and

McClesky, 2002).
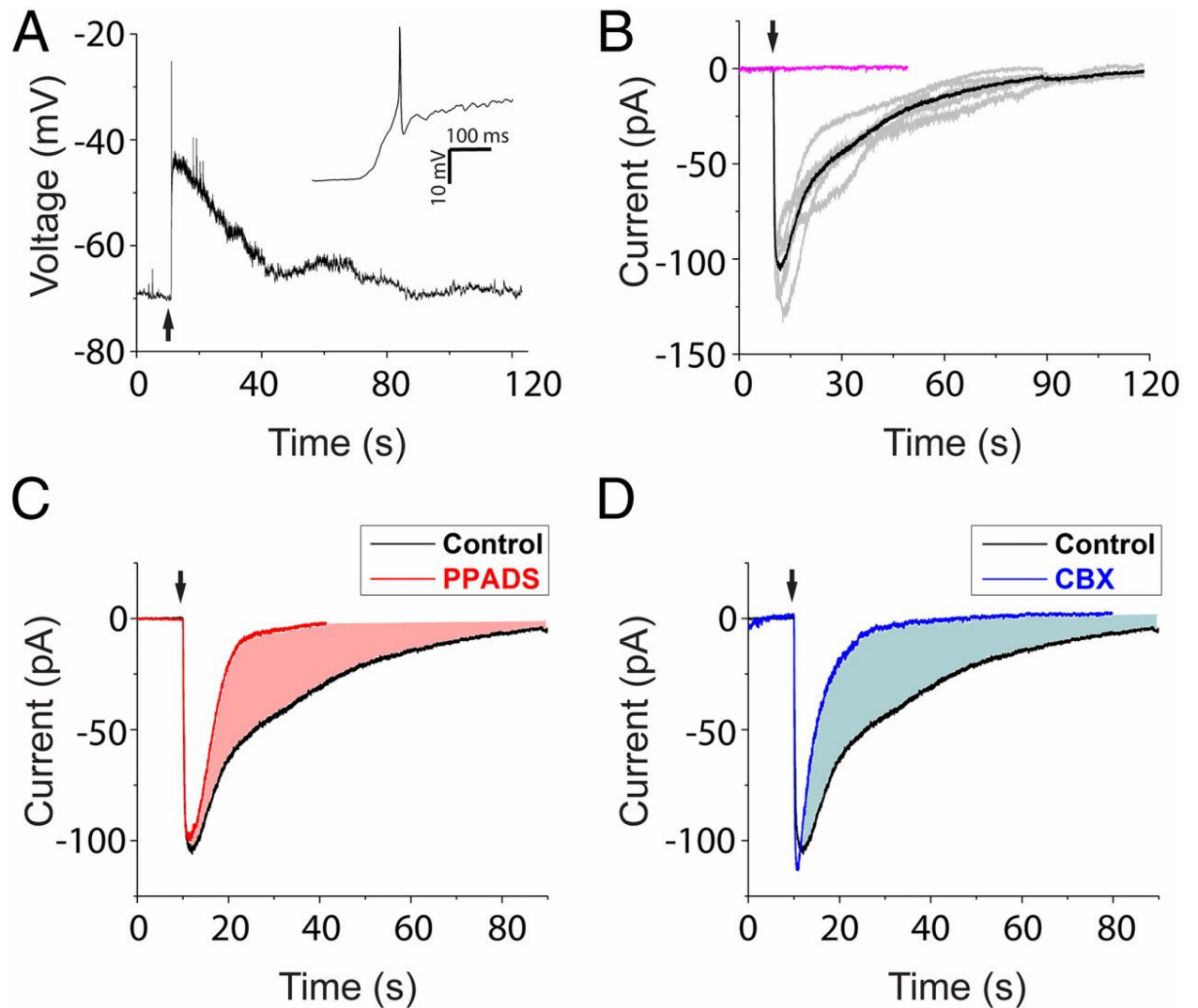
Figure B11: ATP contributes to cell damage-induced response. (A) OHC ablation depolarized type II afferents and triggered action potentials on the rising phase (Inset). (B) Representative traces of damage-induced currents (at −70 mV) from five different type II afferents (gray) and the average (black). Identical needle movement that failed to ablate OHCs induced no current (magenta). (C) Average ablation-induced current in PPADS (red, three trials in three afferents) compared with average control current from B. (D) Average ablation-induced current in CBX (blue, five trials in three afferents) compared with control average. Adapted from Liu et al., 2015.

3.3 Genetic differences

Two separate lines of inquiry have given us insight into the genetic differences between type I and type II cochlear afferents. The first line comes from three separate RNA-seq papers that examined the genetic profiles of type I and type II cochlear afferents (Petitpré et al., 2018; Shrestha et al., 2018; Sun et al., 2018). While the focus of each of the papers differs slightly, all three divide type I afferents into three subtypes based on gene clustering. These three subtypes appear to align well with the classification of type I afferents by their tonic firing rate. Electrophysiological recordings from type I afferents revealed that there is a large variability in their observed firing rates. Recordings performed on the pillar side of the IHC, i.e. closer to the tunnel of Corti, have higher spontaneous firing rates and lower acoustic thresholds. Conversely, type I afferents that synapse with IHCs on the modiolar side (closer to the spiral ganglion) typically have low spontaneous rates and high acoustic thresholds (Liberman, 1982). Interestingly, when noise exposure that causes transient ABR threshold shifts occurs, it can cause a retraction of a percentage of type I afferents, termed synaptopathy (Kujawa and Liberman, 2009). The boutons that disappear with this type of damage tend to be ones from the low spontaneous rate, high threshold, modiolar type I afferents (Furman et al., 2013). It has been hypothesized therefore that synaptopathy can impair the ability to hear clearly in noisy situations when the surviving low threshold type I afferents would be saturated. This has been called "'hidden hearing loss" because it affects the

ability to hear without showing up as an elevated auditory threshold. The genetic profiling of these subtypes allows for identification of genes that may be responsible for differences in function, and the differential survival after noise trauma. "Survival genes" are targets for potential therapeutics. While these studies zero in on type I afferent genetics they also see a cluster that is associated with type II afferents. Just as with the type I afferent subtype data, identification of genetic markers that distinguish type I from type II afferents can aid in the investigation into the function of type II afferents.

The other approach is not to cast as wide of a net but instead find potentially relevant Cre lines that could label type II but not type I afferents and cross them with reporter lines. This approach is more akin to "needle in the haystack" operation. Crossing the lines and performing immunohistochemistry can take a long time to verify if one gene is present in type II afferents but does grant more definitive answers and can be immediately useful if you cross with functional transgenic proteins such as Ai32, an excitatory channelrhodopsin with a conjugated eGFP (Madisen et al., 2012). Recent work has employed this strategy and identified four genes that are associated with type II but not type I afferents. All four of these genes are expressed in a tonotopic gradient with two, tyrosine hydroxylase (TH) and serotonin transport (SERT), expressed more strongly in the apex and the other two, calcitonin gene related peptide alpha (CGRPα) and dopamine receptor 2 (Drd2) expressed more strongly in the base (Vyas et al., 2017; Wu et al., 2018). It should also be noted that with this approach nitric oxide synthase (NOS) was seen to exclusively label type I

afferents with no expression in type II afferents (Vyas et al., 2019) (Figure B12).

The exact genes that enable these investigations could have functional

significance but so far there has been no assay of dopamine, serotonin, or CGRP

release onto or by type II afferents. Combining these two approaches by

targeting Cre lines for genes revealed by the RNA-seq datasets could be like

taking a magnet to find the needle in the haystack and is a promising way

forward to verify and then exploit the genetic differences between these two

populations of neurons.
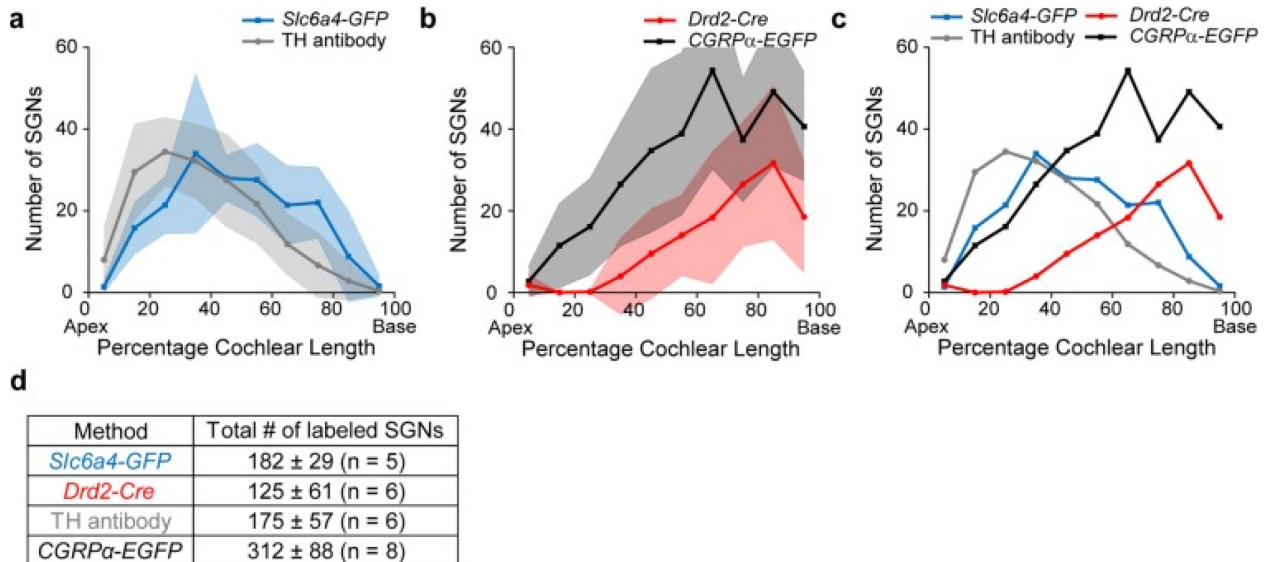
Figure B12: Comparative tonotopic distribution of molecular markers in type II afferents. (**a**) Comparative tonotopic distribution of type II neurons labeled in *Slc6a4-GFP* mice and by TH antibody immunostaining. (**b**) Comparison of the expression pattern of labeled type II neurons in *CGRPα-EGFP* and *Drd2-Cre* mice. (**c**) Average distribution of labeled type II SGNs using different methods. (**d**) Average total number of SGNs labeled by different methods. Age range of mice analyzed: TH immunostaining (P28-~P60), *Slc6a4-GFP* (~P30), *CGRPα-EGFP* (~P30), *Drd2-Cre* (~P30). All graphs show distribution patterns after hearing onset. Each cochlear turn was divided into 10 bins of equal length along the cochlear spiral and the number of labeled SGNs in each cochlear bin was recorded. Shaded areas represent standard deviations. TH immunostaining and *CGRPα-EGFP* mouse line data were reproduced from previous publication (Wu et al., 2018). Adapted from Vyas et al., 2019.

4. Somatosensory Neuron Comparison

A potentially useful comparison for approaching the heterogeneity of response types in cochlear afferents is to look at another set of neurons that are involved in mechanotransduction as well, the somatosensory neurons. Early investigation into the somatosensory neurons of the skin revealed there to be multiple subtypes of neurons that could be identified by the caliber of their axons and thus conduction velocity (Brown et al., 1967; Leem 1993; and reviewed in Abraira and Ginty, 2013 and Figure B13). The larger diameter neurons were referred to as A fibers, which had further subdivisions such as Aβ which conveyed information about touch, and the unmyelinated, small caliber neurons were referred to as C fibers. C fibers that respond to noxious stimuli tend to have free endings extending into the skin and convey information about pain or itch and thus are referred to as nociceptors and pruriceptors, respectively. These C fibers can detect signals that are associated with the lysis of cells such as ATP and protons (Cook and McCleskey, 2002) or are activated by pruritogens such as histamine (Alving et al., 1991) and chloroquine (Liu et al., 2009). A more modern approach of classifying the somatosensory neurons is to take a genetic approach. RNA-seq clustering analysis has revealed a myriad of somatosensory neurons that correspond to different modalities of somatosensation (Hu et al., 2016; Ray et al., 2018). A defining protein family of the nociceptors is the transient receptor

potential family of ion channels (TRP) (Caterina et al., 1997; Caterina and Julius, 2001; Samanta et al., 2018), while many non-histaminergic pruriceptors express another family of G protein coupled receptors, the mast-related G protein receptors (MRGPRs) (Guan et al., 2010). A subset of nociceptive neurons is defined by the expression of genes encoding neuropeptides such as *Calca* (Noguchi et al., 1990; Kestell et al., 2015; Patil et al., 2018) and *Tac1* (Duggan et al., 1988; Kestell et al., 2015).
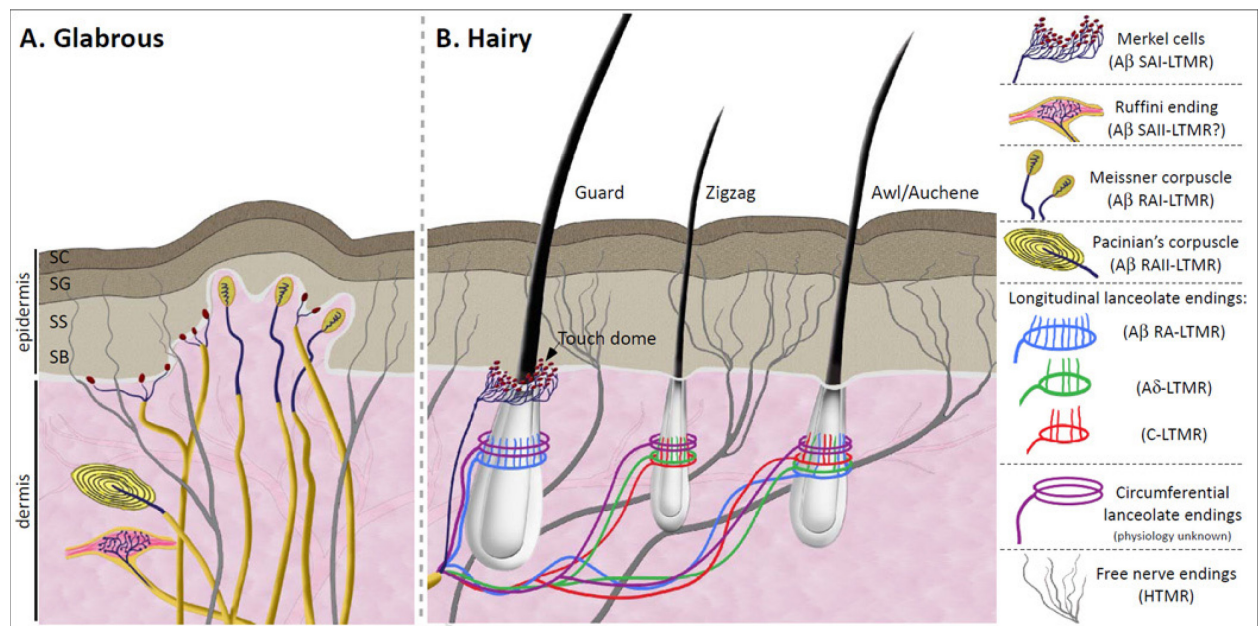
Figure B13: The organization of cutaneous mechanoreceptors in skin. Innocuous touch information is processed by both glabrous (hairless, **A**) and hairy skin (**B**). **A**) In glabrous skin, innocuous touch is mediated by four types of mechanoreceptors. The Merkel cell-neurite complex is in the basal layer of the epidermis and it consists of clusters of Merkel cells making synapse-like associations with enlarged nerve terminals branching from a single Aβ fiber. This complex and its associated SAI-LTMR responses help us in reconstructing acute spatial images of tactile stimuli. Meissner corpuscles are localized in the dermal papillae and consist of horizontal lamellar cells embedded in connective tissue. Their characteristic RAI-LTMR responses detect movement across the skin. Ruffini endings are localized deep in the dermis and are morphologically similar to the Golgi tendon organ, a large and thin spindle-shaped cylinder composed of layers of perineural tissue. Historically, Ruffini endings have been associated with SAII-LTMR responses, which respond best to skin stretch, though such

correlations remain highly controversial. Lastly, Pacinian corpuscles are located in the dermis of glabrous skin where its characteristic onion-shaped lamellar cells encapsulate a single Aβ ending. Their well-recognized RAII-LTMR responses detect high frequency vibration. **B**) In hairy skin, tactile stimuli are transduced through three types of hair follicles, defined in the mouse as guard, awl/auchenne, and zigzag. The longest hair type, guard hairs, are associated with touch domes at the apex and Aβ-LTMR longitudinal lanceolate endings at the base. Awl/auchene hairs are triply innervated by C-LTMRs, Aδ-LTMRs, and Aβ-LTMRs longitudinal lanceolate endings. Zigzag hair follicles are the shortest and are innervated by both C- and Aδ-LTMRs longitudinal lanceolate endings. In addition, all three hair follicle types are innervated by circumferential lanceolate endings whose physiological properties remain unknown. Noxious touch is detected by free nerve endings found in the epidermis of both glabrous and hairy skin and are characterized by both Aδ- and C-HTMR responses. Abbreviations: SA, slowly adapting; RA, rapidly adapting; LTMR, low-threshold mechanoreceptor; HTMR, high-threshold mechanoreceptor; SC, stratum corneum; SG, stratum granulosum; SS, stratum spinosum; SB, stratum basalis. Adapted from Abraira and Ginty, 2013.

Neurons of the cochlea have also followed a pattern of identification by morphology (Spoendlin, 1969; Spoendlin, 1971), electrophysiology (Liberman, 1982; Liberman and Oliver, 1984; Robertson, 1984; Berglund and Brown, 1994; Robertson et al., 1999) ,and more recently genetic analysis (Petitpré et al., 2018; Shrestha et al., 2018; Sun et al., 2018). While cochlear afferent neurons have been able to be classified along these lines, type II afferents have eluded careful examination of their biological function. Unlike somatosensory neurons where neurons can be recorded and assayed easily in a living animal, cochlear afferents are housed in one of the toughest bones of the body. Instead, *in vivo* electrophysiology requires sharp electrode recordings directly from the eighth nerve (Galmbos and Davis, 1943). However, the thin diameter and sparse nature of the type II afferents has made even those recordings exceedingly rare (Berglund and Brown, 1994; Robertson et al., 1999). From all the recordings from the eighth nerve, only a handful have been determined to be putative type II

afferents and from there only one has any recorded response to a sound stimulus. The likeliest conclusions that can be taken from this paucity of responses is that type II afferents are either completely unresponsive to sound stimuli or that they require excessively loud sounds (Flores et al., 2015). An emerging hypothesis about the function of type II afferents is that they act like nociceptors for the auditory system. Like somatic C fibers, type II afferents are also small, unmyelinated fibers that have widely branching dendritic projections (Spoendlin, 1969; Spoendlin, 1971; Perkins and Morest, 1975).

Electrophysiology from the type II afferents has been similarly intractable but has revealed that in the young rat cochlea these neurons can respond to glutamate released from OHCs, but even more so to ATP released from damaged tissue (Weisz et al., 2009; Liu et al., 2015). Research following up these findings showed that type II afferents strongly respond to focal ablation of OHCs, supporting the auditory nociceptor hypothesis (Liu et al., 2015). Genetic investigations to divide up cochlear afferents into subtypes also show expression of certain genes commonly seen in somatosensory neurons, including C fiber associated genes, in type II afferents. These include tyrosine hydroxylase (*Th)* (Brumovsky et al., 2006; Brumovsky et al., 2016; Li et al., 2011; Vyas et al., 2017; Wu et al., 2018) and calcitonin related polypeptide alpha (*Calca)* (Rice et al., 1997, Kestell et al., 2015; Wu et al., 2018).

Modeling type II afferent function after nociceptors also may provide insights for how to think about and combat conditions that lead to persistent painful percepts, such as hyperacusis. Hyperacusis is a condition where

43

presentations of innocuous sounds are now deemed painful but also encompass other distortions of auditory processing (Tyler et al., 2014; Pienkowski et al., 2014). A similar condition in the somatosensory system is allodynia where the threshold for classifying a stimulus as painful is lowered, typically after injury (Jensen and Finnerup, 2014). Sensitization after injury can occur at multiple levels. Shortly after damage, the combination of signals from damaged tissue, such as ATP and protons (Cook and McCleskey 2002; Ren et al., 2006), cytokines and other releasable factors from invading immune cells (Kim and Moalem-Taylor, 2011), and neuropeptides (Li et al., 2018) can cause the peripheral afferent nociceptors to become hyperexcitable such that even quiescent, high threshold nociceptors begin to respond to moderate tactile stimulation (Andrew and Greenspan, 1999; Smith et al., 2013; Murthy et al., 2018). Altered peripheral afferent firing can also cause sensitization of central circuits (Mendell and Wall, 1965) through a myriad of mechanisms (Vikman et al., 2008; Soliman et al., 2005; Afrah et al., 2002; Kawasaki et al., 2004; Blum et al., 2014; Matsui et al., 2010; Clark and Malcangio et al., 2014). Understanding mechanisms and finding viable treatments for allodynia may also prove informative about how to combat hyperacusis.

5. Changes in the Cochlea After Hearing Onset

5.1 Changes in the cochlea with maturity

Mice and many other rodent species are altricial, meaning that at birth they do not possess the ability to see or hear. For mice around 12 days after birth, pups begin to open their eyes and the plug of mesenchymal tissue is cleared from the middle ear (Richter et al., 2010) allowing the cochlea to be driven by sound (Figure B14). Though the sensory epithelium is not driven by external stimuli in this developmental epoch, the tissue is quite active (Beutner and Moser, 2001; Tritsch et al., 2007). As discussed in the previous section, waves of spontaneous activity course through the supporting cells of the cochlea (a similar phenomenon occurs in the retina (see Stellwagen and Schatz, 2002)). In short, activity in the supporting cells can drive action potentials in the spiral ganglion neurons and may be important for establishing appropriate synaptic connections in the downstream cochlear nucleus (Zhang and Poo, 2001; Clause et al., 2014). Spontaneous activity persists even if glutamatergic transmission from IHCs is absent (Babola et al., 2018) but terminates around the time hearing comes online and with the loss of the transient supporting cells in Kölliker's organ.
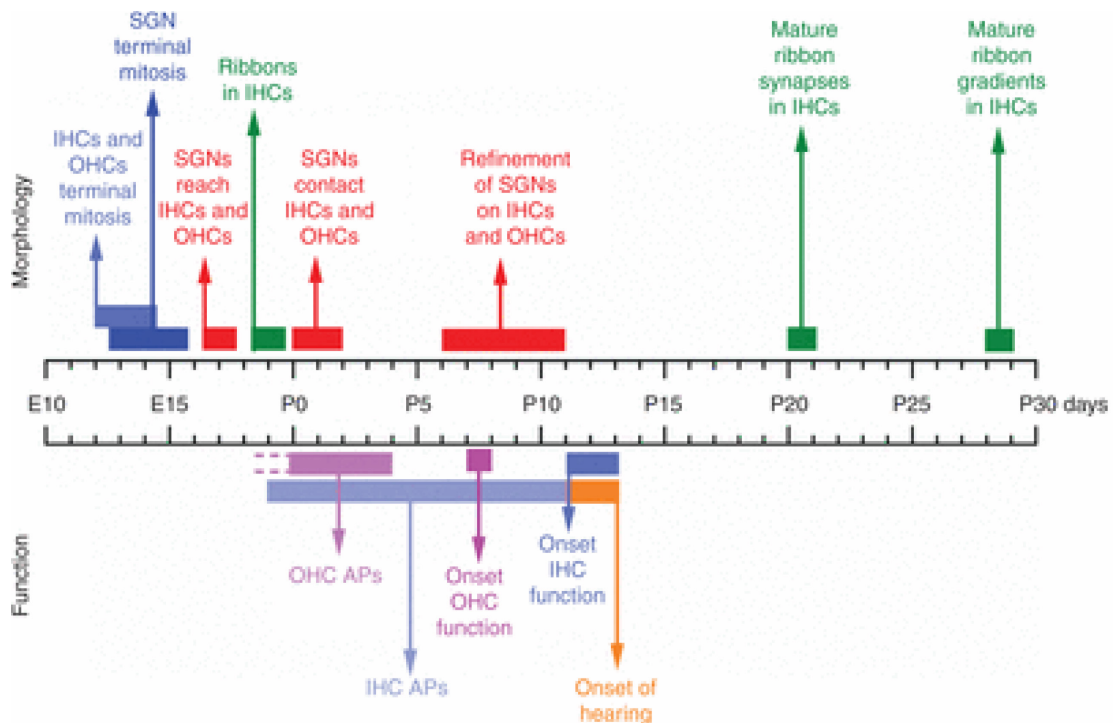
Figure B14: Maturation of the mouse cochlea. Diagram showing the morphological and functional maturation of spiral ganglion neurons (SGNs) and hair cells in the mouse cochlea. Adapted from Johnson et al., 2019.

Another transient phenomenon in the pre-hearing cochlea is the transient synapsing of medial olivocochlear efferent neurons (MOCs) onto IHCs (Glowatzki and Fuchs, 2000). MOCs in the adult typically only synapse onto the OHCs (Katz et al., 2004). These neurons are principally cholinergic and release acetylcholine (ACh) that binds and activates a special nicotinic ACh receptor (Elgoyhen et al., 1994). These nAChRs contain α9/α10 subunits which have strange properties including the sensitivity to strychnine but are not activated by nicotine (Erostegui et al., 1994) as would be expected for most nAChRs. And while ACh causes a non-specific influx of cations, the overall effect of ACh is inhibitory hyperpolarization of the hair cell (Evans, 1996). This occurs because there are

46

Ca^{2+} gated K$^+$ channels (SK2 or BK) that associate with the α9/α10 subunit containing nAChRs and cause a two part current flow, a small inward current that is followed by a much larger outward current at the cell's resting potential (Oliver et al., 2000; Wersinger et al., 2010). These MOC-hair cell synapses also typically present with a subsynaptic structure called a cistern that runs parallel to the hair cell's cell membrane (Lioudyno et al., 2004; Fuchs et al., 2014; Zachary and Fuchs, 2015). The cistern is thought to contain the Ca^{2+} signal as well as possibly acting as a Ca^{2+} reservoir to facilitate the association of Ca^{2+} entering from the nAChR with the Ca^{2+} gated ion channel (Zachary et al., 2018). The subsynaptic cistern appears when MOCs synapse onto IHCs and disappears once the synapses retract. It is not clear what developmental function the transient MOC-IHC synapses serve. It is possible that the inhibitory action of ACh may shape the discharge from IHCs to create a more naturalistic bursting input for the type I afferents (Marcotti et al., 2004; Johnson et al., 2011). There is also some evidence that disrupting efferent to IHC transmission affects the development of inner hair cell vesicle release Ca^{2+} sensitivity (Johnson et al., 2007; Johnson et al., 2013a; Johnson et al., 2013b) and the formation of neuronal connections in the auditory brainstem (Clause et al., 2014; Di Guilmi et al., 2019). Around the onset of hearing, at the earliest P6, MOCs establish the appropriate synapses onto OHCs (Roux et al., 2011) (Figure B15). Shortly after this time the other set of cochlear efferent neurons, the lateral olivocochlear neurons (LOCs), form axodendritic synapses onto the type I afferent boutons (Guinan et al., 1983; Simmons, 2002; Fuchs and Lauer 2019). The function of LOCs is much more

47

obscure than the MOCs. Though, it is presumed that the LOCs are involved in

directly altering the firing patterns of their synaptic partners, the type I afferents.
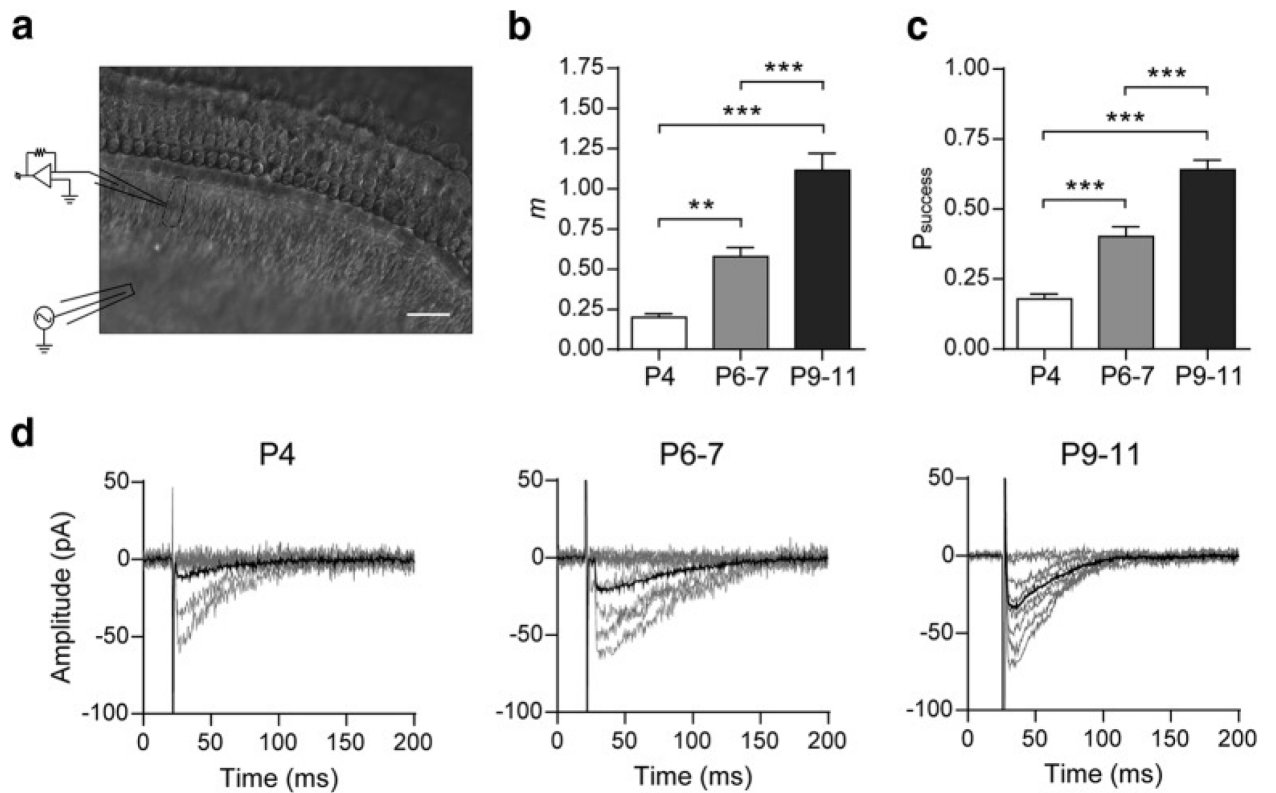
Figure B15: Synaptic strength at the mouse MOC–IHC synapse increases during postnatal development. *a*, Micrograph of the mouse cochlear preparation used in the present study. IHCs were recorded with a patch pipette at a holding potential of −90 mV and MOC fibers were electrically stimulated using a monopolar electrode placed ~80 μm modiolar to the base of the IHCs. Scale bar, 20 μm. *b*, Bar graph showing the progressive increase in *m* from P4 to P9–P11. *c*, Bar graph illustrating the increase in *P*success during the same period shown in *b*. *d*, Representative individual (gray) and average (black) traces of eIPSCs recorded at P4, P6–P7, and P9–P11 IHCs. Average eIPSC amplitudes include failures of release. Data from P9–P11 are shown for comparison and were taken from Zorrilla de San Martín et al. (2010). Error bars indicate SEM. **$p < 0.01$, ***$p < 0.001$. Adapted from Kearney et al., 2019.

Besides the refining of synaptic connections within and outside of the

cochlea the onset of hearing is also a watershed moment in maturation of ion

channel physiology. Hair cells in the first week of life in rodents can support mostly Ca^{2+}-dependent action potentials (Beutner and Moser, 2001; Jeng et al., 2020). Potassium currents increase over this time to mature levels hyperpolarizing the resting membrane potential, preventing action potentials and instead causing graded responses to depolarization (Kros et al., 1998; Marcotti et al., 1999; Marcotti and Kros, 2003) (overview in Figure B16). In the OHCs potassium currents increase in the first week after birth with near mature levels of KCNQ4 expression about the same time that Prestin is strongly being expressed (He et al., 1994; Oliver and Fakler, 1999; Marcotti and Kros, 1999). Prestin expression is dependent on the transcription factor Helios. Expression of Helios in IHCs can even drive them to develop functional Prestin-dependent electromotility (Chessum et al., 2018). In the first week of life calcium currents increase but then after P6 decrease to mature levels while becoming more efficient in driving vesicle release (Beutner and Moser, 2001; Johnson et al., 2005). Around this time CaV1.3 is organized and clustered around the presynaptic ribbons. By increasing the density of Ca^{2+} channels around the ribbons, "nanodomains" or "microdomains" (Graydon et al., 2011; Johnson et al., 2017b), can form increasing the Ca^{2+} concentrations sensed by otoferlin such that vesicles can be released even with only a relatively small Ca^{2+} influx. Many of these developmental properties are sensory input-independent but still activity-dependent, needing the pre-hearing spontaneous activity to become fully mature hair cells. Mutations in genes that affect this spontaneous activity such as, Eps8 (Tavazzani et al., 2016), α9 nAChR subunit, (Johnson et al., 2013a), SK2

(Johnson et al., 2007), CaV1.3 (Brandt et al., 2003), Gata3 (Bardhan et al., 2019), TMC1 (Corns et al., 2018), and connexin 26/30 (Johnson et al., 2017a) can cause defects in the linearization of the Ca^{2+} sensitivity of vesicle release, retention of efferent connections, and/or the expression of mature hair cell ion currents.

Maturation of the cochlear afferents also appears to depend on the activity levels of the presynaptic hair cells. As mentioned in other sections, type I cochlear afferents can be subdivided into three subtypes depending on their genetic sequences and appear to correlate with their physiological properties, e.g. spontaneous firing rate (Petitpre et al., 2018; Sun et al., 2018; Shrestha et al., 2018). Sun et al. observed that these genetic differences are not established at birth but become evident over the first few weeks of life. The distribution of subtypes was disrupted in VGlut3 KO mice where glutamatergic transmission from IHCs is prevented suggesting that hair cells may instruct the fate of the postsynaptic type I afferents. It appears that the high spontaneous rate fibers develop later (Wu et al., 2016) with synaptic pruning occurring earlier among the modiolar, low-spontaneous rate fibers (Markowitz and Kalluri, 2020).

The relationship is not unidirectional, i.e. type I afferents can also influence presynaptic properties of the inner hair cells. After conditionally knocking out the transcription factor Pou4f1, which is expressed in one subtype of type I afferents, there was a change in how Ca^{2+} enters the cell and the sensitivity of the ribbon synapses (Sherrill et al., 2019).

While there is less evidence, it does seem that early activity may be important for type II development as well. Knocking out Connexin 30 causes aberrant morphology of the type II neurites under the OHCs, possibly causing changes in the synaptic inputs onto the type II afferent (Ceriani et al., 2019) (Figure B17).
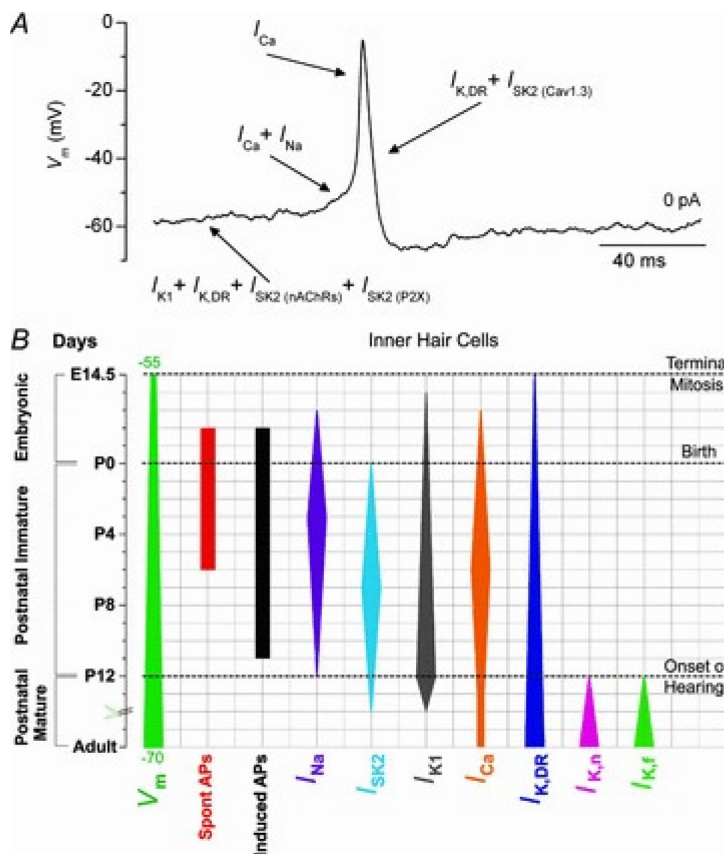
Figure B16: Role of various membrane currents in shaping IHC action potentials. *A*, an action potential recorded from a spontaneously active postnatal day 3 IHC. The different phases of an action potential are primarily determined by different basolateral currents expressed in immature IHCs (indicated by arrows). The IHC resting membrane potential is mainly set by the interplay of the following three currents: a classical delayed rectifier K+ current (IK,DR; Marcotti *et al.* 2003*a*); an inward rectifier K+ current (IK1; Marcotti *et al.* 1999); and a small-conductance Ca2+-activated K+ current (ISK2) gated by Ca2+ influx through α9α10 nicotinic

acetylcholine receptors (ISK2(nAChRs); Marcotti *et al.* 2003*a*; Johnson *et al.* 2007) or purinergic receptors (ISK2(PX2); Johnson *et al.* 2011*b*). While the Ca2+ current carried by CaV1.3 Ca2+ channels is essential for the generation of action potentials (ICa; Marcotti *et al.* 2003*b*; Johnson *et al.* 2011*b*), the Na+ current is required for speeding up the time to spike threshold (INa; Marcotti *et al.* 2003*b*). Finally, IHC repolarization after an upstroke is determined by both IK,DR and the SK2 current, which (different from that described above) is activated by Ca2+ flowing through closely colocalized CaV1.3 Ca2+ channels (ISK2(Cav1.3); Marcotti *et al.* 2004*b*; Johnson *et al.* 2007). *B*, developmental changes in the expression of some IHC biophysical properties (mainly from mice). The width of the vertical bars provides an indication of the developmental change in the size of the currents or membrane potential (*V*m) in apical IHCs. The day of birth (P0) corresponds to embryonic day 19.5 (E19.5). Adapted from Marcotti, 2012.
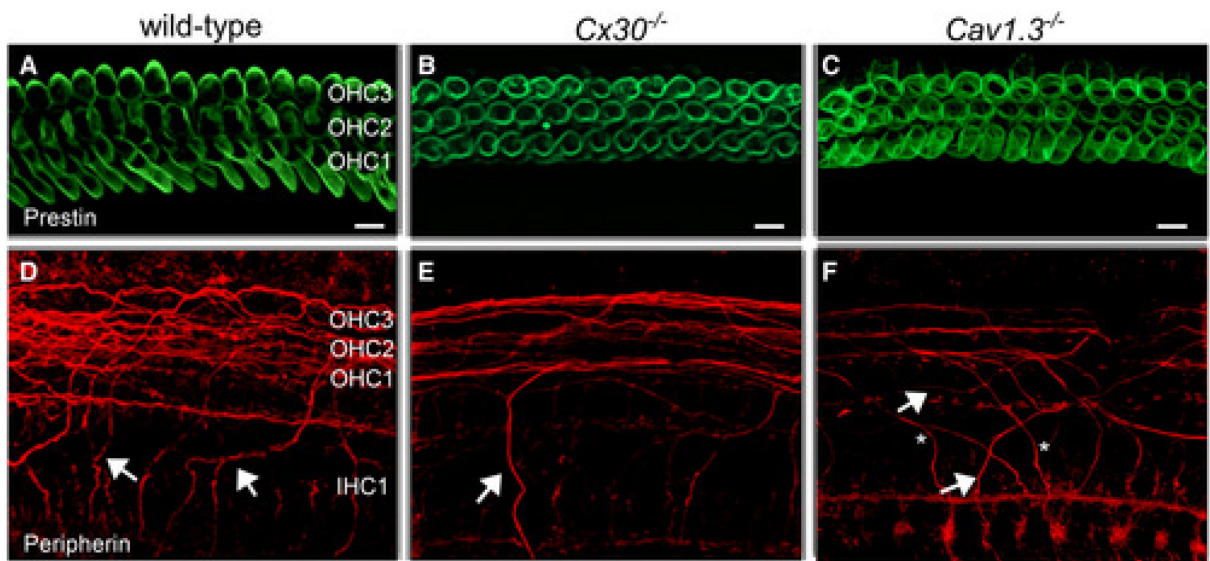
Figure B17: Genetic knockouts disrupt type II afferent arborization. Maximum intensity projections of confocal *z*-stacks taken from the apical cochlear region of wild-type (left column), *Cx30−/−* (right column) and *Cav1.3−/−* mice at P11 using antibodies against prestin (green) and peripherin (red). Each panel represents a different mouse.A–C.Prestin labelling was similar between the different mouse strains and as such was used as an OHC marker. Scale bars 10 µm.D–F.Immunostaining for peripherin (red) highlights outer spiral fibres (arrows) of type II spiral ganglion neurons in the wild-type mouse cochlea (D). These outer spiral fibres cross below IHCs and spiral below OHCs towards the cochlear base. In *Cx30−/−* (E) and *Cav1.3−/−* (F) mice, there are fewer peripherin-labelled outer spiral fibres than in wild-type. In *CaV1.3−/−* mice (F), the outer spiral fibres travel towards the cochlear base (arrows), as in the wild-type (D), but some also spiral apically (asterisks). Adapted from Ceriani et al., 2019.

5.2 Mechanisms employed to reduce damage in the cochlea

Once the cochlear epithelium matures, changes can still occur with senescence (Wu et al., 2019; Liberman and Liberman, 2019), genetic maladies (Mathur and Yang, 2015), and exposure to environmental insults such as ototoxic drug exposure (Schacht et al., 2012) or loud sound stimulation (Ohlemiller 2008; Liberman 2017). Insults to hair cells and spiral ganglion neurons are especially deleterious in mammals because they do not regenerate, whereas avian and reptilian hair cells do (Burns et al., 2013; Burns and Corwin 2013). To protect these cell types there are a few mechanisms that can be employed by the system. The middle ear reflex is triggered by loud sounds (Chertoff et al., 2018) and stifles the amount of vibration on the tympanic membrane and thus dampens the amount of hair cell stimulation as well (Marks and Siegel, 2017). The reflex is most likely directly triggered from activity of the type I afferents and not the type II afferents (Valero et al., 2016).

Type I afferent activity is also the likely input onto MOC efferents which project back to the cochlea to hamstring the amplifying effects of the OHCs. This is due to the sensitivity, tuning, and speed of the efferent responses to sound (Robertson and Gummer, 1985; Liberman and Brown, 1986; Maison et al., 2016). Some have also argued that type II afferents may be involved in activating MOC efferents but these two studies may just reflect compensatory actions when type I afferents are impacted in some way (Froud et al., 2015 and Li et al., 2018). As discussed previously ACh from MOC efferents hyperpolarizes OHCs through a two-channel mechanism. The hyperpolarization therefore reduces the electromotility effect of Prestin in the cell membrane, causing less shearing force

on the stereocilia of the IHCs. Alterations to the nicotinic ACh receptors necessary for the inhibition that cause increased cation influx instills resistance to noise- and age-related decreases in hearing (Boero et al., 2018; Boero et al., 2020) whereas the AChRα9 knockout increased the risk for noise-related hearing deficits (May et al., 2011).

It is less well determined if lateral olivocochlear (LOC) efferents can have similar protective effects but based on their synaptic connections onto the type I afferents are well poised to serve that function. LOCs can contain a wide array of putative neurotransmitters, such as acetylcholine, dopamine, and GABA (Fex and Altschuler, 1986), that could have modulatory effects on IHCs or type I afferents but the effects of these molecules have been less conclusive than the effect of ACh on OHCs. Perfusion of dopamine *in vivo* has been shown to decrease the firing rate of auditory nerve fibers (d'Aldin et al., 1995; Oestreicher et al., 1997; Ruel et al., 2001; Ruel et al., 2006). Additionally, mice with dopamine receptor knockouts are more susceptible to noise trauma than wild-type mice (Maison et al., 2012). A recent report observed that LOC efferents can shift to expressing tyrosine hydroxylase (TH), the rate limiting enzyme to produce dopamine, after long bouts of mildly loud sounds. The potential inhibitory effect of dopamine on type I afferent firing may mean that the upregulation of TH in LOCs may be a protective mechanism to tamp down type I activity in the face of persistent noise (Wu et al., 2020).

Other molecules that could be released during damaging levels of sound have also been investigated to see if they prevent cellular damage and auditory

threshold shifts. For example, ATP is reported to increase in concentration in the endolymph following noise exposure (Muñoz et al., 1995) and can affect cochlear microphonics and decrease the endocochlear potential by increasing the ability of supporting cells to shunt away K^+ (Bobbin and Salt, 2005, Housley et al., 2013). Mice with the P2X2 receptor knocked out also seem to be more susceptible to noise exposure (Yan et al., 2013).

The final preventative measure the cochlea can employ is to shut down mechanotransduction through disrupting tip link connections. As discussed previously, tip links are the linkers between the stereocilia and are vital for mechanotransduction by the MET channels. After traumatic levels of acoustic stimulation (Pickles 1987), tip links can break, but the breakage is reversible and can reform within 24 hours, causing the return of MET currents (Jia et al., 2009). In one review on hair cell damage and repair mechanisms, the authors propose that tip links may act as a "circuit breaker" to prevent excessive transmission from hair cells in the event of loud, persistent noise (Wagner and Shin, 2019).

5.3 Damage and repair mechanisms in the cochlea

If these mechanisms fail, events such as extremely loud sounds can cause irreparable damage to the auditory sensory cells. After a loud stimulus event OHCs and type I afferents are more likely to die than IHCs and type II afferents. OHCs seem particularly susceptible to cell death, especially the high

frequency OHCs of the cochlear base (Fettiplace and Nam, 2019). Both excessive noise and exposure to aminoglycosides can lead to hair cell death. Noise exposure causes mostly apoptosis early after the insult but later both apoptosis and necrosis can occur (Yang et al., 2004). Apoptosis of hair cells from mechanical damage or aminoglycosides activate the ERK1/2 in nearby supporting cells in a Ca^{2+} and ATP dependent process. Elimination of the ATP dependent Ca^{2+} waves through connexin blockers can block the ERK1/2 activity and prevent cell death (Lahne and Gale, 2008). Antibiotic-induced hair cell death also tends to prefer apoptotic mechanisms but can also cause necrosis (Jiang et al., 2006) One possible explanation is that with their smaller volume the OHCs (Dannhof et al., 1991) are less effective at sequestering Ca^{2+} which can lead to apoptotic pathway initiation. Compounding this, basal OHCs have larger MET currents (Johnson et al., 2011) allowing more Ca^{2+} to enter with similar stimulations (Beurg et al., 2006). Even though basal OHCs have the highest concentration of proteinaceous calcium buffers (Hackney et al., 2005), they have the fewest Ca^{2+} pumps, PMCA2. PMCA2 is located in OHC stereocilia (Dumont et al., 2001; Chen et al., 2012) but as basal OHCs have much shorter stereocilia as compared to apical OHCs (Roth and Burns, 1992) there are fewer pumps to extrude excess Ca^{2+}. PMCA mutations can cause outright deafness (Ficarella et al., 2007; Street et al., 1998) or a progressive high-frequency to low-frequency deafness based on the severity of effect on PMCA2 pumping ability (Spiden et al., 2008; Bortolozzi et al 2010). Overall, this increased susceptibility appears to cause progressive OHC death in the base of the cochlea causing age-related

loss of high frequency hearing (Wu et al., 2019). Basal OHCs also are more

susceptible to aminoglycoside toxicity (Ryan et al., 1980) as well as noise

exposure (Liberman and Kiang, 1978).

With sufficient sound stimulation, type I afferent boutons can swell and die

from glutamatergic excitotoxicity (Puel et al., 1998). The retraction of these

synapses can happen over the next few days. Synaptopathy and the resultant

phenomenon of hidden hearing loss were discussed previously (Kujawa and

Liberman, 2009) (Figure B18). If the damage is massive, the type I afferents can

degenerate over the course of about 4 weeks (Kaur et al., 2015). Ribbon

synapses can also degenerate over the course of aging. One study found that

the size of the remaining ribbons however, in mice with age-related hearing loss

might compensate for that loss by increasing in volume, though that is if larger

ribbons have an appreciable compensatory effect (Jeng et al., 2020).
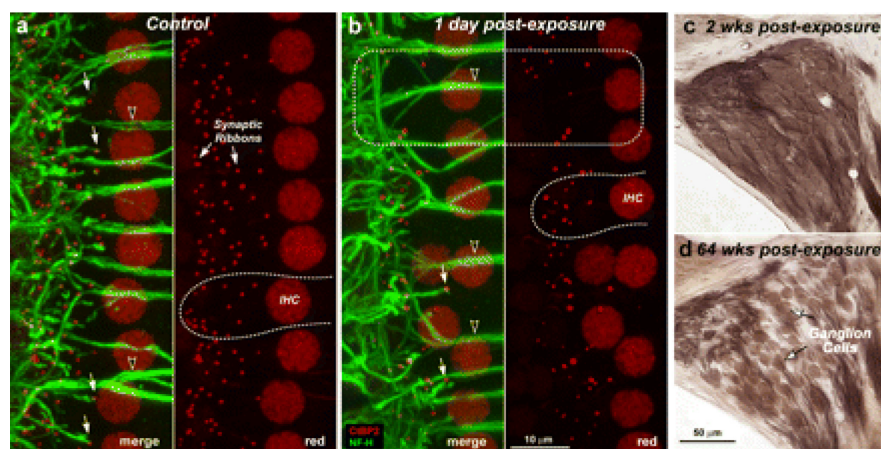
Figure B18: Despite reversibility of threshold shift and intact sensory cells, noise-exposed ears show rapid loss of cochlear synaptic terminals (*a* , *b*) and delayed loss of cochlear ganglion cells (*c* , *d*). Immunostaining reveals synaptic ribbons

(red, anti-CtBP2) and cochlear nerve dendrites (green, anti-neurofilament) in the IHC area of a control (*a*) and an exposed (*b*) ear at 1 d post noise. Outlines of selected IHCs are indicated (*a* , *b* : dashed lines); the position of IHC nuclei is more irregular in the traumatized ears. Each confocal image (*a* , *b*) is the maximum projection of a z-series spanning the IHC synaptic region in the 32 kHz region: the viewing angle is from the epithelial surface (see **Fig. 1**). Each image pair (red/merge) shows the same confocal projection without, or with, the green channel, respectively. Merged images show juxtaposed presynaptic ribbons and postsynaptic terminals, in both control and exposed ears (*a* , *b* : filled arrows), and the lack of both in denervated regions (*b* : dashed box). Anti-CtBP2 also stains IHC nuclei; anti-neurofilament also stains efferent axons to OHCs (*a* , *b* : unfilled arrowheads). Cochlear sections show normal density of ganglion cells 2 weeks postexposure (*c*) compared with diffuse loss after 64 weeks (*d*): both images are from the 32 kHz region of the cochlea. Adapted from Kujawa and Liberman, 2009.

Regardless of age or level of sound stimulation, the type II afferents are resilient. The number of type II afferents does not change significantly with age or noise exposure (Ryan et al., 1980; Wu et al., 2019). They seem to persist after transection, which is how they were first discovered (Spoendlin, 1971; Spoendlin 1973). One major difference between the two types of spiral ganglion neurons that may contribute to their differential survival is the expression of Na$^+$K$^+$-ATPases in the type I afferents. Prolonged bouts of cation influx can interrupt normal ionic homeostasis through depleting ATP needed for pumping ions against their electrochemical gradients. Ouabain, which is a toxin that acts on Na$^+$K$^+$-ATPase, kills nearly every type I neurons but leaves type II afferents untouched (Schmiedt et al., 2002; Lang et al., 2005). After type I afferent synapses retract from the IHCs it is possible that efferents can populate the empty space where the type I synapses used to be. Evidence of this in years old C57Bl6j mice was observed by electron microscopy (Lauer et al., 2012) as well as electrophysiologically (Zachary and Fuchs, 2015). In some recordings from

these senescent mouse IHCs, efferent synaptic responses and inward currents after puffing on ACh were observed. Even if this is not some freak anomaly, it is unclear whether this also could occur after noise-induced synapse retraction. It is possible that post-damage efferents on IHCs would protect from further damage but at the cost of increasing the threshold for sound detection. The return of the efferent innervation may reflect reduced activity due to faulty mechanotransduction as mutants lacking MET current also have efferent reinnervation (Corns et al., 2018).

Once tissue in the cochlea is damaged there are a few pathways to help mitigate and remove the damage. Supporting cells of the cochlea have been shown to extrude damaged hair cells from the organ of Corti and engulf the debris (Forge, 1985; Raphael and Altschuler, 1991; Anttonen et al., 2014; Monzack et al., 2015; Hirose et al., 2017). Immune cells are also known to be attracted to ATP released from damaged tissue to clear debris (Chen et al., 2006; Elliott et al., 2009; Hirose et al., 2017; Oishi and Manabe, 2018). Macrophages can be seen in greater numbers in the vicinity of the organ of Corti after loud sounds (Fredelius and Rask-Andersen, 1990; Hirose et al., 2005). Cytokines, such as IL-1β, IL-6, and TNF-α; and chemokines, such as CCL2, that can cause immune cell infiltration (Taub et al., 1995; Proost et al., 1996) and movement of the resident macrophages to the site of damage are expressed over two weeks, peaking at 6 hours and 7 days following noise exposure (Fujioka et al., 2006; Tan et al., 2016; Frye et al., 2017; Frye et al., 2019). A knockout of the chemokine fractalkine during hair cell ablation prevented macrophages from

invading the cochlea and is associated with more spiral ganglion neuron death (Kaur et al., 2015). In the same animals, lost ribbon synapses did not recover and more IHCs and cochlear afferents died after noise exposure (Kaur et al., 2018). Overall, it appears that macrophages facilitate synaptic repair and cochlear cell survival after damage occurs.

6. Approach and Goal of the Thesis

The study of type II afferents has been problematic for many reasons over the years. Anatomically, besides the defining peripheral arbors and hair cell synapses, the somata of type II and type I neurons are not distinct enough to differentiate easily. The caliber of their fibers and their overall scarcity has also made blind approaches yield few results. When those studies did on occasion stumble across a type II afferent, they did not respond strongly to any tested stimulus (Berglund and Brown, 1994; Robertson et al., 1999). Overall, focused investigation on type II afferents with traditional tools has been met with frustration on many fronts. So far, the most definitive and in-depth studies require patch clamp electrophysiology on the thin dendrites of type II afferents underneath the OHCs (Weisz et al., 2009; Weisz et al., 2012; Weisz et al. 2014; Liu et al., 2015). This already difficult technique becomes intractable when trying to expand to situations beyond the most favorable condition, pre-hearing apical cochleae. However, it is uncertain how applicable it is to extrapolate results from these recordings to any time past early postnatal development. As was laid out in this introductory chapter, there are tonotopic effects and many developmental changes that occur throughout the cochlea especially around the time of hearing onset. So far, the only experiment that attempted to address any change after the onset of hearing determined that the current resulting from a puff of ATP decreased in post-hearing animals (Weisz et al., 2009) (Figure B19). ATP has

been a major focus of these experiments and has been the basis for the main

theory about type II afferent function as auditory nociceptors. However, with the

current data it is equally likely that ATP sensitivity is transient and is just

developmentally relevant. It is known that ATP is important for the development

of the pre-hearing cochlea in that disrupting the supporting cells that release

periodic boli of ATP causes developmental defects for both type I and II afferents

(Kelsell et al., 1997; Cohen-Salmon et al., 2002; Hilgert et al., 2009; Ceriani et

al., 2019). The question now stands whether ATP is still relevant for type II

afferents once this spontaneous activity disappears, but that is difficult to test

systematically with cellular electrophysiology.
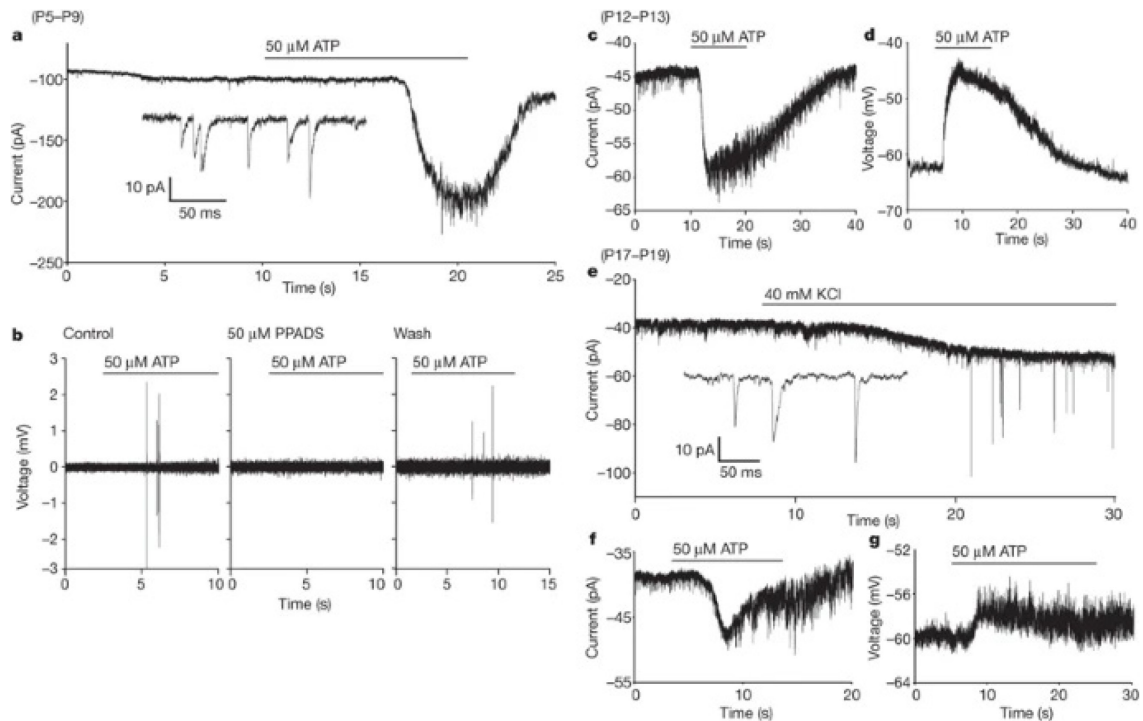
Figure B19: Effect of ATP on rat type II afferents. a, ATP-evoked inward currents in postnatal (P5–P9) fibres (142.7 ± 73.6 pA, $n = 6$) and increased EPSC frequency. Inset: ATP (1 µM) induced EPSCs in another cell. b, PPADS reversibly blocked ATP-induced repetitive action potentials (loose-patch extracellular record). c, ATP-induced inward current (29.9 ± 17.4 pA, $n = 5$) and

EPSCs in P12–P13 fibres. d, ATP depolarized P12–P13 fibres (12.6 ± 4.8 mV, n = 4). e, 40 mM extracellular potassium induced EPSCs in a P18 fibre. Inset: expanded waveforms, same cell. f, ATP evoked inward currents in three of six P17–P19 fibres (10.1 ± 3.6 pA, n = 3). g, ATP depolarized P17–P19 fibres (3.1 ± 0.2 mV, n = 2). Adapted from Weisz et al., 2009.

The recent explosion of genetic tools has been conducive for many avenues of investigation and is extremely promising for studying type II afferents. Although the discovery of genetic markers for type II afferents is nascent and requires more attention, there is a unique opportunity afforded by these advancements. For example, targeting fluorescently labelled type II afferents circumvents the issues that plagued blind recordings. Another major genetic tool that can be applied to studying type II function is calcium imaging.

Calcium signaling within a cell is tightly regulated and important for many cellular processes. Measuring calcium transients is a viable alternative to measuring membrane potentials with techniques like patch clamp electrophysiology for determining the activity of cells (Tian et al., 2012; Anderson et al., 2017). Calcium transients can be measured either through calcium sensitive dyes or through genetically encoded calcium indicators (GECIs). Calcium sensitive dyes can be added to the tissue around the time of investigation but there is variability in the amount that will be loaded across cells depending on cell density. GECIs expressed in transgenic animals provide a more uniform expression of indicator and can be restricted to genetically defined cell types. The most prominent line of GECIs are the GCaMPs. These proteins have a calmodulin-based moiety that confers a conformational change that

allows for bright photon emission from the attached fluorophore when Ca^{2+} binds (Akerboom et al., 2009).

While the sensitivity, temporal precision and reliability of recording events like action potentials is better, electrophysiological techniques require direct access to the tissue. For tissues such as the organ of Corti, the inaccessibility and dense packing of cells make patch clamp recordings exceedingly difficult. Optical imaging techniques not only can more easily penetrate through cell types but leaves the overlying structure intact. This is of particular interest when studying cell types that are responsive to tissue damage such as type II afferents. Another benefit of the calcium imaging technique is the possibility of recording the activity of multiple cells simultaneously which would not be feasible with a technique like patch clamp electrophysiology. Considering all the difficulties that arise from not being able to differentiate type II from type I afferents except at their peripheral terminals, genetic approaches seem to be the best way forward.

As will be detailed in the following chapters, this thesis describes the first attempts to study the activity of type II afferents through genetic methods. By crossing the GECI GCaMP6f with two previously described type II preferring genes and one newly described one, we have been able measure calcium transients in type II afferents to manipulations across the length of the cochlea, at adult ages, and alongside other cell types. While there are many new and exciting paths to explore with this new tool, we first focused on testing the most established hypothesis, that type II afferents act as auditory nociceptors, in

contexts that were heretofore unobtainable. By addressing the strongest

argument levied against the nociceptor hypothesis we seek to strengthen or

discard this concept depending on evidence we gather. In other words, the main

target of this thesis is to determine whether sensitivity to ATP and focal damage

persists along the tonotopic axis and after the onset of hearing. Another aspect of

interest is whether prior damage, such as through loud noise exposure,

sensitizes type II afferents in a fashion similar to the sensitization of somatic

nociceptors after insults to the skin. If the reduced sensitivity to ATP is true and

reduces the ability of type II afferents to respond to focal damage in the adult

cochlea, there are two main outcomes: either ATP and damage only activate

type II afferents during development or the sensitivity to ATP returns following

large scale insults to allow for enhanced detection of damage when the tissue is

at increased risk of impairment. In the former case, the nociceptive hypothesis

would suffer a blow, but in the latter case the nociceptive hypothesis would be

supported. From there, it can be decided which path to pursue to finally begin to

understand these long mysterious neurons.

Materials and Methods

Mice

      Five mouse models were used as part of these studies (Table M1). Th^{CreER} and Drd2^{Cre} homozygous mouse lines were backcrossed to the C57Bl/6j strain and maintained independently. F1 offspring of either sex of Th^{CreER}, Drd2^{Cre}, or Tac1^{Cre} bred with homozygous GCaMP6f$^{fl/fl}$ mice were generated and used for the experiments in this thesis. Tamoxifen (Sigma, #T5648) was administered by gavage at P3-4 for the Th^{CreER}:GCaMP6f animals at a dosage of 0.2 mg in corn oil (Sigma, #C8267). Care of the animals followed all institutional guidelines of the Animal Care and Use Committee of JHU SOM.

Name	Genotype	Source
Th$^{2A\text{-}CreER}$		Abraira et al., 2017
Drd2^{Cre}	B6.FVB(Cg)-Tg(Drd2-cre)ER44Gsat/Mmucd	RRID:MMRRC_032108-UCD
Tac1^{Cre}	B6;129S-*Tac1$^{tm1.1(cre)Hze}$*/J	IMSR Cat# JAX:021877, RRID:IMSR_JAX:021877
GCAMP6f$^{fl/fl}$	C57BL/6N-*Gt(ROSA)26Sor$^{tm1(CAG\text{-}GCaMP6f)khakh}$*/J	IMSR Cat# JAX:029626, RRID:IMSR_JAX:029626
Ai9	B6.Cg-*Gt(ROSA)26Sor$^{tm9(CAG\text{-}tdtomato)Hze}$*/J	IMSR Cat# JAX:007909, RRID:IMSR_JAX:007909

Table M1: List of genotypes used in the thesis with sources.

Calcium Imaging

Mice were euthanized based on ACME guidelines appropriately for the age of the animal immediately prior to imaging. Pre-weaned animals were placed on heating pad to maintain core body temperature prior to euthanasia. The hemi-dissected head was placed in ice-cold 2.5 mM K$^+$ external solution and was excised from the temporal bone. Then, the bone overlying the cochlear epithelium was removed. The cochlea was mounted in utility wax for observation. A gravity perfusion system was constructed on a motorized stage of a 710 LSM

Zeiss microscope with a GaAsP detector and Cameleon 2-photon laser. Dissected cochleae were placed in external solution and imaged using a 20x non-coverslip-corrected water-immersion objective.

Solutions for Bath Application

2.5 mM K⁺ external solution was composed of 2.5 mM KCl, 148 mM NaCl,1.3mM $CaCl_2$, 0.9mM $MgCl_2$, 0.7 mM NaH_2PO_4, 5.6 mM D-glucose and 10 mM HEPES, pH 7.4. 40 mM K⁺ external solution was composed of 40 mM KCl, 104 mM NaCl, 1.3mM $CaCl_2$, 0.9mM $MgCl_2$, 0.7 mM NaH_2PO_4, 5.6 mM D-glucose and 10 mM HEPES (pH 7.4). Alternative concentrations of K⁺ were made by diluting the 40 mM K⁺ external solution with proportions of 2.5 mM K⁺ external solution to achieve the desired concentration. For experiments testing the effect of P2X receptor blockade, PPADS (Tocris, #0683) was added to the 2.5 mM K⁺ extracellular solution to achieve a 100 µM concentration. Preparations of other agonists such as caged glutamate were created in a similar fashion by diluting to the appropriate concentration in 2.5 mM K⁺ extracellular solution.

Ca^{2+} Signaling Image Acquisition

Zen black software was used to control the Cameleon 2-photon laser. Imaging parameters were set at 2x digital zoom and 512x128 pixels allowing for acquisition of time series at 80 ms a frame. Imaging was performed at 8% laser power. For laser ablation, laser power was increased to 100% with up to 1000 iterations within a hand-drawn ROI. Due to the sensitivity of the GaAsP detector, the sample was not imaged during laser ablation for a median time of 8.4 seconds.

Quantification of Change in Fluorescence

Time series images were transformed into a 255 point black scale projection image using standard deviation for the projection type in FIJI. This type of projection image highlighted the areas of the field of view with the largest changes in fluorescence. Regions of interest (ROIs) were created using the polygon selection tool with care to prevent overlapping regions. One region was selected as the background; the values from this region were subtracted from each of the other regions (ΔF). The equivalent of 30 seconds from the control condition of the time series was used as the baseline fluorescence of all regions ($F_{baseline}$). The resulting equation is thus:

$$\Delta F/F = (F_{ROI} - F_{background})/F_{baseline}$$

The data was then plotted as $\Delta F/F$ for every ROI in each frame. All $\Delta F/F$ are reported as fold change, e.g. a value of 1 equals baseline activity and 2 equals a doubling and so on. An ROI was considered responsive if its max $\Delta F/F$ was more than 3 standard deviations above the baseline before laser ablation and/or at the end of the recording.

To compare between videos and genotypes, traces were scaled with the maximum set at 1 ($\Delta F/F=1$). This allowed for calculations of time of response. Total time of response includes the time of the laser ablation to the time at which the trace has fallen to within 3 standard deviations of the baseline fluorescence for at least five consecutive frames. Time constants of decay were estimated by fitting to exponential decays using the Excel add-in Solver.

TTX application

Type II afferents were imaged on a Nikon NiE upright microscope attached to an A1R=MP confocal scan head with a CFI60 Apo40X W NIR objective (NA=0.8m W.D =3.5mm) at 4 frames per second. Each type II afferent was imaged three times. Before each imaging session there was no acquisition followed by a 20 second epoch where the background fluorescence was collected. In the first imaging session the tissue began in 5.8 mM K^+ external solution and then had of 40 mM K^+ external solution perfused through a multibarrel pipette with a 100 μm aperture for a 20 second period and a washout for another 20 second period. This process was repeated but with 5 μM tetrodotoxin citrate (TTX, Tocris) in each of the solutions. Lastly, all these steps were repeated after washing out all the TTX to determine if there were long-lasting irreversible effects of the TTX.

Immunofluorescence

Whole-mount immunostaining and imaging was performed as previously described (Martinez-Monedero et al., 2016; Vyas et al., 2017; Wu et al.,2018; Vyas et al., 2019). Briefly, grossly dissected inner ears were perfused with 4% PFA in 1XPBS through the round window then post-fixed for 30 minutes on a 3D-Rotator. P7-10 and adult inner ears were then washed in PBS (3x30min) and dissected into turns of the organ of Corti. Adult inner ears were washed (3x30min) in PBS then in an additional step decalcified in 125 mM EDTA in PBS for 2 hours. Cochlear turns were immunolabeled with Goat anti-GFP (Sicgen, AB_2333099) to label GCaMP6f protein. Donkey anti-Goat Alexa 488 (Invitrogen, AB_2762838) was used along with Alexa-647-conjugated Phalloidin

(Thermofisher, #A22287) and 4',6-diamidino-2-phenylindole (DAPI, Roche) for GCaMP6f, hair cells, and nuclei, respectively. Cochleae and dorsal root ganglia from Tac1^{Cre}:Ai9 animals were immunolabeled with the following polyclonal antibodies: Goat anti-tdTomato (Sicgen, AB_2722750) and Rabbit anti-CGRPα (Immunostar, AB_572217). Alexa-568-conjugated Donkey anti-Goat (Invitrogen, AB_142581) and Alexa-488-conjugated Donkey anti-Rabbit (Invitrogen, AB_141708) secondary antibodies were used for tdTomato and CGRPa, respectively. Cochlear turns were mounted using ProLong Fade Gold Antifade Mountant (Thermofisher, #P36930) and imaged on a 700 LSM Zeiss confocal microscope.

Cell Number Quantification

Tac1^{Cre}:Ai9 quantification of cochlear afferent somata was based on the previously published procedure for counting SGNs (Wu et al., 2018). Briefly, the organ of Corti was divided into bins of 10% of the total length beginning at the apex (0%) to the base (100%) and straight tangential lines segmented the spiral ganglion. Cochlear afferent somata within each bin were counted.

Experimental Design and Statistical Analysis

Data was processed and analyzed in R studio, Graphpad Prism, and Excel. Statistical testing for success rate data used a generalized linear model with the family set to binomial. Paired data within the same animal used the Wilcoxon ranked sum test. Data with even numbers of across multiple conditions were tested with one- or two-way ANOVAs. Data that stemmed from uneven numbers of multiple recordings across mice were analyzed with a linear mixed

model with the mouse identity as a fixed effect. The number of mice used (N) or number of videos (n) used in a statistical test is reported with p-values. Occasionally, multiple videos from the same animal are taken over the course of an experiment. Videos are not taken in the same location after the tissue is damaged and were taken at a location with healthy tissue tens of microns apical to the site of damage to avoid recording from the same neurons.

Methods specific for Chapter 5:

Mice

C56Bl/6j (RRID: IMSR_JAX:000664) mice purchased from Jackson Laboratories were bred and maintained at Johns Hopkins University School of Medicine under the guidance of the Institutional Animal Care and Use Committee (IACUC). Mice were placed on a 12-hour light-dark cycle, fed an autoclaved Teklad diet, and housed in cages with automatic water and filtered air until adulthood. All experiments take place between 6-9 weeks of age. Male and female mice were used in all experiments to avoid sex-specific variation.

Noise Exposure

C57Bl/6j mice were transferred to a low noise satellite housing facility from the day before noise exposure through the week after noise exposure until the endpoint for histology. Due to the susceptibility of C57Bl/6j mice to age-related hearing loss, (Johnson et al., 1997) all experiments were performed with 6-week old mice. Awake, unrestrained mice were exposed to 110 dB SPL broadband white noise for 2 hours. Two set-ups were used to perform noise exposure. This sound chamber and noise exposure set-up have been previously described (Wu

et al. 2020). All other animals were exposed to noise in a reverberant sound attenuating chamber (58cm x 40cm x 30 cm; width, depth, height) with 3 overhead, Promaster TW47 1200W dome tweeter speakers that produced maximum energy in the sound spectrum from 2-16 kHz. Speakers were approximately 25 centimeters above the heads of the mice. Broadband noise was generated by 2-JKT-tone and noise generators (KV2 audio, Czech Republic) powered by Neewer nw-100 phantom power sources. The noise generators were connected to 2 Crown Drivecore XLS2502 amplifiers: one driving the two peripheral speakers in input Y mode, the other driving a central speaker in bridge mode. The sound spectra and decibel level were tested in each set-up using a Larson-Davis LXT sound level meter with a 1/2-in free field microphone. Care was taken to measure the sound level at the position of the head of the experimental animals.

Auditory Brainstem Response (ABR)

The ABR system, procedures and quantification software used for this study have been previously described (Lauer and May 2011, Lina and Lauer 2013). Mice were anesthetized with an intraperitoneal injection of 0.1cc per 20g body weight of a mixture of ketamine (100 mg/kg) and xylazine (20 mg/kg) in 14% ethanol before being placed on a gauze covered heating pad in the ABR chamber. The animals' eyes were swabbed with petrolatum-based ophthalmic ointment to prevent corneal ulcers during anesthesia. Subdermal platinum electrodes were placed at the vertex of the head (non-inverting), the left pinna (inverting), and on the left side at the base of the tail (ground). 300 repetitions of

a click or pure-tone stimulus (10 stimuli/sec) were used to generate averaged

ABR waveforms. Each tonal stimulus was 5 ms in duration with a 0.5-ms rise and

fall time. A Fostex dome tweeter speaker (model FT28D) in a foam-lined

chamber was used to present the stimuli to mice 30 cm away. The ABR

threshold was defined with custom MatLab software by calculating the averaged

peak-to-peak voltage during a 5-ms interval, beginning 1 ms after the onset of

the stimulus, compared to the averaged peak-to-peak voltage in a 5-ms window

20 ms after the stimulus. The threshold was determined as the stimulus level

where the peak-to-peak response was greater than 2 standard deviations above

the electrical noise.

Fluorescent Immunolabeling and Confocal Microscopy

Cochleae from control and noise-exposed mice were dissected from the

temporal bone and processed as described above. Primary antibodies were

diluted at 1:200 in blocking buffer containing 10% normal donkey serum, 0.6%

Triton 100, and 2% BSA weight by volume in PBS overnight on a shaker at 4°C.

Mouse IgG1 anti-CtBP2, (Clone 16, BD Biosciences, AB_39943) was used to

label ribbon synapses. Mouse IgG2a anti-Tubulin β3 (Clone Tuj1, Biolegend,

AB_2313773) was used to label neurons. Rabbit anti – MyoVIIa (polyclonal,

Proteus, AB_10015251) was used to label hair cells. Cochlear turns were

washed 3x for 10 minutes in PBS then incubated with secondary antibodies

diluted 1:1000 in blocking buffer diluted 1:1 with PBS for 2 hours at room

temperature. Secondary antibodies used: Alexa-568-conjugated goat anti-mouse

IgG1(Invitrogen, AB_2535766), Alex-488-conjugated goat anti-mouse IgG2a

(Invitrogen, AB_2535771), and Alexa 647-conjugated donkey anti-rabbit IgG

(Invitrogen, AB_2536183) 4'6-Diamidine-2'-phenylindole dihydrochloride (DAPI,

Roche) was used to stain nuclei. These images were then analyzed with the

Measureline plugin (Eaton-Peabody Laboratories Mass. Eye and Ear Infirmary)

in FIJI to determine the locations of each frequency region. Whole mount

preparations then were imaged using an oil immersion 40x objective with 2x

digital zoom for a region of 80µm by 80µm at each frequency location indicated.

Quantification of Synapses with Virtual Reality Software

To quantify cochlear ribbon synapses, images were analyzed using

ImageJ and syGlass Virtual reality Software (Istovisio, Inc) and the Oculus Rift

Virtual Reality Headset. syGlass was used to localize the hair cells and cut away

the tectorial membrane, as necessary. The counting tool in syGlass was used to

count afferent ribbon synapses above and below nuclei of whole hair cells.

Colors were assigned to hair cells and CtBP2 puncta in different locations for

reproducibility. Additional analysis included counting the number of whole OHCs

in each tonotopic imaging region with 0, 1, 2, 3, or 4+ CtBP2 immunopuncta. The

observer was blinded until all quantification was completed.

Statistical Model

Mathematical modeling of ribbon and action potential estimates were

generated with RStudio software. The numbers of ribbons were generated

randomly from a normal distribution centered around the mean number of

ribbons per 9 OHCs based on counts from immunofluorescence images. This

was replicated 1000 times to create a distribution of estimated ribbons per type II

afferent. Given an average probability of release of 0.26 for an individual ribbon, a binomial function was used to determine the probability of at least 7 concurrent excitatory postsynaptic potentials (EPSPs) for each type II afferent neuron, from the estimated number of ribbons (Weisz et al. 2012). Seven concurrent EPSPs are required to reach the action potential threshold. For each set of 1000 neurons, the probability for suprathreshold release was averaged and multiplied by 1000 to generate the number of action potentials fired across the population.

Results

Chapter 1: Application of GCaMP6f Expression in Type II Afferents to Record Activity Optically

1.1 Introduction

Patch clamp recordings from the dendrites of type I and type II cochlear afferents have helped inform our understanding of synaptic transfer from hair cells onto these neurons (Glowatzki and Fuchs, 2002; Weisz et al., 2009; Weisz et al., 2012; Weisz et al., 2014; Liu et al., 2015). However, the intractability of recording from type II afferent dendrites hinders detailed investigations needing large sample sizes and has hampered more difficult recordings from type II afferents of the base of the cochlea and from mature animals. While technically easier, recordings from the somata of type II afferents in the spiral ganglion have not been successful so far in reporting the small synaptic events from the distant dendritic terminals (Jagger and Housley, 2003; Martinowitz and Kalluri, 2020). Ideally, it would be possible to observe activity at the level of the dendrites without needing to directly access the type II afferent peripheral process. Now, with the advent of genetic lines that differentiate type I and type II afferents, GCaMP6f can be expressed in the type II afferents specifically (Vyas et al., 2017; Wu et al., 2018). While calcium imaging sacrifices some resolution of synaptic events, it allows for the observation of activity localized to the dendrites without damaging the OHCs first and permits simultaneous viewing of nearby type II

afferents. Without the need for removing all the overlying bone, placing the organ of Corti under an insect pin, or lowering in a glass pipette to report electrical activity; the tissue can be left more intact, speeding up dissections. Faster, less invasive dissections translate to less damage to the hair cells and neurons, resulting in healthier samples. The health of the tissue is imperative in studies of type II afferent function because they have been shown to be sensitive to adenosine triphosphate (ATP), which is released with cell rupture (Cook and McClesky, 2002; Liu et al., 2015). Additionally, the health of the tissue after dissection was the limiting factor for recording type II afferent activity from basal and/or mature tissue. This chapter deals with establishing the calcium imaging and dissection techniques required to record type II afferent events under all situations and verifying that calcium transients in type II afferents correspond to the activity of the neuron.

1.2 Verification of GCaMP6f expression in type II cochlear afferents

The spiral organization of the cochlea subserves its function (Bekesy 1960, Mann and Kelley, 2011, Fettiplace & Nam 2019). Many parameters from hair cell size (Dannhof et al., 1991) to stiffness of the basilar membrane (Teudt and Richter, 2014) vary with the position along the coiled length of the cochlea. These variations sum together to create a tonotopic map where high frequency sounds are transduced by hair cells of the base and low frequency sounds are transduced by hair cells of the apex. Hair cells at each location synapse with cochlear afferents to pass the frequency-specific information to the central

nervous system. One observed difference between type II cochlear afferents along the tonotopic axis is gene expression (Flores-Otero and Davis, 2011, Liu and Davis, 2014, Wu et al. 2018, Vyas et al, 2019). Tyrosine Hydroxylase (TH) and Serotonin Transporter (SERT) are expressed in type II cochlear afferents along a gradient with strong expression favored in the apex which drops off by the base. Calcitonin gene-related polypeptide alpha (Calca) and Dopamine Receptor Subtype II (Drd2), on the other hand, prefer labeling type II cochlear afferents of the base over the apex (Wu et al, 2018, Vyas et al. 2019). Each of these four genes are not exclusive to type II cochlear afferents, but at least seem to differentiate type II cochlear afferents from type I cochlear afferents.

We leveraged these gradients of gene expression in type II cochlear afferents to express GCaMP6f in all parts of the cochlea: TH^{CreER}:GCaMP6f for apical type II cochlear afferents and Drd2^{Cre}:GCaMP6f for basal type II cochlear afferents (Figure 1.2.1 A-C). Expression of GCaMP6f was confirmed first with immunohistochemistry and recapitulated the reported expression patterns for each genotype. TH^{CreER}:GCaMP6f was expressed in apical type II afferent dendrites and Drd2^{Cre}:GCaMP6f was expressed in basal type II somata and dendrites with no expression in type I afferents in either genotype. As well, we never saw appreciable expression in the MOC neurons but occasional expression in LOC neurons in Drd2^{Cre}:GCaMP6f animals. LOC neurons expression never interfered with imaging type II afferents however, because LOC axons are localized to the IHC region.

1.3 Two-photon imaging and more intact tissue preparation

The next step was to image type II afferent calcium transients in acutely dissected cochleae. In pre-hearing tissue before the cochlear bones have ossified, dissections that remove the organ of Corti do not cause destruction of the structure unlike at older ages. Once the bones ossify, it is difficult to extract the organ of Corti without crushing the tissue or having the bones slice the tissue apart. In some experiments with tissue from the apex of pre-hearing animals, we prepared the tissue as was done for electrophysiological preparations where glass pipettes require physical access to the cells. However, to adapt tissue preparation for calcium imaging for mature as well as basal tissue, we instead left most of the cochlea and chipped away the overlying bone to create a window for optical access. For basal preparations more bone was removed from the top of the cochlea and the first apical turn was excised. This "mostly intact preparation" resulted in less damage to the organ of Corti and preserved more of the natural architecture and curvature inherent to the cochlea.

As most of the tissue was left intact, two-photon microscopy was preferred over light or confocal microscopy to overcome the scattering from thick tissue. Two-photon microscopy involves shining light, usually at near infrared wavelengths, that can excite fluorophores at half their wavelength when two of the photons act constructively (Svoboda et al., 1997; Cruz and Lüscher, 2005, Svoboda and Yasuda, 2006). The use of infrared wavelengths allows for deeper penetration into the tissue and is therefore more suitable for dense, thick tissue like the organ of Corti, especially in more intact preparations. Additionally, the

requirement of two in-phase photons to excite the fluorophore reduces the amount of spread, enhancing the resolution. Lastly, two-photon microscopy reduces the amount of bleaching and tissue damage because the longer wavelength light has less power. Overall, the combined use of mostly intact preparations and two-photon microscopy allows imaging within acutely dissected cochleae from previously unobtainable mature animals even in the basal turn.

1.4 GCaMP6f fluorescence corresponds to type II afferent depolarization but not necessarily action potentials

With mostly intact cochlear preparations and two-photon microscopy, type II afferent activity could be monitored in acutely dissected cochleae. Type II cochlear afferents were consistently bright in the presence of depolarizing 40 mM K^+ external solution and became progressively dimmer by decreasing the potassium concentration by introducing increasing volumes of 5.8 mM K^+ external solution (Figure 1.2.1D). The change in brightness was measured by averaging the steady state values at the last 30 seconds in each concentration of K^+ and normalizing it to the steady state value from the lowest K^+ concentration to counteract the effects of washing in solution. The average decrease in fluorescence from multiple regions of interest (ROIs) from multiple neurons was well correlated with the decrease in the K^+ concentration with an R^2 value of 0.886. The approximate halfway point between maximum and minimum fluorescence levels occurred when the tissue was bathed in 15mM K^+ solution. For many of the following experiments 15 mM K^+ solution was used to find

responsive type II afferents without maximal stimulation. Additionally, 2.5 mM K$^+$ and 5.8 mM K$^+$ external solutions were used interchangeably in most experiments as both produced similarly weak fluorescent signals.

Type II cochlear afferents were also able to respond swiftly and reversibly to perturbations of K$^+$ concentration changes (Figure 1.2.1E-H). After bathing in 40 mM K$^+$ external solution, application of 5.8 mM K$^+$ solution reduced the fluorescence of type II afferent processes several fold. Levels returned to nearly their original values when 40 mM K$^+$ solution was reintroduced. While 40 mM K$^+$ solution has been shown to depolarize type II afferents and cause action potentials in pre-hearing animals, it is unclear to what extent the calcium transients induced by high concentrations of K$^+$ solutions is due to action potential generation. To explore the role of action potentials in internal calcium levels 40 mM K$^+$ was introduced first without 5 µM tetrodotoxin (TTX), returned to 5.8 mM K$^+$ solution, and then compared to the fluorescence change when adding in 40 mM K$^+$ solution with TTX. Afterwards there was another puff of 40mM K$^+$ to wash out the lingering TTX (Figure 1.2.1I). TTX is a voltage-gated Na$^+$ channel blocker which prevents the initiation of action potentials. Therefore, if there is a decrease in the $\Delta F/F$ signal it is indicative of calcium increases that arise from action potentials. In the three P7 TH^{CreER}:GCaMP6f mice that were tested there was no fluorescence signal from somata but the peripheral dendrites clearly expressed GCaMP6f. In all three animals the largest fluorescence increase occurred when there was TTX present, approximately 20% larger than either the initial 40 mM K$^+$ bolus or the washout with 40mM K$^+$ solution and appeared to last

longer. It is unclear without further follow-up if the increase in fluorescence

change with 5 μM TTX present reflects a rapid, robust change in the type II

afferents or simply had no effect. At the very least, because there is no decrease

in the ΔF/F signal with TTX present, it can be concluded that either no action

potentials were generated or there is no additional free calcium in the dendrites

when action potentials do occur.
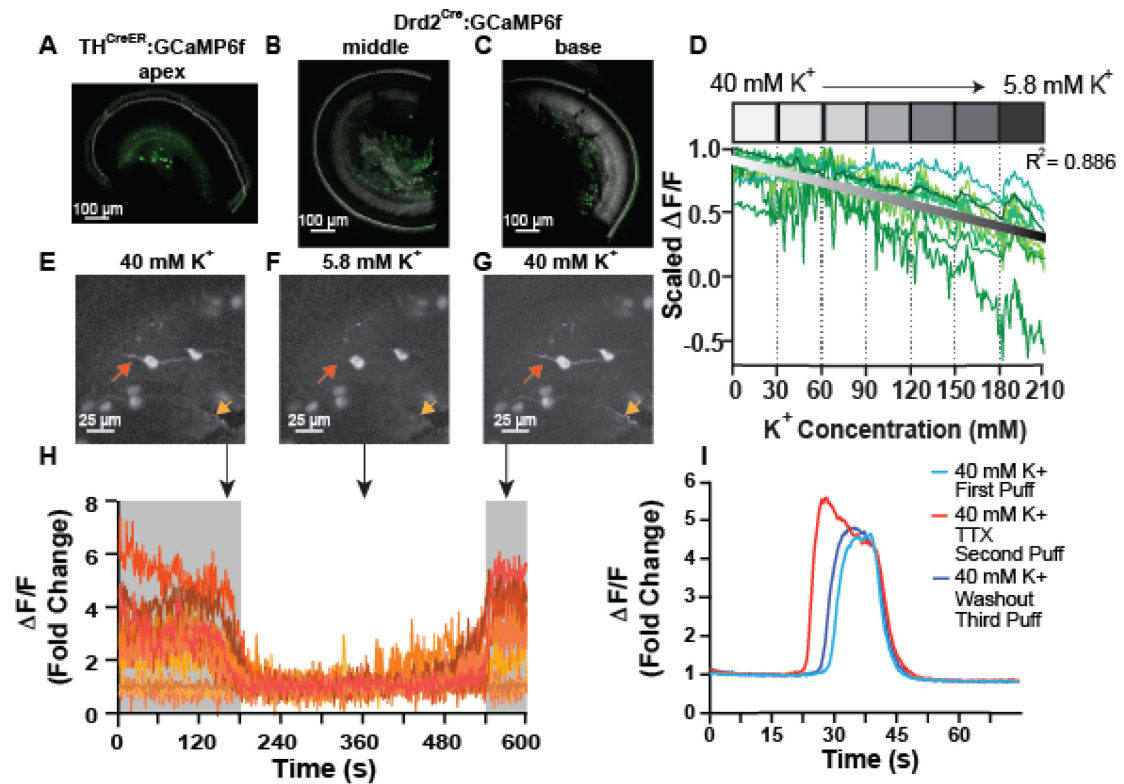
Figure 1.2.1: GCaMP6f can be functionally expressed in type II cochlear afferents throughout the cochlea. A. 5x magnification confocal image of the apex of a pre-hearing TH[CreER]:GCaMP6f mouse cochlea. Green channel anti GFP to label GCamP6f expression. White channel Phalloidin (F-actin) to label hair cells. Scale bar 100 μm. B-C. 5x magnification confocal image of the middle section (B) and base (C) of a pre-hearing Drd2[Cre]:GCaMP6f mouse cochlea. Scale bar = 100 μm. Green channel anti GFP to label GCamP6f expression. White channel Phalloidin (F-actin) to label hair cells. D. Scaled ΔF/F for multiple hand-drawn neuronal ROIs from a single Drd2[CreER]:GCaMP6f as the K$^+$ concentration in the extracellular solution progresses from 40 mM to 5.8 mM. White-to-black gradient line represents the linear regression for the traces. R^2 = 0.886. Traces from

individual ROIs represented by green colored lines. Vertical dashed bars and overlying boxes designate epochs of the last 30 seconds of recording from discrete changes in extracellular solution concentration. E-G. Standard deviation projection images of a pre-hearing Drd2^{Cre}:GCaMP6f mouse spiral ganglion starting in 40 mM K$^+$ (E) to 5.8 mM K$^+$ extracellular solution (F) and back to 40 mM K$^+$ (G). Scale bar = 25 µm. Orange arrows point to two example type II processes that are transiently suppressed in 5.8mM K$^+$ extracellular solution. H. ΔF/F traces of type II afferent fibers from E-G. Gray shading represents the time when 40 mM K$^+$ was present in the extracellular solution. Black arrows point to the time periods where the images from E-G. occurred. I. Overlaid ΔF/F traces of an example type II afferent fiber in response to 40 mM K$^+$ external solution puffs. Light blue trace represents the first puff of 40 mM K$^+$ solution. Red trace represents the second puff where 5 µM TTX was present in the bath solution and the 40 mM K$^+$ solution. Dark blue trace represents the last puff of 40 mM K$^+$ solution after washing out the 5 µM TTX.

1.5 Investigation of potential type II afferent agonists

Observing fluorescence changes in GCaMP6f expressing animals with agonist application could be a quick diagnostic tool to determine if certain agonists modulate type II afferent activity. The most likely agonists that would cause a fluorescence change in these dendrites is ATP and glutamate which are agonists known to cause depolarization of type II afferents. Although application of 100 µM ATP sometimes caused fluorescence increases throughout the cochlear tissue, it also caused the tissue to move out of focus frequently. With the ambiguity of bath applications of ATP, we next attempted to see if known agonists of type II afferent function were sufficient to drive calcium transients when delivered through caged agonists. To assess if caged agonists could be the solution to problems with the shifting of the focal plane, we first turned to caged forms of glutamate and ATP. While uncaging glutamate and ATP, we employed the bleaching settings of the two-photon microscope over hand-drawn regions of interest (ROIs). We adjusted the laser power and number of iterations

84

to control the amount of uncaging. If the number of iterations was below 15, the fluorescence of the tissue within that ROI would decrease every time (0 out of 6, **p=0.031** Wilcoxon ranked sign test). A decrease in the total area within the ROI means that the laser "bleached" the tissue where the fluorophores lose their ability to emit light and does not reflect a biological process (Kalies et al., 2011). If the number of iterations exceeded 30 iterations the laser would consistently cause tissue damage where the affected cell would expand and burst. Intermediate number of iterations only caused bleaching of the tissue half of the time but did not seem to have any effect on the fluorescence level of type II afferent fibers. Overall, uncaging either glutamate or ATP is unfeasible if the amount of light needed to uncage the agonists causes physical damage to the tissue which can cause a confounding release of ATP.

1.6 Discussion

Through improvements in dissection technique, type II afferent activity can be observed by tracking calcium transients *ex vivo* with two-photon microscopy. Basal type II afferents which eluded study previously, are accessible by removing the top of the cochlea in Drd2^Cre:GCaMP6f animals and remain healthy for longer than completely dissected basal organs of Corti. GCaMP6f is functional in type II afferents and accurately reflects the extent of depolarization within a minute of potassium application both at the peripheral dendrites and the somata in the spiral ganglion. The near linear relationship between K^+ concentration and fluorescence suggests that the fluorescence level is a reliable readout of the type

II afferent's membrane potential. Experiments with TTX, however, cast doubt on the ability to use calcium imaging in this system to track action potential activity. In the future, it will be interesting to see if the action potentials that arise from 40 mM K^+ solution cause further calcium influx in the somata closer to where action potentials are generated. Assuming the somata have action potential dependent calcium influxes, one could determine if OHC ablation can cause action potentials by evoking damage and observing calcium transients in the somata with and without TTX. This will require some technical advances because it requires quickly shifting the field of view of the microscope from the OHCs for the damage event to the somata to record the calcium response. This will also likely cause a delay in recording not only because of the movement but because of the GaAsP detector shutting off from the bleaching event. Without the early phase of the response it could be difficult to observe the effect of TTX so these technical limitations would have to be overcome first.

The techniques described in this chapter also allow for the preservation of the natural structure of the cochlea and organ of Corti and reduce the damage experienced by the tissue. Any dissection will inherently cause tissue damage that will result in the release of ATP and other molecules that signal distress. Type II afferents have been shown to respond to at least ATP and could respond to other elements caused by dissection. Limiting the exposure of type II afferents to ATP could prevent processes, such as desensitization, which can cause spurious results about type II afferent function. A more naturalistic tissue preparation could be especially important in mature tissue where the response to

ATP is currently unknown and where there is a high potential amount of damage incurred by dissection. It is unfortunate that most attempts with agonists in the bath were not sufficient to cause a strong response in the type II afferents, even for cases where the agonist is known to depolarize type II afferents. More care will be required to determine a way to reliably introduce potential agonists while recording calcium transients without causing tissue movement or damage. A possible solution is to use a perfuse a small amount of agonist directly onto the imaging area as was done for the TTX experiments. Improving the drug application system will be important for determining if type II afferents are activated by anything other than ATP or glutamate and if that changes with maturity.

With future innovations in microscopy and clearing techniques it might be possible to image through the bone of the cochlea and image without any disturbance to the tissue, especially if it could be done in a manner similar to cranial windows that allow for imaging brain tissue *in vivo* (Osswald and Winkler, 2013). *In vivo* recording is the ultimate goal to understand type II afferent function in behavior. Little is known about the stimuli that drive type II activity in behaving animals. By systematically testing different auditory parameters and measuring type II afferent calcium activity, we would come closer to understanding what the purpose is of type II afferents.

Chapter 2: Focal Ablation Causes ATP-Dependent Calcium Transients in Type II Afferents

2.1 Introduction

In pre-hearing cochleae, ATP is an important signaling molecule that coordinates activity of neighboring supporting cells and hair cells (Tritsch et al., 2007; Tritsch et al., 2010; Ceriani et al., 2019). In the first patch clamp recordings from type II afferent dendrites, application of ATP caused large inward currents (Weisz et al., 2009). Follow up experiments determined that ATP released by the rupture of nearby OHCs caused an ATP-dependent current that could cause action potential firing in type II afferents (Liu et al., 2015). A caveat of this work is that most of these recordings were restricted to apical turns of the cochlea in pre-hearing animals. Another complication is that ATP is constantly present and responsible for numerous developmental changes in the pre-hearing cochlea. The sample size for these investigations were small due to the intractability of the technique, often in the low tens of neurons (Weisz et al., 2009; Liu et al., 2015). With the previously described success of calcium imaging to capture type II afferent activity, we wanted to determine the efficacy of GCaMP6f in reflecting the inward currents induced by OHC rupture. Partially, these experiments would serve to verify the kinetics and thresholds for measuring calcium events compared to similar established metrics from whole cell patch clamp data. It would also allow us to extend those data to the middle and base of the cochlea which were excluded from those original analyses. Lastly, because of the large field of view in these recordings, we could examine the activity of multiple type II

afferents concurrently in response to the same stimulus to determine the

effective area that is affected by a single focal ablation and the likelihood that

neurons within that area respond to the stimulus.

2.2 Laser intensity and cell death

Early in calcium imaging experiments, when using the two-photon

microscope at higher magnifications, we noticed that the tissue appeared to

become distressed. To take advantage of this phenomenon, we programmed the

bleaching settings of the two-photon microscope that were described above for

uncaging photosensitive agonists to set both the intensity and duration of the

laser within a hand drawn ROI. When bleaching with 100% laser power for

multiple iterations, the resulting heat caused expansion of the OHCs until they

ruptured (Gale et al., 2004, Sirko et al., 2019). In determining the right

parameters for destroying tissue, we held the intensity at 100% laser power

constant for most ablations but adjusted the number of iterations that the laser

would raster through the hand drawn ROI, ranging from 10 to 2500, with a

chance of causing cell death whenever the number was higher than 30. The

most common values were 500 and 1000 to ensure damage occurred.

Depending on the amount of damage incurred however, we occasionally scaled

the number of iterations to cause less or more damage as needed to have a

repeatable amount of damage across animals. In all recordings that caused a

noticeable "scar" after laser ablation there was no effect of age or genotype on

the size of the scar. However, the size of the scar was larger in recordings that

eventually caused a neuronal response suggesting there is some threshold of

damage needed to cause neuronal response. A limitation of this method is that during the rastering period we could not image the tissue for a median time of 8.4 seconds, meaning we may have occasionally missed the peak response and observed only the tail end of the response.

2.3 Tonotopic effects of calcium response to focal tissue damage

To assess the functionality of the type II cochlear afferents we sought to repeat the finding that type II cochlear afferents respond strongly to focal ablation of nearby hair cells (Liu et al., 2015). To accomplish the ablation, we utilized the bleaching function described above to raster the laser of the two-photon microscope at 100% power over a rectangular region of interest about the size of 1-3 outer hair cells (OHCs) hundreds of times. Videos were taken only once at each location within the cochlea of an individual animal unless there was healthy tissue tens of microns apical to the site of damage. Because type II afferents turn basally moving apical from the previous recording location minimizes the chance of recording a neuron that experienced a previous ablation. Previous damage at a distant site did not increase the chance of type II afferents to respond to the subsequent ablation.

Following ablations that caused visible rupture, 65% of the time at least one type II neurite underneath the OHCs would experience a transient increase in fluorescence in pre-hearing tissue (Figure 2.3.1). The responses to damage in pre-hearing type II afferents was typically monotonically decreasing with the peak occurring sometime between the start of laser ablation and when images could

be captured. The average time constant of decay for all pre-hearing type II afferents was 27.5s ± 11.7s and the time from the observed peak in response to returning within three standard deviations of the steady state value was 45.5s ± 25.0s. As expected, the time constant of decay and the time to reach steady state for each recording were highly correlated with r = 0.692. These response times are similar in length to the currents recorded from type II afferents with whole cell patch clamp recording methods (Liu et al., 2015), a 90% decay time of 58.0 ± 9.5 s, suggesting that the GCaMP6f fluorescence closely follows the membrane potential of the type II afferent.

Transient calcium events occurred both in type II afferents of the apex and base of the cochlea. To observe activity at any location along the cochlear spiral, videos were recorded with the entire cochlea mostly intact. The bone on top of the cochlea was carefully chiseled away with forceps exposing the apical organ of Corti underneath. For basal recordings, more bone and the apical turn were removed to reveal the basal turn of the organ of Corti. There were no obvious differences between responses from pre-hearing TH (apical) or Drd2 (basal) expressing type II cochlear afferents. Both classes of neurons responded to damage in near equal proportions (Table 4.2.1, TH 13/40 vs. Drd2 24/53) and had similar kinetics (Figure 2.4.1G, TH 54.6 ± 19.7 s vs. Drd2 45.8 ± 33.8 s).
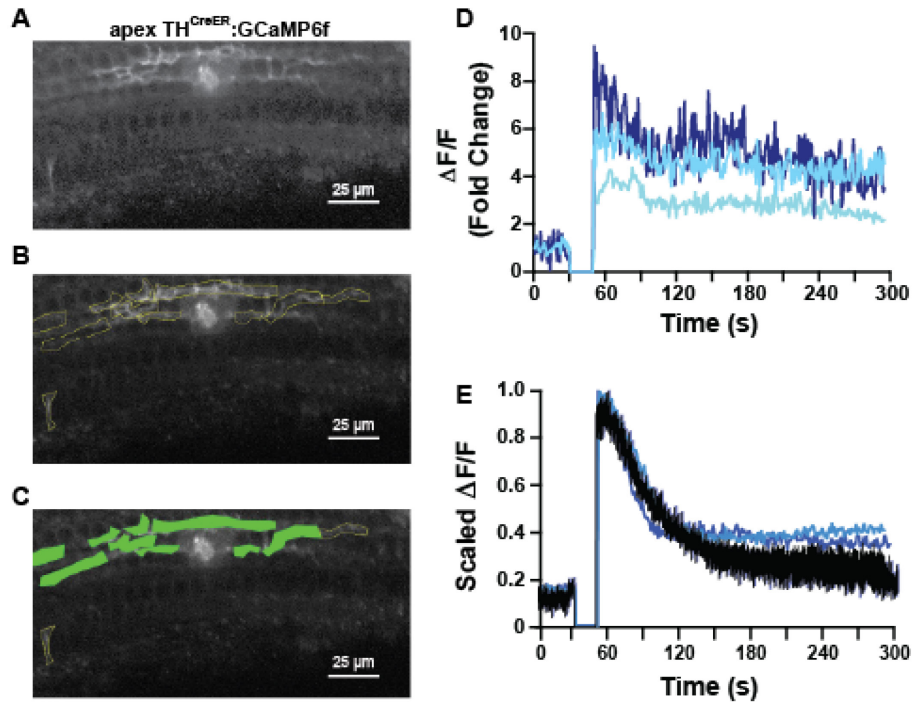
Figure 2.3.1: Focal photoablation causes transient calcium events in apical pre-hearing type II cochlear afferents expressing GCaMP6f. A. A standard deviation image of a pre-hearing TH[CreER]:GCaMP6f mouse cochlea after focal ablation of OHCs with 1000 iterations of 100% laser power. B. Same image as A. but with hand drawn regions of interest overlaid. C. Same image as B. but with the responsive regions of interest filled in green. Scale bars = 25 μm. D. ΔF/F traces of responsive ROIs from C. ΔF/F at time of photoablation and until imaging restarts is set to 0. E. Averaged and scaled ΔF/F traces from each pre-hearing TH[CreER]:GCaMP6f with different shades of blue per animal. Black line is the average of all the animal average traces. ΔF/F at time of photoablation and until imaging restarts is set to 0.

2.4 ATP dependence for pre-hearing response to tissue damage

ATP is an important signaling molecule within the developing cochlea and is a major contributor to the response of type II cochlear afferents to focal OHC ablation (Liu et al, 2015). 100 μM pyridoxalphosphate-6-azophenyl-2',4'-disulfonic acid (PPADS), a selective P2 receptor antagonist, did not appear to reduce the probability of recording calcium transients in at least one type II cochlear afferent (Table 4.2.1, no PPADS 28/71 vs. PPADS 9/21). However, 100 μM PPADS

significantly restricted the total area of responding neurons to those just proximal to the site of damage (Figure 2.4.1H, no PPADS 62.7% ± 26.0% vs. PPADS 37.7% ± 21.8%, p=**0.033**, n=25 videos, linear mixed model Satterthwaite's method), suggesting that the spread of the damage signal is dependent on ATP. Binding of ATP on supporting cells of the cochlea can cause further ATP release (Anselmi et al., 2008), amplifying and propagating the ATP signal throughout the epithelium. By blocking the propagation of supporting cell activity and the activation of purinergic receptors on the type II cochlear afferent, PPADS might block the distant response of neurons. However, eliminating the effects of ATP is insufficient to prevent responses in all areas of the visible type II afferent dendrites, presumably because other contents of ruptured cells can depolarize neurons (e.g. H^+, K^+, glutamate, etc.) (Cook and McClesky, 2002). Blocking purinergic receptors with 100 μM PPADS while patch clamping apical pre-hearing type II cochlear afferents caused the inward current to narrow, but not disappear, after rupturing OHCs with a sharp electrode (Liu et al., 2015). The remaining depolarization observed while patch clamping a type II cochlear afferent dendrite in the presence of PPADS most likely also causes calcium transients in the proximal type II cochlear afferent segments.
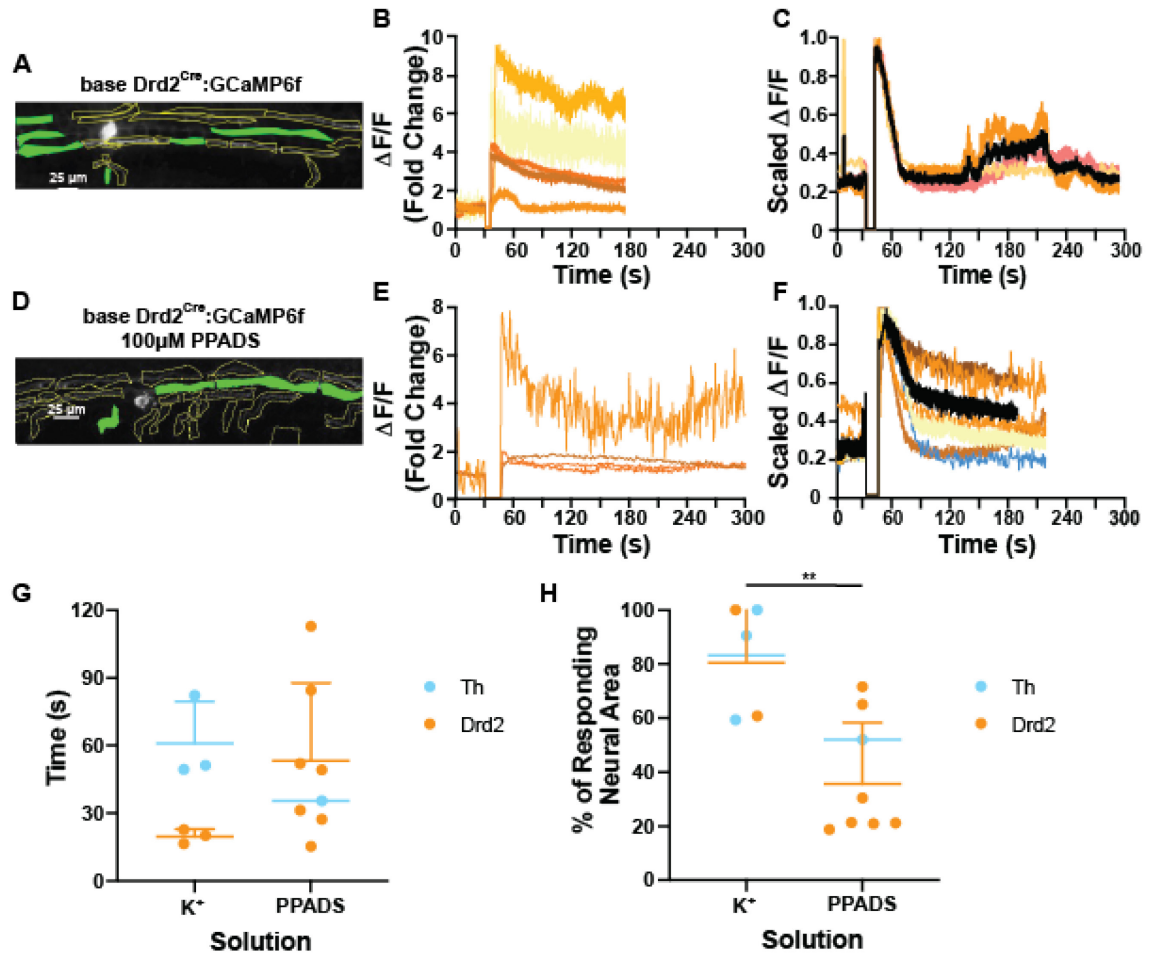
Figure 2.4.1: ATP blockade prevents the response of distant type II cochlear afferent fibers. A. A standard deviation projection image of a pre-hearing Drd2^{Cre}:GCaMP6f with hand drawn ROIs. Green filled in ROIs represent responsive ROIs. Scale bar = 25 μm. B. ΔF/F traces of the transiently responding ROIs in A. ΔF/F at time of photoablation and until imaging restarts is set to 0. C. Averaged and scaled ΔF/F traces of each pre-hearing Drd2^{Cre}:GCaMP6f animal without 100 μM PPADS in the extracellular solution presented with different shades of orange per animal. Black line represents the average of all the animal average traces. ΔF/F at time of photoablation and until imaging restarts is set to 0. D. A standard deviation projection image of a pre-hearing Drd2^{CreER}:GCaMP6f with 100 μM PPADS in the extracellular solution with hand drawn ROIs. Green filled in ROIs represent responsive ROIs. Scale bar = 25 μm. E. ΔF/F traces of the transiently responding ROIs in D. ΔF/F at time of photoablation and until imaging restarts is set to 0. F. Averaged and scaled ΔF/F traces of responses from each pre-hearing Drd2^{Cre}:GCaMP6f animal when 100 μM PPADS was in the extracellular solution with orange colors representing different Drd2^{Cre}:GCaMP6f animal and blue representing TH^{CreER}:GCaMP6f. Black line is the average of all the animal average traces. ΔF/F at time of photoablation and until imaging

restarts is set to 0. G. Histogram of the time of response from the observed peak to the time the response returns within three standard deviations of the steady state. Blue dots represent TH^{CreER}:GCaMP6f animals and orange dots represent Drd2^{Cre}:GCaMP6f animals. Horizontal bar and vertical line represent average and standard deviation for each group. H. Histogram of the proportion of the area of responding neural ROIs to total area of neural ROIs for recordings from pre-hearing mice in 100 µM PPADS and without 100µM PPADS in the extracellular solution. Blue dots represent TH^{CreER}:GCaMP6f animals and orange dots represent Drd2^{Cre}:GCaMP6f animals. Horizontal bar and vertical line represent average and standard deviation for each group.   ** = $p < 0.01$.

2.5 Discussion

The present study combined fluorescent calcium imaging with a novel

dissection strategy to record the activity of basal type II cochlear afferents *ex*

vivo. Moreover, by utilizing a fluorescent calcium reporter, we were able for the

first time to monitor the activity of multiple type II cochlear afferents concurrently

to discover the level of coordination between type II cochlear afferents in varying

conditions. Through these technical innovations, we were able to describe an

ATP dependent activation of distant type II cochlear afferents in response to focal

tissue damage. An interesting difference between electrophysiological

investigation of damage responses in type II afferents and the present damage-

induced calcium transients is that blocking ATP with PPADS had varying effects

(Liu et al., 2015). In the whole cell patch clamp setting PPADS reduces the

kinetics but not the peak current in response to focal ablation. While the calcium

transients closely matched the kinetics of control damage stimuli, PPADS did not

shorten the response time. However, with the benefit of recording multiple

neurons simultaneously responding to a single damage event, there was a

noticeable effect of PPADS on the number of neural ROIs activated by OHC

rupture. The disparity might be explained by the technical differences between

the two approaches: voltage clamp electrophysiology directly measures ion current and the calcium imaging indirectly measures free internal calcium concentrations. Although blocking P2 receptors with PPADS is expected to reduce the current flow after focal ablation there may be other mechanisms that cause rises in internal calcium and either by the natural buffering of Ca^{2+} or by the internal off kinetics of GCaMP6f falls off at the same rate regardless if purinergic receptors are available. It would be helpful to compare the peak $\Delta F/F$ values with and without PPADS in the external solution but because the GaAsP detector shuts off immediately after the ablation event for several seconds the true peak values are unobtainable.

The gradient of genetic markers throughout the cochlea demonstrate that type II cochlear afferents are not a homogeneous population. The two neuron specific Cre driver lines utilized in this chapter subdivide the population of type II cochlear afferents along the tonotopic axis. For all the tested parameters, however, we could not refute the null hypothesis that there are no differences between TH and Drd2-positive neurons besides the position of the type II cochlear afferents within the cochlear spiral. In our recordings, we did note heterogeneity in type II cochlear afferent responses to tissue damage especially across animals, but this was independent of the Cre driver lines. It is possible that these variable responses suggest there are subtypes of type II cochlear afferents, but the present study was not able to distinguish between these as is seen in type I cochlear afferents (Petitpré et al., 2018; Sun et al., 2018; Shrestha et al., 2018). There may be other facets by which TH and Drd2-positive type II

96

cochlear afferents differ, responsiveness to certain neurotransmitters for

example, but the present study was unable to uncover any such differences.

Chapter 3: Focal Ablation Causes Epithelial Cell Activity and is Correlated with Type II Afferent Activity

3.1 Introduction

Calcium signaling in supporting cells has been studied extensively within the cochlea, especially during development, and in response to tissue damage (Gale et al., 2004; Piazza et al., 2007; Tritsch et al., 2007; Sirko et al., 2019). ATP that is either released from connexin hemichannels or from ruptured cells can cause rises in internal calcium and cause further ATP release, resulting in a wave of activity through the supporting cells. Blocking gap junctions had nearly an equal effect of reducing the duration of type II afferent responses to acute tissue damage as direct purinergic antagonists suggesting that the supporting cells may contribute to the damage induced inward currents (Liu et al., 2015). Presumably, the ATP released from the rupture of 1-3 OHCs was amplified through this ATP-mediated ATP release in supporting cells which then can cause a prolonged type II afferent response (Liu et al., 2015). While many supporting cells can still respond to ATP in maturity, the peak in sensitivity occurs around the time of hearing onset when the spontaneous ATP dependent crenations that drive neural activity still occur cells (Berekméri et al., 2019a; Berekméri et al., 2019b; Horváth et al., 2016). Many of these studies utilize a calcium sensitive dye that permeates through the supporting cell syncytium to visualize internal calcium levels among all supporting cells. It is also possible to cross a genetic line that is ubiquitously expressed in supporting cells of the cochlea like Sox2[Cre] with a GCaMP to measure calcium levels (Cox et al., 2012). However, with both

techniques the large spread of fluorescence from the calcium indicators in all supporting cells would occlude fluorescence changes in the thin type II afferent fibers that run mostly between the rows of Deiters' cells. To overcome this limitation while trying to record supporting cells and type II afferents simultaneously we detailed crenation-like non-GCaMP associated fluorescence events (NGAF) and characterized a new genetic line, Tac1[Cre], that has a special tonotopic expression pattern that permits the visualization of type II afferent and supporting cells responses together after focal OHC rupture. Overall, this chapter investigates the response of the epithelial cells, both supporting and hair cells, to focal damage and asks whether the neuronal and epithelial cell responses are related.

3.2 Description of non-GCaMP6f associated fluorescence

To test whether ATP is acting through the supporting cells to cause activation of type II cochlear afferents removed from the site of damage, we needed to be able to observe supporting cell activity concurrently with type II cochlear afferent activity. Unexpectedly, as we imaged the cochlear epithelium, we noticed episodes of autofluorescence transients in the tissue not related to GCaMP6f function, heretofore referred to as Non-GCaMP6f-Associated-Fluorescence or NGAF. This NGAF usually occurs transiently in large swaths of tissue either in the greater epithelial ridge region in pre-hearing animals (Figure 3.3.1A-C) or in the area of the OHCs (Figure 3.3.1D-F). Given the location and duration of events we hypothesized that NGAF was the consequence of

crenations. Crenations are spontaneous waves of supporting cell activity that cause physical shrinkage of the cochlear epithelium and thus can be observed even with differential interference contrast (DIC) imaging (Tritsch et al, 2007; Tritsch and Bergles, 2010). The sensitivity of the two-photon microscope in principle should be able to detect movements of the tissue at this scale.

Incidents of NGAF also occurred throughout the tissue immediately following focal OHC ablation. Moreover, over all conditions, the proportion of times where any neuron responded and where any NGAF was observed were highly correlated (Table 4.2.1, r = 0.89). Both the spontaneous and evoked NGAF events occurred in a mouse with no GCaMP6f expression in any cell type under similar recording conditions suggesting that this phenomenon was not caused by ectopic expression of GCaMP6f but instead is intrinsic to the tissue (Figure 3.3.1A-C).

3.3 Effect of PPADS on non-GCaMP6f associated fluorescence

We counted the proportion of pixels above a certain brightness threshold over time and then took the area under the curve of increases in brightness to measure the magnitude of the NGAF in each video. Videos were taken occasionally from the same cochlea but once a location was ablated no new videos were taken at that spot and instead were moved to a new location far away from the damage. When pooling across animals, there was no significant effect of 100 µM PPADS on NGAF magnitude in videos where an ablation event occurred (Figure 3.3.1G, n=28 videos). This may be due to the large variability

observed across animals and due to the sparsity of videos with NGAF with 100

μM PPADS in the external solution. To circumvent the differences between

recordings, comparisons were made between paired recordings in the same

cochlea with and without 100 μM PPADS in the bath. Videos with 100 μM

PPADS in the bath had reduced area under the curve measures 13 out of 16

times as compared to non-PPADS videos in the same animal with similar testing

protocols (data not shown, p=**.026**, Wilcoxon Ranked Sum Test). Moreover, in

single videos where 100 μM PPADS was introduced during the video, the area

under the curve dropped in 14 out of 18 videos after PPADS was pushed in

(Figure 3.3.1H, p= **0.016**, Wilcoxon Ranked Sum Test). Overall, the dynamics,

location, and ATP dependence of the NGAF suggests these events reflect ATP-

dependent waves of activity among the supporting cells of the cochlea. (Gale et

al. 2004, Ceriani et al. 2016, Sirko et al., 2019).
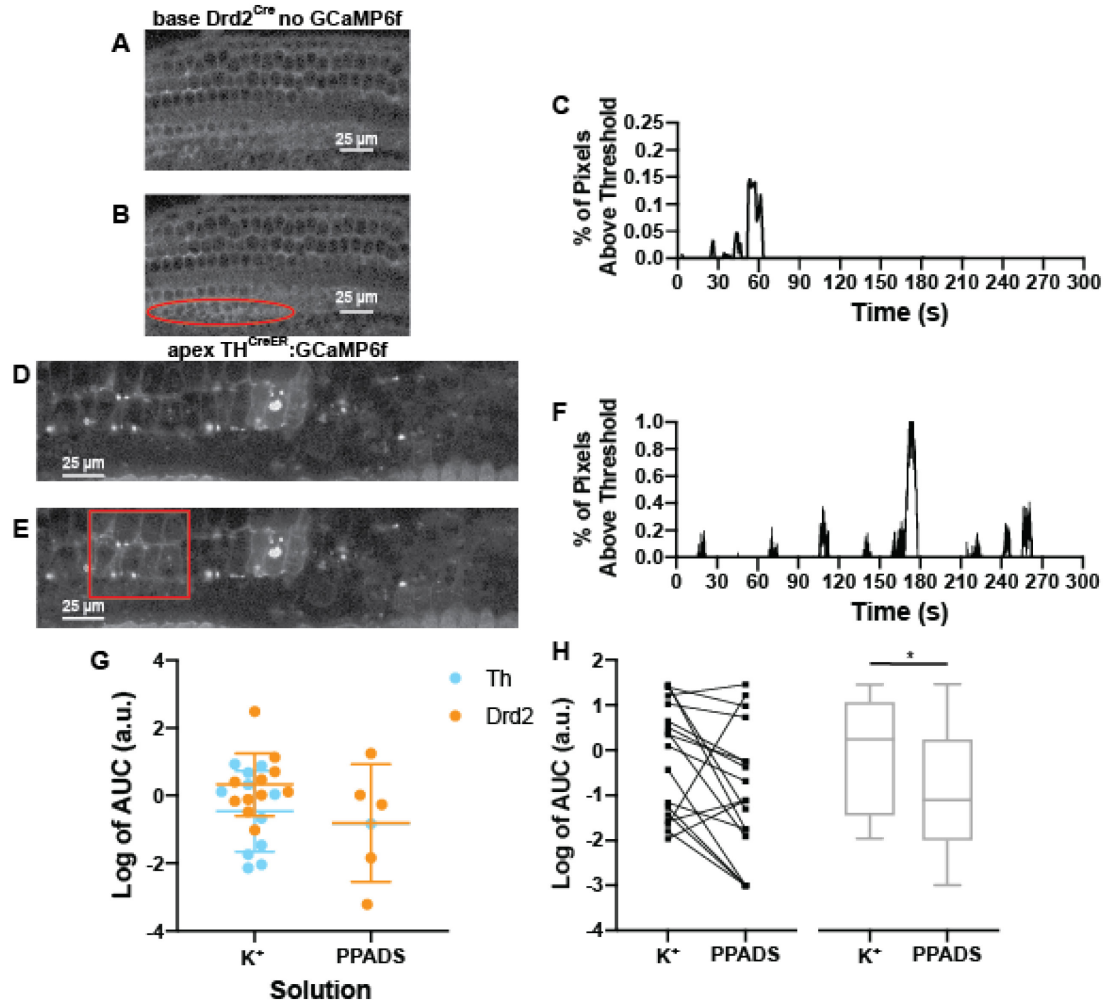
Figure 3.3.1: Non-GCaMP6f associated fluorescence (NGAF) is PPADS sensitive and can occur spontaneously. A. Standard deviation image of a recording from a pre-hearing Drd2Cre animal with no GCaMP6f expression. B. Same image as A. but with a red outline overlaid where a spontaneous increase in fluorescence occurred. Scale bars = 25 µm. C. Percent of total green pixels above an arbitrary threshold from spontaneous events from the recording in A. D. Standard deviation image of a recording from a mature Drd2Cre:GCaMP6f animal. E. Same image as D. but with a red outline overlaid where a spontaneous increase in fluorescence occurred. Scale bars = 25 µm. F. Percent of total green pixels above an arbitrary threshold from spontaneous events from the recording in E. G. Histogram of log transformed values from taking the area under the curve of spontaneous increases in green pixels above an arbitrary threshold. Blue dots represent the value from single videos from THCreER:GCaMP6f animals and orange dots single videos represent Drd2Cre:GCaMP6f animals. Horizontal bar and vertical lines represent average and standard deviation for each group. H. (Left) Paired dot and (Right) box and whisker plot of log transformed area under the curve values from paired recordings before and after the addition of 100 µM PPADS in the extracellular solution. * = p<0.05.

3.4 Generation and verification of Tac1[Cre]:GCaMP6f mouse model

Despite the evidence that the observed NGAF corresponds to supporting cell activity, NGAF is not as reliable or as bright a signal as the fluorescence from the GCaMP6f expressing cells, with GCaMP6f-mediated ΔF/F signals approximately an order of magnitude larger than NGAF signals (Figure 3.4.2B). A better system would be to have both supporting cells and type II cochlear afferents express GCaMP6f jointly. Without resorting to a combinatorial approach, no reported expression pattern would allow for this arrangement. Even with a genetic calcium reporter in the supporting cells, the percentage of supporting cells expressing the reporter would need to be reduced to see the neurites of the neurons underneath. Other researchers have taken to electroporating calcium dyes into supporting cells in a hemicochlea preparation to observe calcium transients in adult supporting cells (Berekméri et al., 2019a; Berekméri et al., 2019b; Horváth et al., 2016). However, this approach would not be helpful as the anatomy of type II cochlear afferents prevent the hemicochlea preparation and single cell electroporation would not reveal the extent of the supporting cell response spread.

To overcome these limitations, we crossed Tac1[Cre] mice with floxed GCaMP6f mice to express GCaMP6f in all cell types that have expressed Tac1 at any point during development. Tac1 is a gene that through alternative splicing leads to the production of four different neuropeptides, including Substance P (Krause et al., 1987). Tac1 is known to be expressed in peptidergic somatosensory neurons in the dorsal root ganglia (Kestell et al., 2015). Recent

RNA-seq work on cochlear afferents suggested that type II cochlear afferents and one subtype of type I cochlear afferents could express Tac1 (Shrestha et al., 2018). When we crossed Tac1[Cre] mice with Ai9, floxed tdTomato, reporter mice, we noticed a unique expression pattern. Most strikingly, there is a smooth gradient of expression across epithelial cells (both hair cells and supporting cells) with the apex having nearly every cell expressing Ai9 and the base having no expression in any epithelial cell (Figure 3.4.1A,F,G). In stark contrast, the spiral ganglion has a subset of neurons expressing Ai9 corresponding to all type II cochlear afferents that is constant in proportion across the cochlear length except at the extreme apical tip (Figure 3.4.1H, **p=0.0082**, N=5 mice, one-way ANOVA). Even in all other genetic lines that label type II afferents there is little to no expression at the extreme apex suggesting there may be no neurons located at that position due to the geometry of the spiral ganglion within the cochlea (Figure B12C, Vyas et al., 2019). If one excludes the counts from the first 10% of the cochlea, there is no significant difference between the remaining areas along the cochlear spiral (p=0.17, N=5 mice, one-way ANOVA). Ai9 was expressed in a greater number of neurons than any other type II afferent specific genetic line as well. For example, Drd2 was expressed in 125 ± 61 neurons whereas Tac1 was expressed in 393 ± 55 neurons (Figure B12D, Vyas et al., 2019). This could partly be because Drd2 is expressed in the basal half of the cochlea while Tac1 is strongly expressed in over 90% of the cochlea. The remaining difference could mean that a small percentage of type I cochlear afferents also express Tac1.

This is a distinct possibility because RNA-seq showed expression of Tac1 in type II afferents as well as a subset of type I afferents (Shrestha et al., 2018).

This expression pattern is unlike any other published reporter that labels type II cochlear afferents. In the apex, Tac1 expression appears like the ubiquitous expression pattern of Sox2Cre reporters and could be useful for observing large scale epithelial cell activity (Cox et al., 2012). Recordings from this area in pre-hearing Tac1Cre:GCaMP6f show large spontaneous wave-like events in the greater epithelial ridge region just as would be expected from crenation events (Figure 3.4.1B-C). Focal ablation in the OHC region causes calcium increases across the entire visible portion of the cochlea (Figure 3.4.1D-E). Additionally, ablating in the presence of 100 µM PPADS appears to reduce the spread of the damage signal through the epithelial tissue as well.

In the base, the Tac1 expression is similar to the Drd2 expression and could be used as another model to image basal type II cochlear afferents by themselves. Even though there are very few or even no epithelial cells expressing GCaMP6f in the base of the cochlea we still observe NGAF in the Tac1Cre:GCaMP6f model (Figure 3.4.2D-E). In conjunction with immunostaining for GCaMP6f, the coexistence of real GCaMP6f signals alongside the NGAF phenomenon in the same animal, even occasionally in the same video, suggests that the NGAF is not due to ectopic expression of GCaMP6f in epithelial cells.

The most novel use of the expression pattern, however, is the imaging in the middle turn where there is a haphazard arrangement of epithelial cells allowing for concurrent viewing of type II cochlear afferent neurites through the

gaps in epithelial cell expression (Figure 3.4.2A-C). Analysis of videos in this region allow us to observe calcium events happening simultaneously in epithelial cells and type II cochlear afferents. The difference between NGAF events and real GCaMP6f dependent changes in fluorescence in epithelial cells is readily apparent. In the cases with GCaMP6f, the brighter signals are restricted to cell membranes instead of the more diffuse signal seen in NGAF events (Figure 3.4.2A-B). Each individual epithelial cell has brief calcium transients that can repeat multiple times (Figure 3.4.2E). Even when averaging the total response of multiple epithelial cells together, these GCaMP6f dependent responses have a significantly shorter time constant of decay than the NGAF signal or the GCaMP6f signal in the type II afferents (Figure 3.4.2G, NGAF 30.9 ± 21.5 s, type II GCaMP6f 36.0 ± 24.3 s, vs. epithelial cell GCaMP6f 11.9 ± 7.8 s, **p= 0.014**, n=15 videos, linear mixed model Satterthwaite's method). This contrasts with NGAF events which persist longer, similar to the neuron time constants, than responses in epithelial cells with actual GCaMP6f expression. This suggests that NGAF events are not exact readouts of calcium within the epithelial cells, but instead are the products of slower, mechanical changes in the tissue, such as crenations.
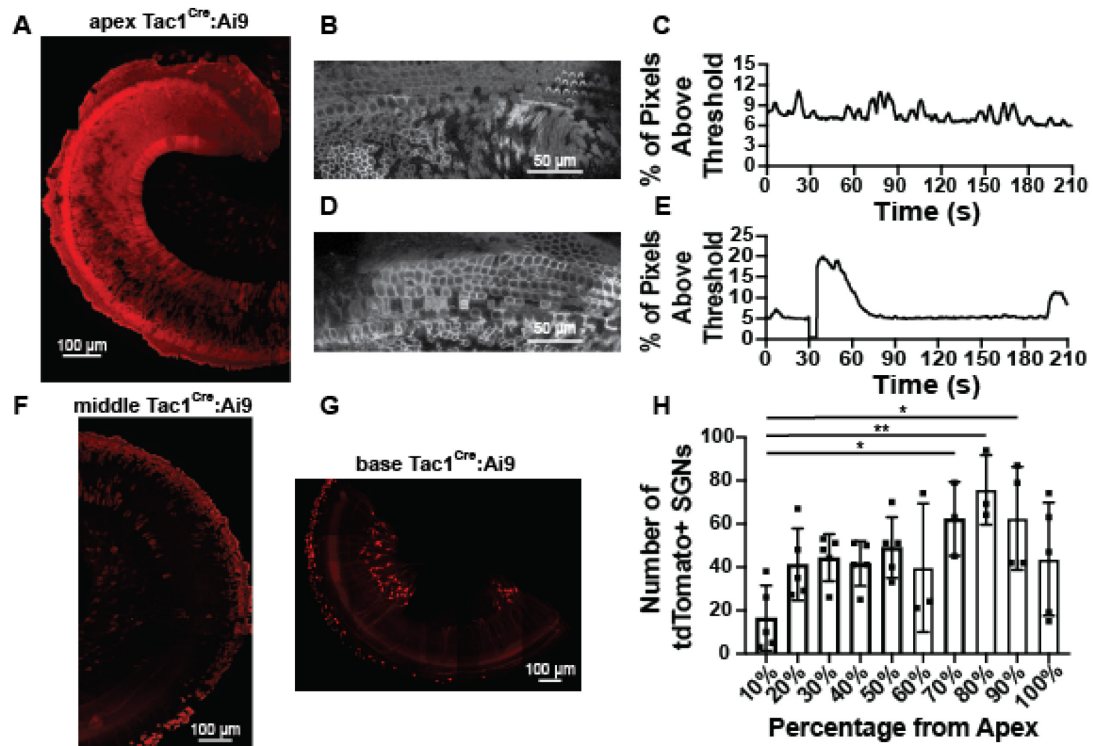
Figure 3.4.1: Expression of GCaMP6f by Tac1^{Cre} driver labels type II afferents along the tonotopic axis and has broad supporting cell expression in the apex. A. 5x magnification confocal image of a pre-hearing Tac1^{Cre}:Ai9 mouse apical section of cochlea. Red channel is anti tdTomato (Tac1^{Cre} expressing cells). Scale bar = 100 µm. B. Standard deviation image of an apical section of a pre-hearing Tac1^{Cre}:GCaMP6f mouse cochlea undergoing spontaneous crenations. Scale bar = 25 µm. C. Trace of percent of pixels above an arbitrary brightness threshold over time for the video shown in B. D. Standard deviation image of a focal ablation in the same region as the video from B. in the apical section of a pre-hearing Tac1^{Cre}:GCaMP6f mouse cochlea. Scale bar =25 µm. E. Trace of percent of pixels above an arbitrary brightness threshold over time for the video shown in D. Percent of bright pixels at time of photoablation and until imaging restarts is set to 0. F. 5x magnification confocal image of a pre-hearing Tac1^{Cre}:Ai9 mouse middle section of cochlea. Red channel is anti TdTomato (Tac1^{Cre} expressing cells). Scale bar = 100 µm. G. 5x magnification confocal image of a pre-hearing Tac1^{Cre}:Ai9 mouse basal section of organ of Corti. Red channel is anti TdTomato (Tac1^{Cre} expressing cells). Scale bar = 100 µm. H. Histogram of spiral ganglion cell somata count with 10 bins across the tonotopic axis. * = $p<0.05$., ** = $p<0.01$.
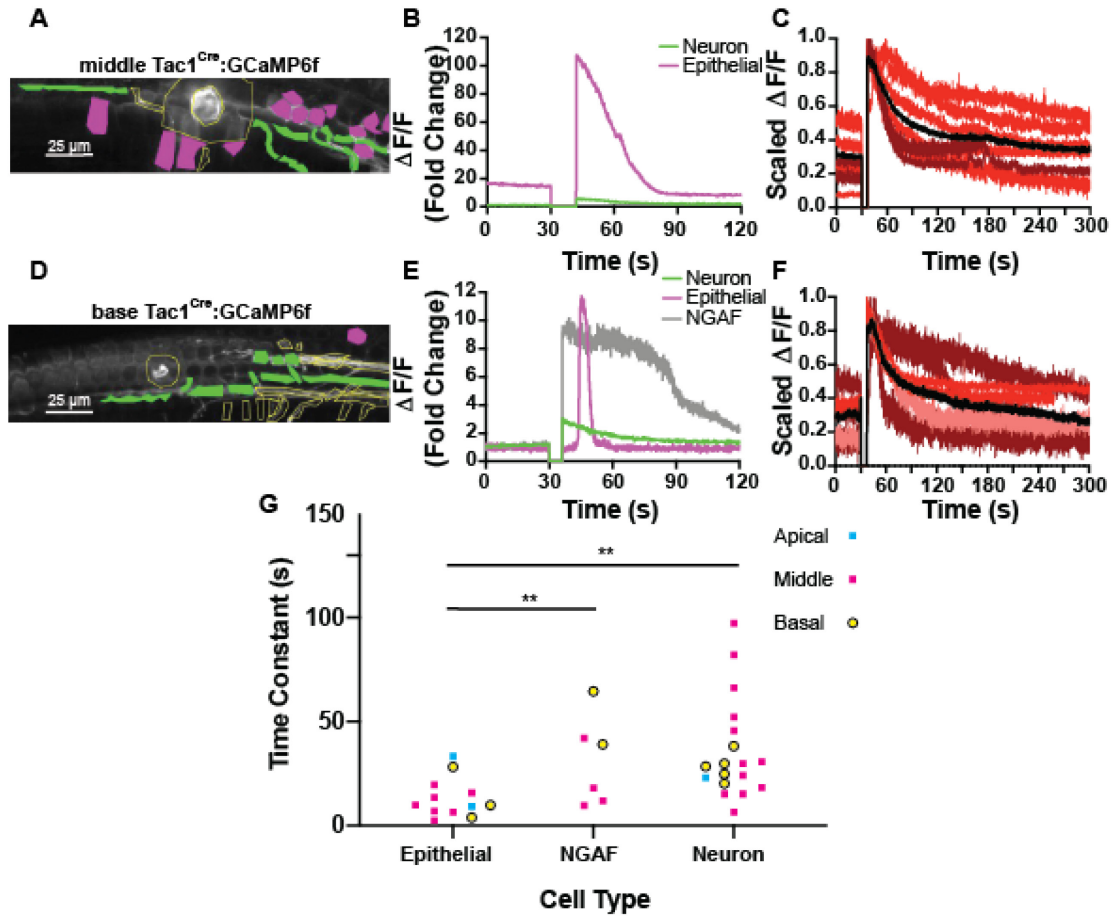
Figure 3.4.2: Expression of GCaMP6f by Tac1[Cre] driver reveals type II afferent activity in the base as well as epithelial cell calcium activity in the middle section of the cochlea. A. Standard deviation image of a focal ablation in the middle section of a pre-hearing Tac1[Cre]:GCaMP6f mouse cochlea with hand drawn ROIs around segments of neurons and epithelial cells. Scale bar = 25 μm. Green filled neuronal segments represent neurons that significantly respond to the stimulus and magenta filled epithelial cells represent epithelial cells that significantly respond. B. Average ΔF/F traces from responding ROIs in A. Supporting cell response average shown in magenta and average neuron trace in green. ΔF/F at time of photoablation and until imaging restarts is set to 0. C. Averaged and scaled ΔF/F traces for neuronal responses (shades of red) from the middle sections of Tac1[Cre]:GCaMP6f mice. Black line is the average of all the animal average traces. ΔF/F at time of photoablation and until imaging restarts is set to 0. D. Standard deviation image of a focal ablation in the basal section of a pre-hearing Tac1[Cre]:GCaMP6f mouse cochlea with hand drawn ROIs around segments of neurons and epithelial cells. Scale bar = 25 μm. Green filled neuronal segments represent neurons that significantly responded to the stimulus and magenta represent epithelial cells that significantly respond. E. Average ΔF/F traces from responding ROIs in D. Non-GCaMP6f associated fluorescence trace shown in gray, average epithelial cell response in magenta and average neuron response in green. ΔF/F at time of photoablation and until

imaging restarts is set to 0. F. Averaged and scaled ΔF/F traces for neuronal responses (shades of red) from the basal sections of Tac1^{Cre}:GCaMP6f mice. Black line is the average of all the animal average traces. ΔF/F at time of photoablation and until imaging restarts is set to 0. G. Histogram of the individual time constants of decay for responses from NGAF, epithelial cell and neuron ROIs across all Tac1^{Cre}:GCaMP6f mice across the cochlea. Blue dots represent responses from apical cochlea sections, magenta from middle cochlea sections, and yellow from basal cochlea sections. ** = $p < 0.01$.

3.5 Discussion

Supporting cells are known to release ATP in a wave-like manner after focal damage to cochlear tissue (Gale et al., 2004). It follows that type II afferents could respond to both the initial ATP released from the rupture of cells and the subsequent supporting cell activity but supporting cells and type II afferents have not been studied concurrently before this study. The closest example is the use of a connexin blocker while recording type II afferent current changes to focal OHC ablation. The connexin blocker had a similar effect as PPADS in the recorded neurons suggesting that the longer ATP effect could have been solely from the ATP released from supporting cells and the initial current influx that remains after these blockers is from the direct products released from inside the damaged cells, such as K^+, glutamate, etc.

The high sensitivity of two-photon microscopy allowed for the imaging of type II afferent dendrites with high spatial resolution but also can capture slight movements in the tissue that cause changes in optical density. In a majority of the videos from pre-hearing animals there was fluorescence that based on the location and the susceptibility to PPADS suggests that the NGAF signal is the result of movement of epithelial cells. The timing of the NGAF events was similar

to that of the neuron responses which could reflect the amount of time that ATP was present in the nearby extracellular fluid, driving both the crenation-like activity and the neuronal calcium transients. Unfortunately, because of the lag between ablation and recording we could not determine whether NGAF preceded neuronal responses or vice versa. An approach that does not use the bleaching settings of the two-photon microscope such as sharp electrode ablation may allow for continuous recording and could elucidate the timing of the spread of NGAF and neuronal responses and their temporal ordering.

Alongside the two previously reported genetic markers, we described a new genetic marker and its expression profile throughout the cochlea. The unique expression pattern of Tac1^{Cre} in the cochlea combined with previously described technical advancements allowed for the first simultaneous recording of type II cochlear afferents and epithelial cell calcium transients. Substance P, a neuropeptide encoded by the Tac1 gene (Krause et al., 1987), is commonly released by peptidergic somatosensory neurons that typically convey noxious stimulus information. Peptidergic somatosensory neurons frequently co-express Calca, the gene encoding CGRPα (Kestell et al., 2015). Interestingly, a tonotopically restricted subpopulation of type II cochlear afferents also expresses Calca (Wu et al., 2017). As with TH and Drd2 expression in certain subpopulations of type II cochlear afferents it is uncertain whether Tac1 or Calca expression signifies functional release from the neurons, let alone production under any circumstance. It is presumed that synaptic transmission from type II cochlear afferents to their downstream targets in the cochlear nucleus is

glutamatergic just like the type I cochlear afferents (Hackney et al., 1996), but this has not yet been verified. There have been suggestions that type II cochlear afferents make local synapses in the periphery (Fechner et al., 2001). Thus, it is also possible that type II afferents could utilize alternative release methods such as bulk transmitter or peptide release within the cochlea with any or all these signaling molecules.

Chapter 4: Effects of Maturity and Traumatic Noise Exposure on Epithelial Cell and Type II Afferent Activity

4.1 Introduction

Both as the cochlea matures and following traumatic noise exposure, many anatomical and cellular changes occur. Around the time of hearing onset, the supporting cells that release ATP periodically to activate neighboring type I afferents disappear. This process also affects type II afferent development as interrupting this ATP signaling by knocking out connexin 30 causes defects in the arborization of type II dendrites underneath the OHCs (Ceriani et al., 2019). The transient nature of ATP availability combined with the possible reduced response of type II afferents to ATP (Weisz et al., 2009) suggests that ATP, and by extension damage, responses may be restricted to the pre-hearing developmental time window. However, systematic study of mature type II afferents has been hindered by the difficulty of adult recordings. The calcium imaging and improved dissection techniques described here have allowed for the first glimpses into type II afferent responses to damage in mature cochleae.

Another potentially significant change in type II afferent function, if they serve as auditory nociceptors, is after traumatic noise exposure. If type II afferents act as nociceptors, they might become sensitized after damage, like what happens with somatic nociceptors in allodynia (Andrew and Greenspan, 1999; Smith et al., 2013; Murthy et al., 2018). Noise damage also can cause ribbon loss and dendrite retraction in the type I afferent synapses (Kujawa and Liberman, 2009; Kaur et al., 2015). However, both the anatomical and

physiological changes in the OHCs and type II afferents have been overlooked. In this chapter, mature responses to damage before and after traumatic noise is investigated to determine the role of type II afferents in responding to damage in hearing animals.

4.2 Type II afferent responses to tissue ablation are reduced but not eliminated in adult cochleae

Imaging the organ of Corti in mostly intact cochleae not only allowed recording of basal neurons, but also extended the capabilities of recording activity in fully mature tissue which was previously intractable. Adult type II cochlear afferents were still capable of responding to focal ablation stimuli (Figure 4.2.1A-I); however, responses happened about one third as often as in cochleae from young animals, even in cases where neurons were clearly visible and damage occurred (Table 4.2.1, mature 15/63 vs. pre-hearing 28/43, p=**4.92e-05,** generalized mixed model). Although in the mature condition there were more failures to produce damage, the decrease in response rate when damage occurred could not be explained by a decrease in the amount of damage caused by the focal laser ablations because the area of damage was not significantly different between the pre-hearing and mature animals. Interestingly though, the size of the scar caused by the laser was significantly larger (with response 305.8 ± 251.6 μm^2 vs. without response 209.8 ± 182.7 μm^2, **p=0.0085**, n=153 linear mixed model Satterthwaite's method) in cases where the damage caused type II afferent responses, regardless of age. This suggests there may be

some correlation between the amount of damage and the neuronal response or at least a minimum threshold needed to evoke neuronal responses.

In recordings featuring transiently responding neurons, the time from observed peak to steady state was significantly longer in adult as compared to pre-hearing animals (Figure 4.2.1L, mature 73.5 ± 74.9 s vs. pre-hearing 42.5 ± 25.0 s, p= **0.025**, n=42 videos, linear mixed model Satterthwaite's method). Interestingly, in the adult cochleae there were incidents of neurons having delayed responses to the ablation (Figure 4.2.1C, Figure 4.3.2). In contrast, nearly all the pre-hearing neurons responded with a calcium transient immediately after the ablation and with no secondary, delayed responses. Moreover, the neuronal area was significantly reduced when comparing adult and pre-hearing responses without the presence of PPADS (Figure 4.2.1J, pre-hearing 63% ± 26% vs. mature 41% ± 15%, p=**.0030,** n=41 videos, linear mixed model Satterthwaite's method). The neuronal area in adult cochleae, however, was not affected by PPADS unlike what was seen in the pre-hearing animals (interaction between age and PPADS linear mixed model Satterthwaite's method, p=**.0036**).

As expected, if NGAF reflects epithelial cell activity, the frequency of observed NGAF is reduced in adult tissue compared to young tissue, but not completely eliminated (Table 4.2.1, mature 48/163 vs. pre-hearing 52/107, p= **.0052,** generalized mixed model). The magnitude of these events was also decreased by measuring the area under the curve of transient increases in brightness (Figure 4.2.1K, pre-hearing 13.0 ± 55.9 au vs. mature 3.3 ± 8.4 au,

p=**0.0026,** n=73 videos, linear mixed model Satterthwaite's method). When these transient autofluorescence events did occur, they were situated mostly in the OHC region instead of the greater epithelial ridge region as was the case in the pre-hearing animals (Sirko et al., 2019).

Age-related deficits in responding to stimuli appear to have two dissociable elements: an increase in the threshold for neuronal responses and a decrease in the ATP-dependent signal. The decrease in the neuronal area and the deficits in the NGAF signal mirror the effects of PPADS in the pre-hearing animals. Buttressing this finding is the fact that the effect of PPADS is occluded by the effects of aging. PPADS does not further reduce the neuronal area or the magnitude of NGAF events presumably because there is so little ATP in the adult cochlea. One major difference between the recordings of pre-hearing tissue with PPADS and recordings in mature tissue, however, is the smaller proportion of mature recordings with any neuron response or any NGAF event at all. This phenomenon could point to a change in the likelihood to initiate events in an ATP-independent manner.
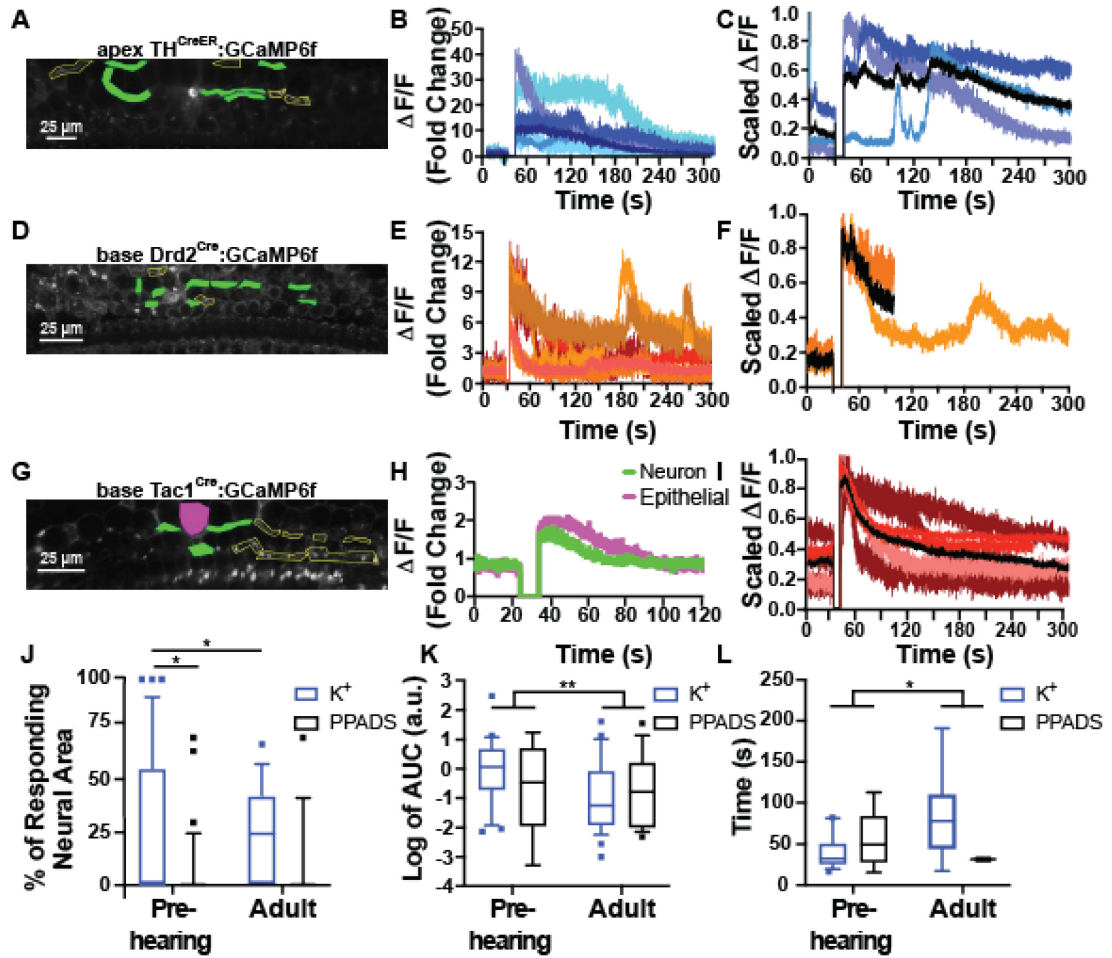
Figure 4.2.1: Mature organs of Corti have reduced spread of non-GCaMP6f associated fluorescence and neuronal activation. A. Standard deviation image of a mature TH[CreER]:GCaMP6f mouse apical cochlea after focal ablation with hand drawn regions of interest around segments of neurons. Green filled neuronal segments represent neurons that significantly responded to the stimulus. Scale bar = 25 µm. B. ΔF/F traces from responding ROIs in A. Black line is the average of all the animal average traces. ΔF/F at time of photoablation and until imaging restarts is set to 0. C. Averaged and scaled traces of all mature TH[CreER]:GCaMP6f recordings. Black line is the average of all the animal average traces. ΔF/F at time of photoablation and until imaging restarts is set to 0. D. Standard deviation image of a mature Drd2[Cre]:GCaMP6f mouse basal cochlea after focal ablation with hand drawn ROIs around segments of neurons. Green filled neuronal segments represent neurons that significantly responded to the stimulus. Scale bar = 25 µm. E. ΔF/F traces from responding ROIs in D. Black line is the average of all the animal average traces. ΔF/F at time of photoablation and until imaging restarts is set to 0. F. Averaged and scaled traces of all mature Drd2[Cre]:GCaMP6f recordings. Black line is the average of all the animal average traces. ΔF/F at time of photoablation and until imaging restarts is set to 0. G. Standard deviation image of a mature Tac1[Cre]:GCaMP6f mouse basal cochlea

116

after focal ablation with hand drawn ROIs around segments of neurons. Green filled neuronal segments represent neurons that significantly responded to the stimulus and magenta filled segment for the responding epithelial cell. Scale bar = 25 µm. H. ΔF/F traces from responding ROIs in G. Black line is the average of all the animal average traces. ΔF/F at time of photoablation and until imaging restarts is set to 0. I. Averaged and scaled neuronal traces of all mature Tac1^{Cre}:GCaMP6f recordings. Black line is the average of all the animal average traces. ΔF/F at time of photoablation and until imaging restarts is set to 0. J-M. Box-and-whisker plots of (J.) the proportion of area of responding neural ROIs to total area of neural ROIs, (K.) log transformed values of the area under the curve of spontaneous increases in fluorescence, and (L.) time of response from the observed peak to the time the response returns within two standard deviations of the steady state for recordings from mature mice in 100 µM PPADS (black) and without 100µM PPADS in the extracellular solution (dark blue). * = $p < 0.05$, ** = $p < 0.01$.

	Pre-hearing	Mature	Apex (Th)	Base (Drd2)	External	PPADS	Total
Total # of videos	129	147	122	152	220	56	276
# with neurons in view	90	102	71	121	150	42	192
Total # of mice	23	25	20	27	48	24	48
# of mice with neurons in view	20	24	20	24	44	17	44
# Photoablation with neural response	28	9	13	24	28	9	37
# Photoablation without neural response	21	35	27	29	43	13	56
# Photoablation with no damage	11	35	16	30	41	5	46
# with NGAF	80	53	53	78	106	27	133

Table 4.2.1: Number of videos recorded in various conditions for TH^{CreER}: and Drd2^{Cre}:GCaMP6f animals. The original dataset consisted of 48 mice of both sexes and 276 videos. Due to exclusion criteria, this was cut down to 192 videos from 44 mice of both sexes. To determine the rate of success for photoablation take the proportion of (# photoablation with neural response/ # photoablation with neural response + # photoablation without neural response) within a single column. To determine the proportion of videos with NGAF take the proportion of (# with NGAF/ total # of videos) within a single column.

	Pre-hearing	Mature	Apical	Mid	Basal	External	PPADS	Total
Total # of videos	36	38	14	50	10	58	16	74
Total # of mice	6	8	9	10	6	12	8	14
# Photoablation with response	14	7	3	13	5	18	3	21
# Photoablation without neural response	6	8	2	11	1	7	7	14
# Photoablation with no damage	4	9	2	9	2	12	1	13
# with supporting cell response	24	4	11	14	3	23	5	28
# with NGAF	2	13	0	11	4	10	5	15

Table 4.2.2: Number of videos recorded in various conditions for Tac1[Cre]:GCaMP6f animals. The original dataset consisted of 14 mice of both sexes and 74 videos. To determine the rate of success for photoablation take the proportion of (# photoablation with neural response/ # photoablation with neural response + # photoablation without neural response) within a single column. To determine the proportion of videos with NGAF take the proportion of (# with NGAF/ total # of videos) within a single column.

4.3 Change in response profile of type II afferent from noise damaged mice

To test if previous traumatic noise exposure affects the damage response of type II afferents, we subjected mice to 2 hours of 110 dB broadband noise and compared their responses 7 days later to their control untraumatized littermates and to two wild-type C57Bl6j mice. Hearing thresholds as measured with ABRs

were significantly elevated in both genotypes after acoustic trauma (Figure 4.3.1, two-way ANOVA, N=25 mice, p= <0.0001). The control littermates were not significantly different from the other non-noise-exposed adult mice used in other experiments in terms of bleach success rate, NGAF rate, or any other tested metric. Therefore, for some analyses that were lacking in sample size noise-exposed animals were compared to all non-noise-exposed adult mice. Noise-exposed animals had a significantly higher occurrence of NGAF at some point within the video (Table 4.3.1, noise-exposed 37/74 vs. non-noise-exposed 26/79, p= **.049,** generalized linear model) than even their non-noise-exposed littermates but, overall, there was not a significant effect on the magnitude of those events when they occurred. When comparing the initial time back to baseline neuronal activity after an ablation event between noise-exposed and all non-noise-exposed adult mice, the noise-exposed animals had a significantly longer time of response (noise-exposed 166.2 ± 79.5 s vs. non-noise-exposed 73.5 ± 74.9 s, **p= .014,** n=16 videos, linear mixed model Satterthwaite's method). Interestingly, the control littermates also had significantly larger magnitude NGAF events as compared to the other non-noise-exposed adult mice (8.1 ± 14.0 au vs. 3.3 ± 8.4 au, **p=0.015**, n=16 videos, linear mixed model Satterthwaite's method). Neuronal area was not affected however with similar proportions of neuronal activation after a damage event among all adult mice.

Upon closer inspection, many of the NGAF events in these noise-exposed animals and their non-noise-exposed adult littermate controls happened several minutes after the onset of focal ablation. On occasion, the late NGAF response

was accompanied by a late neuronal response (Figure 4.3.2A-C, E). A late

NGAF and/or neuronal response trended towards significance when compared

with their control littermates (Figure 4.3.2D, noise-exposed 16/31 vs. non-noise-

exposed 10/34, p= 0.081, Fisher's exact test for count data). Noise-exposed

animals have a delayed response to focal ablation when compared to all non-

noise-exposed adults (Figure 4.3.2D, noise-exposed 16/31 vs. non-noise-

exposed 22/89, **p= 0.0075,** Fisher's exact test for count data). For example,

epithelial cells from the mid-apical turn of a noise damaged Tac1^{Cre}:GCaMP6f

animal underwent waves of activity that persisted for tens of minutes after focal

ablation. In this example animal a second focal ablation in PPADS prevented

delayed action (data not shown). Only in a few cases was this phenomenon ever

witnessed in pre-hearing animals (3/54). Overall, noise exposure seems to

increase the frequency of NGAF events and alter the time course of cochlear

responses such that responses last longer and repeat themselves minutes after

the damage stimulus has ended.
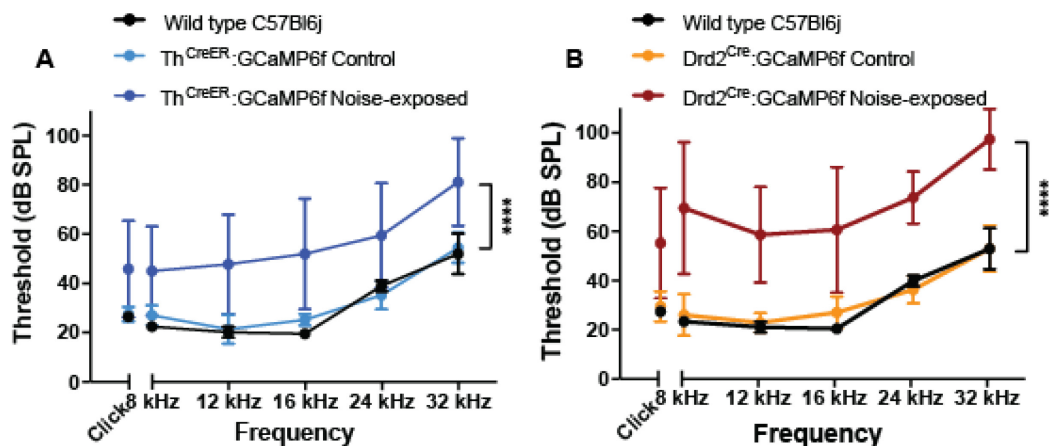
Figure 4.3.1: Acoustic trauma causes elevated thresholds in TH[CreER]:GCaMP6f and Drd2[Cre]:GCaMP6f mice. A. Average ABR threshold measurements from noise-exposed TH[CreER]:GCaMP6f mice and their control littermates seven days after acoustic trauma. Light blue trace represents control mice and dark blue represents noise-exposed mice. Black trace represents 2 control wild type mice tested. B. Average ABR threshold measurements from noise-exposed Drd2[Cre]:GCaMP6f mice and their control littermates seven days after acoustic trauma. Orange trace represents control mice and red represents noise-exposed mice. Black trace represents the same 2 control wild type mice tested in A. **** = p<0.0001.
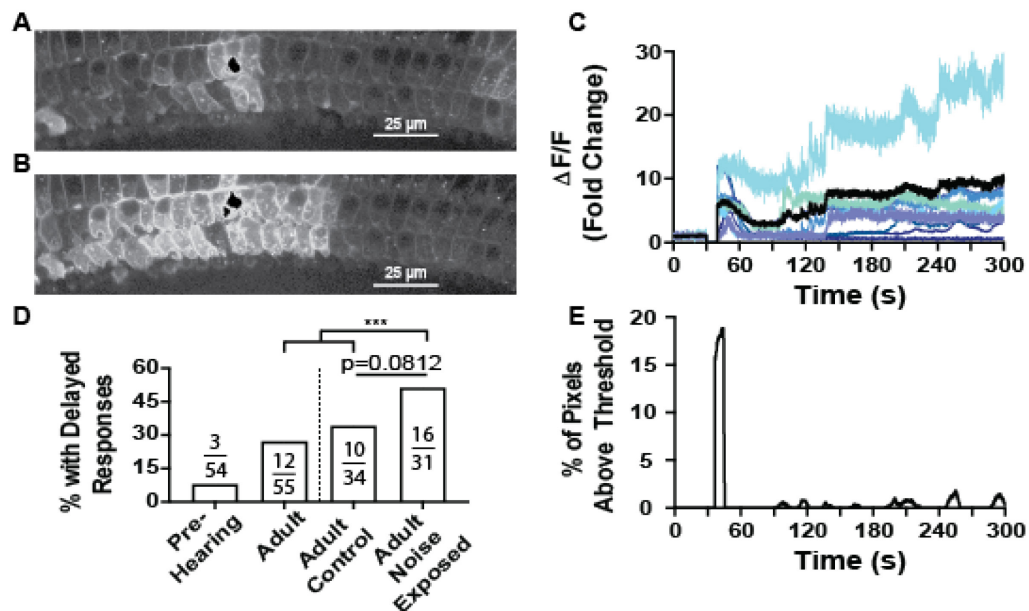
Figure 4.3.2: Previous acoustic trauma increases the chance for cochlear activity long after an acute damage stimulus has subsided. A. Standard deviation image of a mature 7 days post-noise exposure TH[CreER]:GCaMP6f mouse apical cochlea 30 seconds after focal ablation for 30 seconds. B. Standard deviation image of the mature 7 days post-noise exposure TH[CreER]:GCaMP6f mouse apical cochlea from A. minutes after focal ablation for 30 seconds. Scale bars = 25 µm. C. ΔF/F traces from responding neural segments in A-B. Black line is the average of all the animal average traces. ΔF/F at time of photoablation and until imaging restarts is set to 0. D. Bar plot of the proportion of videos that have NGAF and/or neural activity re-emerge minutes after the photoablation in different conditions. Number of videos with delayed response over the number of videos with an ablation event displayed in each bar of the bar graph. *** = p<0.001. E. Percent of total green pixels above an arbitrary threshold from spontaneous events from the recording in A-B.

	NE	Control	TH	Drd2	External	PPADS	Total
Total Number of Videos (#)	74	79	108	45	127	26	153
# with neurons in view	52	62	89	25	93	21	114
Total # of mice	12	13	18	7	25	14	25
# of mice with neurons in view	11	12	18	5	25	14	23
# Photoablation with neural response	9	7	16	0	15	1	16
# Photoablation without neural response	12	17	22	7	22	7	29
# Photoablation with no damage	1	4	4	1	3	2	5
# with NGAF	27	18	33	12	36	9	45
# with delayed response	16	10	23	3	25	1	26

Table 4.3.1: Number of videos recorded in various conditions for TH[CreER]: and Drd2[CreER]:GCaMP6f litters where half were noise-exposed and the other half were controls. The original dataset consisted of 25 mice of both sexes and 153 videos. Due to exclusion criteria, this was cut down to 114 videos from 23 mice of both sexes. Ages ranged from 7-9 weeks. NE stands for noise exposed. To determine the rate of success for photoablation take the proportion of (# photoablation with neural response/ # photoablation with neural response + # photoablation without neural response) within a

single column. To determine the proportion of videos with NGAF take the proportion of (# with NGAF/ total # of videos) within a single column.

4.4 Noise exposure increases subnuclear OHC ribbon synapses and can cause increased action potential generation in type II afferents

The preceding studies focused on the role that waves of ATP release by supporting cells might play in activating type II cochlear afferents. A separate question is whether glutamate release from OHCs also might be altered after acoustic trauma and thus contribute to type II activation. In pursuit of this question, a similar noise exposure protocol in a different cohort of animals was found to increase the number of presynaptic ribbons of OHCs (Wood et al., in press). The total number of CtBP2 puncta was not significantly affected by noise exposure but more ribbons were localized to the synaptic zone underneath the nucleus (Figure 4.4.1C, 1.36 ± 0.19 synaptic ribbons per OHC vs. 1.14 ± 0.22 synaptic ribbons per OHC, **p=0.0065**, N=12 mice, linear mixed model Satterthwaite's method). In the same animals there was a significant decrease in the number of ribbons in IHCs as has been detailed in other studies (Stamataki et al., 2006; Kujawa and Liberman, 2009).

What might be the functional consequence of increased OHC synaptic ribbons? A simple mathematical model was designed to address this question. This asked whether the change in ribbon numbers alone could alter the summed type II afferent activity produced by loud, broad-band sound in a post-trauma cochlea compared to that of control. Previously published intracellular recording from type II afferents showed that there are on average 9 functional presynaptic OHCs per type II afferent (range 1 to 31) (Weisz, Lehar et al. 2012). These

authors also demonstrated that maximal stimulation of an OHC had a one in four

chance of releasing a single vesicle. Each vesicle causes a 4mV depolarization

on average, thus requiring 7 or more concurrent vesicles for the type II afferent to

reach the 25 mV threshold for action potential initiation (Weisz et al. 2012).

To account *in silico* for the wide variability in connectivity, we generated a

normally distributed dataset around the means for the number of ribbons per 9

OHCs for both control and noise-exposed mice, based on the

immunofluorescence counts, while preventing any values less than 1. Each

random value represents the number of ribbons presynaptic to a single type II

afferent (range 1-33). This process was iterated 1000 times to generate the pool

of type II afferents (i.e., 8% of the total 12,350 spiral ganglion neurons in one

mouse cochlea) (Ehret 1983, Nayagam et al. 2011), i.e., a "virtual cochlea". This

entire process was repeated 1000 times to approximate variability among

cochleae, and so provide an average number of ribbons presynaptic to type II

afferents across all virtual cochleae. Averaging across all 1,000,000 virtual type II

afferents, there were 10.16 ± 5.8 and 12.2 ± 6.4 ribbons presynaptic to each type

II afferent for control and noise-exposed mice, respectively (Figure 4.4.1D).

For each virtual type II afferent, a binomial function was run to estimate

the chance of receiving 7 or more vesicle release events given their number of

presynaptic ribbons. The model assumes that all OHCs in the control and noise-

exposed group are fully functional and that all presynaptic ribbons are

independent (Wu et al., 2016). For each of the 1000 sets of 1000 neurons, the

probability of firing an action potential was averaged and then multiplied by 1000

to estimate the number of action potentials produced by the entire population of virtual type II afferents for a maximal stimulus such as one due to a loud, broadband sound. The average number of action potentials for the entire population of type II afferents was 21.9 ± 1.8 in the control condition and 43.7 ± 2.9 for the noise-exposed condition. The two resulting distributions did not overlap. Every estimate in the noise-exposed group was larger than the largest control group estimate (Figure 4.4.1E). Overall, the global 20% increase in OHC ribbon count observed in the noise-exposed mice is estimated to cause a 99% increase in type II action potentials in response to maximal stimulation of OHCs across the population.
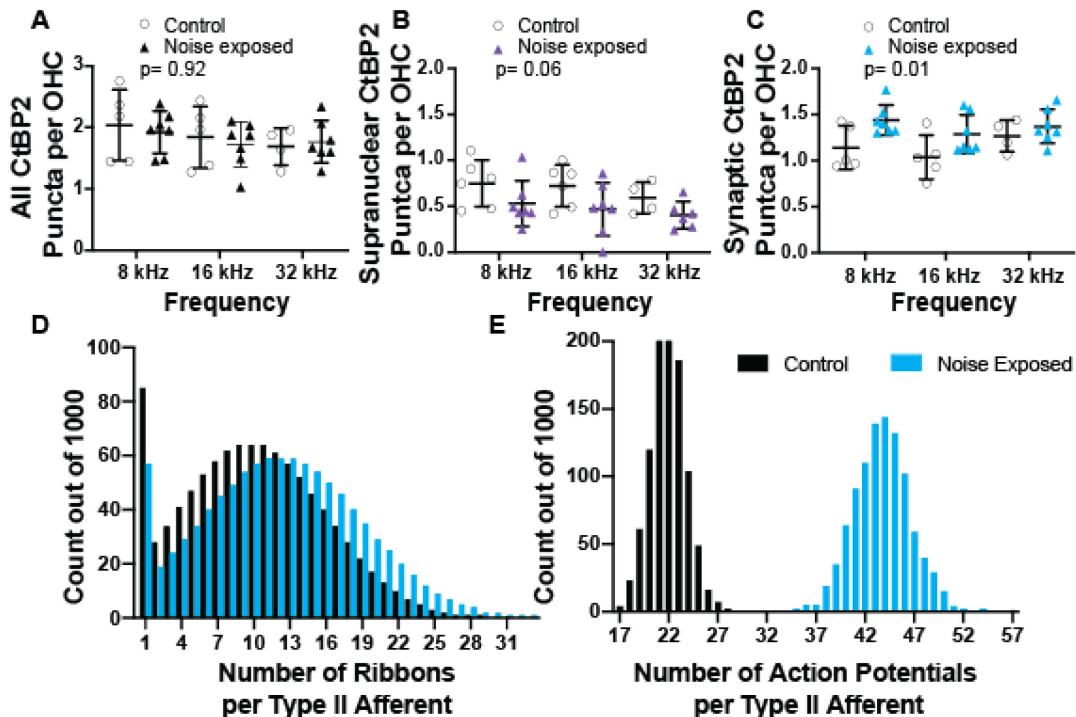
Figure 4.4.1: An increase in synaptic ribbons after acoustic trauma leads to a projected increase in action potential generation in response to maximal OHC stimulation. A. Quantification of all CtBP2 immunopuncta per OHC. Each dot or triangle represents the immunopuncta per OHC from an 80 µm region of the organ of Corti for the frequency region indicated from 1 mouse. Linear mixed

model analysis showed no significant effect for either noise exposure or frequency. Noise exposure: p= 0.92. B. Quantification of supranuclear CtBP2 immunopuncta per OHC. Each dot or triangle represents the immunopuncta per OHC from an 80 μm region of the organ of Corti for the frequency region indicated from 1 mouse. Where both ears were quantified, the average is represented. Linear mixed model analysis shows that the effect of neither noise exposure nor frequency are significant. p= 0.06. C. Quantification of CtBP2 immunopuncta at the synaptic pole per OHC. Each dot or triangle represents the immunopuncta per OHC from an 80 μm region of the organ of Corti for the frequency region indicated from 1 mouse. Where both ears were quantified, the average is represented. Linear mixed model analysis shows significance for only the effect of noise exposure: **p= 0.01**. The interaction between noise exposure and frequency was not significant. Data collected by Keira Mull. D. Histogram of the simulated average number of ribbons presynaptic to the population of type II afferents. Black bars represent estimates derived from control mouse ribbon counts. Cyan bars represent estimates derived from noise-exposed mouse ribbon counts. E. Histogram of the simulated sum of action potentials generated across the population of type II afferents over 1000 iterations. Black bars represent estimates derived from the simulated number of ribbons per type II afferents in control mice from D. Cyan bars represent estimates derived from the simulated number of ribbons per type II afferents in noise-exposed mice from D. Figure adapted from Wood et al., in press.

4.5 Discussion

While the ability to generate calcium transients following focal OHC ablation still exists in mature type II afferents, it is reduced relative to the pre-hearing condition. The response appears not to be affected by PPADS which supports the decreased ATP currents observed from whole patch clamp recordings (Weisz et al., 2009). There is a chance that in mature tissue the purinergic receptors become desensitized after dissection. Despite reducing the amount of damage done with the mostly intact preparation, mature cochleae are encased in hard bone that causes a large amount of damage when broken and the tissue is extremely susceptible to dying from the resulting damage. More experiments are needed to test the extent of the desensitization. If it does exist, it

could mean that mature cochleae have a mechanism to turn off responses to damage which would also result in less neuronal activity from damage sources.

The prolonged initial response and the following delayed response to focal ablation is the first evidence that type II afferents modulate their activity after acoustic trauma. The changes in response kinetics could make signaling to the central nervous system more robust by increasing the total change transfer into the neuron and by having multiple chances for activation from a single stimulus. If delayed epithelial cell responses can elevate the type II afferents' membrane potential for several minutes, then it is likely that type II afferents will increase their probability to fire an action potential in response to OHC vesicle release. A persistent depolarization of 4 mV, the equivalent of an extra vesicle released, could more than double the number of neurons firing after maximal stimulation of the OHCs according to the model described in Figure 4.4.1 (2.2% to 4.8%). This number rises further to 8.5% with the corresponding increase in synaptic OHC ribbons seen in noise-exposed animals.

The mechanism of action for delayed responses requires more work to be fleshed out. It most likely occurs via a postsynaptic mechanism and not by the increased number of functional OHC synapses because there is no stimulus to drive OHC activity at that delayed time and this still occurs without previous noise trauma. It is also likely that the changes derive from the supporting cells and that a mechanism like the wave-like spread of activity in the pre-hearing animals could cause widespread prolonged activity after damage. The origin may not be purinergic in nature as PPADS did not completely block the occurrence of

delayed responses. However, there were not enough recordings to determine if the rate decreased in the presence of PPADS in the external solution. On the other hand, PPADS did block recurrent epithelial cell activity in one example from a noise damaged Tac1^{Cre}:GCaMP6f mouse.

Alongside the change in response to focal ablation, noise exposure appeared to increase the number of ribbons presynaptic to each type II afferent. Although there is a modest increase in the number of OHC synaptic ribbons, the model described here predicted this change could cause a near doubling in action potentials generated by the population of type II afferents. There are, however, limitations to the statistical model. First, it was assumed that before and after damage there are equal numbers of functional, healthy OHCs. While there was not a significant degree of OHC loss following this noise exposure protocol, damage to stereocilia could reduce mechanotransduction. If true, the model would overestimate the number of functional synaptic inputs in noise-exposed animals. Secondly, the dataset used to generate the parameters for the model were taken from a study in young, pre-hearing rats. The number of ribbons in OHCs declines soon after birth, with that change essentially complete in the first postnatal week (Sobkowicz et al., 1986). Nonetheless, species differences and the effects of maturation could alter the number of presynaptic OHCs, their release properties, or the intrinsic excitability of type II afferents. Any of these parameters could change following noise trauma and are potential avenues of future research into the effects of damage on type II afferent function.

Regardless, the present work provides evidence that OHC ribbon numbers increase after acoustic trauma and that change alone could significantly increase sound-evoked type II afferent activity. Combined, the increased likelihood to have prolonged and delayed responses to focal ablation after noise exposure suggest that type II afferents become hyperexcitable with previous damage. In an *in vivo* context, loud sounds could drive type II activity more with the increased number of functional ribbon synapses and that response can be sustained by the delayed activity. These changes could explain how normally unresponsive neurons could signal damage responses only in previously damaged conditions and supports the auditory nociceptor hypothesis. Furthermore, increased acoustic drive from OHCs relates specifically to the phenomenon of hyperacusis whereby previously innocuous sounds become intolerable.

Chapter 5: Discussion and Future Directions

5.1 Discussion

Calcium imaging is a promising new direction for studying the function of type II cochlear afferents. Whereas previous methods could only rarely record one type II afferent at a time, calcium imaging allows for consistent recording of activity from multiple type II afferents in nearly every animal tested. Calcium imaging was able to achieve a sample size about two orders of magnitude greater than previous lower throughput methods (Tables 4.2.1, 4.2.2, and 4.3.1). The ability to draw from the responses of hundreds of type II afferent neurons will enable future studies that require detection of small effects such as determining the effects of modulatory peptides or neurotransmitters. Calcium imaging combined with dissections that leave the cochlea mostly intact allows for investigation of type II afferents at any location along the tonotopic axis of the cochlea and at any age.

Maturation caused a significant change in the response of type II afferents: the likelihood of type II afferents to respond to focal ablation decreased as compared to pre-hearing animals. When these mature neurons do respond to damage, they respond for a longer time, but the damage response is more limited in terms of the number of neurons that respond. The mature cochlear epithelium seems also to respond less, with NGAF events significantly diminished as well (Figure 5.1.1).

Noise exposure caused changes in the number of presynaptic ribbons that could synapse with type II afferents, a greater likelihood for epithelial cells to be

active, and prolonged type II afferent responses immediately after focal ablation. Noise exposure may change how the cochlea reacts to future insults by causing delayed, reverberant activity in the epithelial tissue and type II afferents (Figure 5.1.1). Overall, the methods ventured here pave the way for deeper and more relevant investigation into type II afferent function and could apply equally to the study of other cochlear cell types.

Despite the differences in gene expression, there were no differences between type II afferents of the apex and the base for the tested parameters. There could be yet undetected functional differences between the apical TH expressing type II afferents and the basal Drd2 expressing type II afferents, but it will require more pointed investigation into factors besides their response to focal ablation. For example, an obvious possible difference is the effect of dopamine. Dopamine may be inhibitory but could also have a more modulatory effect that does not involve calcium signaling. Future work should use the techniques described here to generate a large sample size to parse out any effect of dopamine or other catecholamines or even neuropeptides, considering the expression of Calca and Tac1 in type II afferents as well. It is also possible that the functional translation of any of these type II afferent-defining genes only occurs with maturation or after noise damage. There is some evidence that CGRPα peptide, which is not normally present in the peripheral dendrites, is expressed one day after noise exposure (unpublished results, MB Wood).

It may also be helpful to pin down more thoroughly any genetic changes with maturation and after noise trauma, especially changes that cause the

delayed responses to damage in some of the mature animals. Pulsatile waves of activity have been noted for tissue undergoing cell death and could involve secreting factors that attract immune cells (Gale et al., 2004; Kurpius et al., 2007, Lahne and Gale, 2008). What is interesting about the behavior, however, is that this situation can activate type II afferents even though the initial response to focal ablations have similarly low likelihoods to occur as compared to non-traumatized mature animals. During this altered response to damage, do the type II afferents play a role in recruiting immune cells to the dying tissue like nociceptors do in the skin and can their activity signal to the central nervous system that damage is occurring in the cochlea (Chen et al., 2020)? Figuring out the source of this change could be important as recurring activity after loud noises could be one mechanism for initiating tinnitus.

Tinnitus is the perception of phantom noises, often described as a ringing in the ears (Langguth et al., 2013). Along with hyperacusis, tinnitus is common after intense noise exposure and can present in two ways. A short-term effect arises soon after the noise trauma and subsides quickly thereafter. Chronic tinnitus, on the other hand, can be persistent and not tied directly to recent sound exposure. While chronic tinnitus most likely has central origins as it can exist even when the cochlear nerve is transected, acute tinnitus could emerge peripherally. In our experiments once the tissue has been damaged from previous noise trauma, a single initiating event can cause persistent epithelial cell activity for tens of minutes. The delayed activity also involved type II afferent activity in some cases. If type II afferent activity causes the perception of pain or

annoyance like a nociceptor would, traumatic noise may cause a persistent noxious phenotype after a sufficiently loud noise stimulus in people who have already suffered some cochlear damage. The activity could also directly activate type I afferents, like what happens during crenation events in the pre-hearing tissue, but we were not able to record type I afferent activity during these events so that is entirely speculative.

Hyperacusis is another condition that affects auditory perception and is a common sequela of hearing loss. In mice that were noise damaged, not only did the epithelium respond longer after the damaging stimulus, there was a significant increase in the number of OHC ribbon synapses. Modeling the synaptic transfer between OHC and type II afferents with the observed increase in ribbons almost doubled the expected type II afferent activity as a result of a single maximally stimulating event. This should also apply for lower levels of sound and may push normally innocuous sounds into the range that would be perceived as harmful, providing a possible etiology for one form of hyperacusis.

A major question that arises from the work in this thesis is: do the data presented here support or refute the auditory nociceptor hypothesis? In all conditions tested, type II afferents could respond to focal ablation of OHCs; however, the proportion of times when type II afferents responded to damage significantly declined in healthy adult mice. The mature type II afferents also appear to respond to damage in an ATP-independent manner, with PPADS having little effect. With the increased amount of tissue damage required to access the organ of Corti even in the mostly intact preparation, it is possible that

the type II afferent and/or supporting cells desensitize before the focal OHC

responses. This could explain the reduced proportion of times when damage

caused type II calcium transients. It is also possible that the suite of purinergic

receptors shifts to more PPADS-insensitive P2Y receptors that could be

activated by the products of ATP degradation, meaning that the neurons may still

respond to damage but in a less direct way. Even though the mature type II

afferents seem less responsive to damage, there are two lines that suggest they

become sensitized after noise exposure. Both the delayed response phenotype

and increase in subnuclear synaptic OHC ribbons could drive more type II activity

after loud stimuli. In the somatosensory system many nociceptive neurons have

extremely high thresholds until an insult occurs. Afterwards, these neurons can

respond to moderate touch resulting in allodynia. Type II afferents may employ a

similar strategy where in the control mature condition they do not respond to

almost any stimulus but once there is damage, possibly from a bout of intense

noise exposure, they become sensitive to even moderate noise.

The results of this thesis, while supporting a version of the nociceptor

hypothesis where type II afferents are mostly unresponsive in mature animals but

can be recruited to respond to stimuli associated with damage after traumatic

noise exposure, is not conclusive on its own. More direct evidence is required,

most likely involving measuring either *in vivo* type II activity or behavior. Until

then, other hypotheses about type II afferent function cannot be dismissed. The

most prominent alternative is that type II afferents make local synapses in the

organ of Corti, providing quick adjustments to OHC and supporting cell function

during different amounts of sound activation. Some electron microscopy studies have found putative synapses from type II afferents onto supporting cells (Burgess et al, 1997; Fechner et al., 2001) and even reciprocal synapses between OHCs and type II afferents but these reports may just be species specific oddities or due to loss of efferent innervation (Pujol and Carlier, 1982; Thiers et al., 2008). These hypotheses are based on ultrastructural studies only. Currently, there are no direct recordings, or immunolocalizations of pre- or post-synaptic proteins that support these claims.

In this work there was a correlation between the epithelial cells and type II afferents, but the directionality could not be worked out because of the gap in time between photoablation and recording. The Tac1^{Cre}:GCaMP6f animals may be a useful tool in determining the relationship between epithelial cells and type II afferents due to the unique ability to record the activity of both cell types simultaneously. Transgenic animals could also be used to express channelrhodopsin in type II afferents to see if there are synaptic responses in the supporting cells or OHCs with blue light stimulation. It is also possible that instead of classical synapses onto cell types within the organ of Corti, type II afferents bulk release neuromodulators or neuropeptides, possibly explaining the disparate gene expression and wide arborization, to affect cochlear function. Neither of these two hypotheses are mutually exclusive with the nociceptor hypothesis and could supplement the response to damage by reducing further

damage by acting on supporting cells or OHCs.
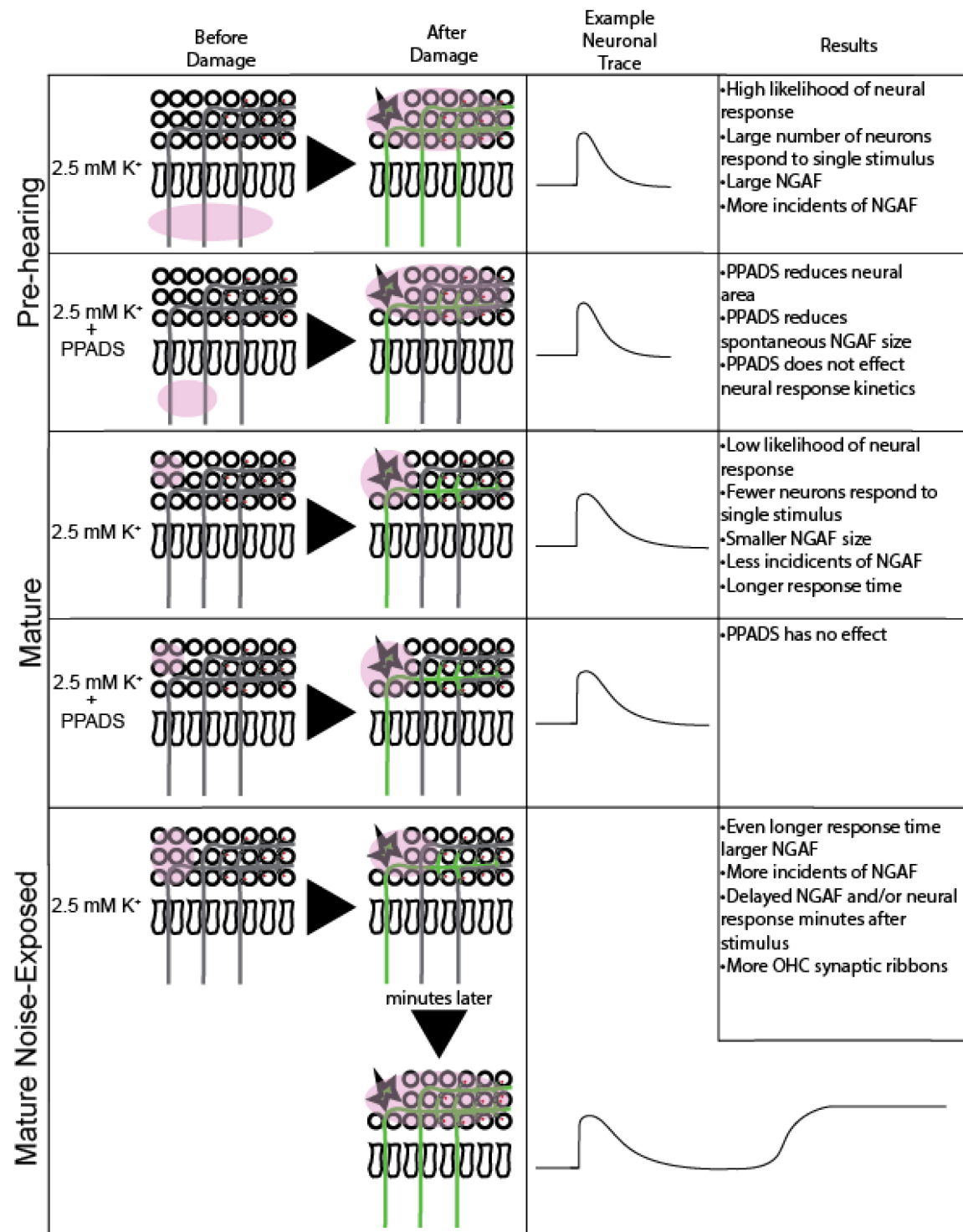
Figure 5.1.1. Summary schematic of the effects of age, noise-exposure, and 100 µM PPADS on responses of type II afferents and epithelial cells to focal ablation. Black circles represent OHCs, black vase-shaped objects represent

137

IHCs, red dots in OHCs represent synaptic ribbons, green and gray lines that run through the hair cells and make a 90-degree turn represent type II afferents with green representing afferents with a response to damage and gray as ones that do not respond, transparent magenta clouds represent NGAF events, jagged star-like object represents the damage caused by focal ablation. The before damage column represents the baseline spontaneous activity in each condition and the after damage column represents an average response to a focal ablation event. The example trace column represents the contour of the average neuronal calcium transient as measured by GCaMP6f. Results column represents the main findings in each condition.

5.2 Future directions

The work presented in this thesis, while expanding the knowledge of type II afferent activity, is not the final word on the function of type II afferents. Instead, the work highlights how important it is to investigate neuronal function from many angles. Patch clamp electrophysiology from type II peripheral dendrites greatly expanded our knowledge of type II afferent function and remains vital for understanding the synaptic currents with exquisite precision. However, one of the major limitations was the dependence on pre-hearing animals when performing whole cell patch clamp electrophysiology. Extrapolating from one time point is unreliable and can cause misconceptions. By expanding the possible conditions where recording type II afferent activity is possible, this works improves our current knowledge and permits many more avenues of research in the future.

For instance, the present work focused on the response to focal ablation because of the precedent set by previous work and because of the success of calcium imaging in that context. However, more dedication will be required to determine if neurotransmitters or neuropeptides can cause calcium responses in type II afferents. It will require many repeated exposures of type II afferents to

various molecules to record responses based on the lack of fluorescence changes seen here. It will also be necessary to repeat all these experiments in mature and noise-exposed animals in case their expression is mutable. Other proteins, such as AMPARs, P2Rs, voltage-gated ion channels, etc.; could be modulated with maturation and following noise exposure. Understanding how type II afferents change under different conditions aids our understanding of type II afferent function overall.

Another unresolved issue with the current work is that the action of ATP was assumed indirectly through NGAF levels and the effects of PPADS. Recently, there has been development of an ATP sensor that can bind to the external surface of cells to measure the level of ATP released into the external fluids (Kitajima et al., 2020). Measuring the levels of ATP directly could provide information about the state of ATP release in mature cochleae after focal ablations and could address whether there is more ATP released from previously noise traumatized tissue.

Although there is much more exploration required with calcium imaging to better understand type II afferent function, GCaMP is not the only transgenic protein that can be employed to study neuronal function. One problem that is not fully resolved is the identity of the postsynaptic targets of type II afferents. Understanding the projection pattern of type II afferents in the central nervous system may help elucidate the function of type II afferents. Selective fluorescence tagging of type II afferent axons, staining for synaptic proteins and

staining for select cochlear nucleus cell types could clarify tonotopic patterns and the identity of the neurotransmitter released by type II afferents.

Neuronal activity can be driven or inhibited through light sensitive channels or through designer receptors exclusively activated by designer drugs (DREADDs). There is a great deal of interest in optogenetic control of cochlear afferent function to build better cochlear implants (Dombrowski et al, 2019; Dieter et al., 2020). The current electrical cochlear implants have a large degree of signal spread causing overlap between the channels and dissatisfaction about the quality of hearing in implanted individuals. With light there should be less spread increasing the sensitivity of the device. Experiments carried out to test the viability of optical cochlear implants so far have targeted all cochlear afferents. It could be possible to selectively target the type II afferent population by introducing a floxed channelrhodopsin into an animal with type II afferent specific Cre expression. From there, one could study the behavioral effects of selective type II afferent activation by stimulating with blue light.

Activation of somatic nociceptors causes nocifensive behaviors such as grooming and freezing (Brodkin et al., 2014). Type II afferent activation could also cause nocifensive behaviors such as covering the ears. One line of evidence suggests that type II afferent activity is not sufficient to cause any overt behavior (Flores et al., 2015). Mice without sound-driven type I afferent function but functioning type II afferents did not attempt to escape from damaging levels of noise. Because the knockout of Vglut3 was not restricted to IHCs, there is a possibility that the behavioral effects were caused by the dysfunction of another

140

cell type. If it is true however, that type II afferents do not denote negative valence, they could still convey salience and when combined with type I activity could drive nocifensive behavior. Therefore, it may be better to pair a tone with type II afferent activation to observe if the animal begins to form a negative association with that tone. Alternatively, type II afferent activity may decrease the threshold for engaging in auditory behaviors related to loud sounds, such as the startle reflex. Inhibitory halorhodospins can also be used to see if the threshold increases with inhibition as well. Injecting the animal with the designer drug for DREADDs is more tractable and less damaging to the cochlea than introducing an optical cochlear implant but it does not have the temporal specificity of light stimulation. The choice between DREADDs and optogenetics will come down to the specifics of the experiment and whether one needs type II afferent activity to be controlled or can be constantly elevated or depressed.

Expression of channelrhodopsin can also be leveraged to identify the desired cell type during electrophysiological recordings, called photostimulation-assisted identification of neuronal populations or more colloquially optotagging (Lima et al., 2009). Cells that express channelrhodopsin will have obvious short latency depolarizations to blue light exposure, therefore, if one has channelrhodopsin expression restricted to a single cell type, quick responses to blue light means one is recording from that specific cell type. This diagnostic technique could be extremely helpful in sharp electrode recordings from the eighth nerve where recordings from type II afferents were marred by the

uncertainty that the cell was actually a type II cochlear afferent (Berglund and Brown, 1994; Robertson et al., 1999).

Select cell types can be ablated by expressing the light chain of the diphtheria toxin or by expressing the receptor and administering the toxin itself. Ablating type II afferents is even more extreme than inhibiting them with DREADDs or halorhodopsin and may provide more obvious defects in behavior. For example, mice may not show a preference for the quieter chamber in a two-chamber choice preference without type II afferent activity. If a reproducible animal model of hyperacusis or tinnitus were to be designed, it would be interesting to see if ablating type II afferents could prevent the development of these disorders or could even alleviate the symptoms.

For all these genetic tools besides GCaMP, where anatomy informs verification of type II afferent identity, there is the issue of specificity to address first. All the Cre lines that have been identified that label type II afferents preferentially over type I afferents, are not entirely selective for type II afferents and are expressed by many other cell types. The search continues for a type II afferent specific marker, but it is unlikely that a specific marker exists without expression in any other cell type. Therefore, it may be necessary to find a gene that is only expressed in type II afferents within the cochlea and then induce expression of a transgenic protein with a spatially restricted method. One possible delivery system would be to inject a virus that expresses a floxed transgenic protein into the cochlea when the only cochlear cell type to express Cre is the type II afferents. Although there is a great deal of work ahead before

these genetic tools can be employed, implementing GCaMP6f into the arsenal of tools to study type II afferents has been promising. The mysteries of type II afferents will most likely be uncovered through employing these diverse genetic tools alongside traditional techniques.

Bibliography

Abraira V, Ginty D. The sensory neurons of touch. *Neuron* 2013;79(4):618-639.

Abraira V, Kuehn ED, Chirila AM, Springel MW, et al., Ginty The cellular and synaptic architecture of the mechansensory dorsal horn. *Cell.* 2017;168(1-2):295-310.

Afrah AW, Fiskå A, Gjerstad J, et al. Spinal substance P release in vivo during the induction of long-term potentiation in dorsal horn neurons. *Pain*. 2002;96(1):49-55.

Akerboom J, Vélez Rivera JD, Rodríguez Guilbe MM, et al. Crystal structures of the GCaMP calcium sensor reveal the mechanism of fluorescence signal change and aid rational design. *Journal of Biological Chemistry*. 2009;284(10):6455-6464.

Alving K, Sundström C, Matran R, Panula P, Hökfelt T, Lundberg JM. Association between histamine-containing mast cells and sensory nerves in the skin and airways of control and capsaicin-treated pigs. *Cell and tissue research*. 1991;264(3):529-538.

Anderson M, Zheng Q, Dong X. Investigation of pain mechanisms by calcium imaging approaches. *Neurosci Bull*. 2017;34(1):194-199.

Andrew D, Greenspan JD. Mechanical and heat sensitization of cutaneous nociceptors after peripheral inflammation in the rat. *Journal of Neurophysiology*. 1999;82(5):2649-2656.

Anselmi F, Hernandez VH, Crispino G, Seydel A, Ortolano S, et al. ATP release through connexin hemichannels and gap junction transfer of second messengers propagate Ca^{2+} signals across the inner ear. *Proceedings of the National Academy of Sciences - PNAS*. 2008;105(48):18770-18775.

Anttonen T, Belevich I, Kirjavainen A, et al. How to bury the dead: Elimination of apoptotic hair cells from the hearing organ of the mouse. *JARO*. 2014;15(6):975-992.

Ashmore, JF. A fast motile response in guinea-pig outer hair cells: The cellular basis of the cochlear amplifier. J Physiol. 1987 Jul; 388: 323–347.

Ashmore J. Cochlear outer hair cell motility. *Physiological reviews*. 2008;88(1):173-210.

Askew C, Rochat C, Pan Ym Ahmed H, Child E, Schneider BL, Aebischer P, Holt JR. Tmc gene therapy restores auditory function in deaf mice. *Sci. Transl. Med.* 2015;7(295):295ra108.

Assad JA, Hacohen N, Corey DP. Voltage dependence of adaptation and active bundle movement in bullfrog saccular hair cells. *Proceedings of the National Academy of Sciences of the United States of America*. 1989;86(8):2918-2922.

Babola TA, Li S, Gribizis A, et al. Homeostatic control of spontaneous activity in the developing auditory system. *Neuron*. 2018;99(3):511-524.e5.

Ballesteros A, Fenollar-Ferrer C, Swartz KJ. Structural relationship between the putative hair cell mechanotransduction channel TMC1 and TMEM16 proteins. *eLife*. 2018;7.

Bardhan T, Jeng J, Waldmann M, et al. Gata3 is required for the functional maturation of inner hair cells and their innervation in the mouse cochlea. *The Journal of physiology*. 2019;597(13):3389-3406.

Becker L, Schnee ME, Niwa M, et al. The presynaptic ribbon maintains vesicle populations at the hair cell afferent fiber synapse. *eLife*. 2018;7.

Beisel KW. Differential expression of KCNQ4 in inner hair cells and sensory neurons is the basis of progressive high-frequency hearing loss. *The Journal of neuroscience*. 2005;25(40):9285-9293.

Békésy G. von (1960) Experiments in Hearing (McGraw-Hill. New York)

Benito-Gonzalez A, Doetzlhofer A. Hey1 and Hey2 control the spatial and temporal pattern of mammalian auditory hair cell differentiation downstream of hedgehog signaling. *The Journal of neuroscience*. 2014;34(38):12865-12876.

Benson T, Brown MC. Postsynpatic targets of type II auditory nerve fibers in the cochlear nucleus. *J. Assoc. Res. Otolaryngol.* 2004;5(2):111-25.

Berekméri E, Deák O, Téglás T, Sághy É, Horváth T, Aller M, Fekete Á, Köles L, Zelles T. Targeted single-cell electroporation loading of Ca^{2+} indicators in the mature hemicochlea preparation. *Hear. Res.* 2019a:371:75-86.

Berekméri E, Fekete Á, Köles L, Zelles T. Postnatal development of the subcellular structures and purinergic signaling of Deiters' cells along the tonotopic axis of the cochlea. *Cells* 2019b:8(10):1266.

Berglund AM, Ryugo DK. Hair cell innervation by spiral ganglion neurons in the mouse. *J. Comp. Neurol.* 1987l255(4):560-70.

Berglund AM, Brown MC. Central trajectories of type II spiral ganglion cells from various cochlear regions in mice. *Hearing Research*. 1994;75(1):121-130.

Berglund AM, Benson TE, Brown MC. Synapses from labeled type II axons in the mouse cochlear nucleus. *Hearing Research*. 1996;94(1):31-46.

Beurg M, Evans MG, Hackney CM, Fettiplace R. A large-conductance calcium-selective mechanotransducer channel in mammalian cochlear hair cells. *Journal of Neuroscience*. 2006;26(43):10992-11000.

Beurg M, Evans MG, Hackney CM, Fettiplace R. A large-conductance calcium-selective mechanotransducer channel in mammalian cochlear hair cells. *Journal of Neuroscience*. 2006;26(43):10992-11000.

Beurg M, Fettiplace R, Nam J, Ricci AJ. Localization of inner hair cell mechanotransducer channels using high-speed calcium imaging. *Nature neuroscience*. 2009;12(5):553-558.

Beurg M, Michalski N, Safieddine S, et al. Control of exocytosis by synaptotagmins and otoferlin in auditory hair cells. *The Journal of neuroscience*. 2010;30(40):13281-13290.

Beurg M, Goldring AC, Fettiplace R. The effects of Tmc1 beethoven mutation on mechanotransducer channel function in cochlear hair cells. *The Journal of general physiology*. 2015;146(3):233-243.

Beutner D, Moser T. The presynaptic function of mouse cochlear inner hair cells during development of hearing. *Journal of Neuroscience*. 2001;21(13):4593-4599.

Blum E, Procacci P, Conte V, Hanani M. Systemic inflammation alters satellite glial cell function and structure. A possible contribution to pain. *Neuroscience*. 2014;274:209-217.

Bobbin RP, Salt AN. ATP-γ-S shifts the operating point of outer hair cell transduction towards scala tympani. *Hearing Research*. 2005;205(1):35-43.

Boero LE, Castagna VC, Di Guilmi MN, Goutman JD, Elgoyhen AB, Gómez-Casati ME. Enhancement of the medial olivocochlear system prevents hidden hearing loss. *The Journal of neuroscience*. 2018;38(34):7440-7451.

Boero LE, Castagna VC, Terreros G, et al. Preventing presbycusis in mice with enhanced medial olivocochlear feedback. *Proceedings of the National Academy of Sciences - PNAS*. 2020;117(21):11811-11819.

Boettger T, Hübner CA, Maier H, Rust MB, Beck FX, Jentsch TJ. Deafness and renal tubular acidosis in mice lacking the K-cl co-transporter Kcc4. *Nature (London)*. 2002;416(6883):874-878.

Boettger T, Rust MB, Maier H, Rust MB, Siedenbecher T, et al. Loss of K-Cl co-transporter KCC3 causes deafness, neurodegeneration and reduced seizure threshold *EMBO J.* 2003;22(20):5422-34.

Bok J, Zenczak C, Hwang CH, Wu DK. Auditory ganglion source of Sonic hedgehog regulates timing of cell cycle exit and differentiation of mammalian cochlear hair cells. *Proc. Natl. Acad. Sci. U S A.* 2013;110(34):13869-74.

Bortolozzi M, Brini M, Parkinson N, et al. The novel PMCA2 pump mutation tommy impairs cytosolic calcium clearance in hair cells and links to

deafness in mice. *The Journal of biological chemistry*. 2010;285(48):37693-37703.

Bourk TR, Mielcarz JP, Norris BE. Tonotopic organization of the anteroventral cochlear nucleus of the cat. *Hear. Res.* 1981;4(3-4):215-41.

Brändle U, Zenner HP, Ruppersberg JP. Gene expression of P2X-receptors in the developing inner ear of the rat. *Neurosci. Lett.* 1999;273(2):105-8.

Brandt A, Striessnig J, Moser T. CaV1.3 channels are essential for development and presynaptic activity of cochlear inner hair cells. *Journal of Neuroscience*. 2003;23(34):10832-10840.

Brandt A, Khimich D, Moser T. Few CaV1.3 channels regulate the exocytosis of a synaptic vesicle at the hair cell ribbon synapse. *Journal of Neuroscience*. 2005;25(50):11577-11585.

Brodkin J, Frank D, Grippo R, Hausfater M, Gulinello M, Achterholt N, Gutzen C. Validation and implementation of a novel high-throughput behavioral phenotyping instrument for mice. *J. Neurosci. Methods.* 2014;224:48-57.

Brown A, Yates PA, Burrola P, et al. Topographic mapping from the retina to the midbrain is controlled by relative but not absolute levels of EphA receptor signaling. *Cell*. 2000;102(1):77-88.

Brown AG, Iggo A, Miller S. Myelinated afferent nerve fibers from the skin of the rabbit ear. *Exp. Neurol.* 1967;18(3):338-49.

Brown MC. Morphology of labeled afferent fibers in the guinea pig cochlea. *Journal of Comparative Neurology*. 1987;260(4):591-604.

Brown MC, Berglund AM, Kiang NYS, Ryugo DK. Central trajectories of type II spiral ganglion neurons. *Journal of Comparative Neurology*. 1988;278(4):581-590.

Brown MC, Ledwith JV. Projections of thin (type-II) and thick (type-I) auditory-nerve fibers into the cochlear nucleus of the mouse. *Hearing Research*. 1990;49(1):105-118.

Brownell W, Bader C, Bertrand D, de Ribaupierre Y. Evoked mechanical responses of isolated cochlear outer hair cells. *Science*. 1985;227(4683):194-196.

Brumovsky P, Villar MJ, Hökfelt T. Tyrosine hydroxylase is expressed in a subpopulation of small dorsal root ganglion neurons in the adult mouse. *Experimental Neurology*. 2006;200(1):153-165.

Brumovsky PR. Dorsal root ganglion neurons and tyrosine hydroxylase—an intriguing association with implications for sensation and pain. *Pain (Amsterdam)*. 2016;157(2):314-320.

Burgess BJ, Adams JC Nadol JB. Morphologic evidence for innervation of Deiters' and Hensen's cells in the guinea pig. *Hear. Res.* 1997;108(1-2):74-82.

Burns JC, Collado MS, Oliver ER, Corwin JT. Specializations of intercellular junctions are associated with the presence and absence of hair cell regeneration in ears from six vertebrate classes. *Journal of comparative neurology* 2013;521(6):1430-1448.

Burns JC, Corwin JT. A historical to present-day account of efforts to answer the question: "What puts the brakes on mammalian hair cell regeneration?". *Hearing Research*. 2013;297:52-67.

Burnstock G, Kennedy C. Is there a basis for distinguishing two types of P_2-purinoceptor? *Gen. Pharmac.* 1985;16(5):433-440.Kubi

Caprara GA, Mecca AA, Wang Y, Ricci AJ, Peng AW. Hair bundle stimulation mode modifies manifestations of mechanotransduction adaptation. *The Journal of neuroscience*. 2019;39(46):9098-9106.

Casimiro MC, Knollmann BC, Ebert SN, et al. Targeted disruption of the Kcnq1 gene produces a mouse model of jervell and lange-nielsen syndrome. *Proceedings of the National Academy of Sciences - PNAS*. 2001;98(5):2526-2531.

Caterina MJ, Schumacher MA, Tominaga M, Rosen TA, Levine JD, Julius D. The capsaicin receptor: A heat-activated ion channel in the pain pathway. *Nature (London)*. 1997;389(6653):816-824.

Caterina MJ, Julius D. The vanilloid receptor: A molecular gateway to the pain pathway. *Annual review of neuroscience*. 2001;24(1):487-517.

Cederholm JME, Ryan AF, Housley GD. Onset kinetics of noise-induced purinergic adaptation of the 'cochlear amplifier'. *Purinergic Signalling*. 2019;15(3):343-355.

Ceriani F, Hendry A, Jeng J, et al. Coordinated calcium signalling in cochlear sensory and non-sensory cells refines afferent innervation of outer hair cells. *The EMBO journal*. 2019;38(9)

Chapochnikov N, Takago H, Huang C, et al. Uniquantal release through a dynamic fusion pore is a candidate mechanism of hair cell exocytosis. *Neuron*. 2014;83(6):1389-1403.

Chen O, Donnelly CR, Ji RR. Regulation of pain by neuro-immune interactions between macrophages and nociceptor sensory neurons. *Curr. Opin. Neurobiol.* 2020;62:17-25.

Chen Q, Mahendrasingam S, Tickle JA, Hackney CM, Furness DN, Fettiplace R. The development, distribution and density of the plasma membrane calcium ATPase 2 calcium pump in rat cochlear hair cells. *European Journal of Neuroscience*. 2012;36(3):2302-2310.

Chen X, Tanner K, Levine JD. Mechanical sensitization of cutaneous C-fiber nociceptors by prostaglandin E2 in the rat. *Neuroscience letters*. 1999;267(2):105-108.

Chen Y, Corriden R, Inoue Y, et al. ATP release guides neutrophil chemotaxis via P2Y2 and A3 receptors. *Science (American Association for the Advancement of Science)*. 2006;314(5806):1792-1795.

Chertoff M, Martz A, Sakumura J, Kamerer A, Diaz F. The middle ear muscle reflex in rat: Developing a biomarker of auditory nerve degeneration. *Ear and Hearing*. 2018;39(3):605-614.

Chessum L, Matern MS, Kelly MC, et al. Helios is a key transcriptional regulator of outer hair cell maturation. *Nature (London)*. 2018;563(7733):696-700.

Clark AK, Malcangio M. Fractalkine/CX3CR1 signaling during neuropathic pain. *Frontiers in cellular neuroscience*. 2014;8:121.

Clause A, Noh J, Kandler K. Tonotopic reorganization of developing auditory brainstem circuits. *Nature Neuroscience*. 2009;12(6):711-717.

Clause A, Kim G, Sonntag M, et al. The precise temporal pattern of pre-hearing spontaneous activity is necessary for tonotopic map refinement. *Neuron*. 2014;82(4):822-835.

Cohen-Salmon M, Ott T, Michel V, et al. Targeted ablation of connexin26 in the inner ear epithelial gap junction network causes hearing impairment and cell death. *Current Biology*. 2002;12(13):1106-1111.

Cohen-Salmon M, Regnault B, Cayet N, et al. Connexin30 deficiency causes instrastrial fluid-blood barrier disruption within the cochlear stria vascularis. *Proceedings of the National Academy of Sciences - PNAS*. 2007;104(15):6229-6234.

Cook SP, McCleskey EW. Cell damage excites nociceptors through release of cytosolic ATP. *Pain.* 2002;95(1-2):41-7.

Corey DP, Akyuz N, Holt JR. Function and dysfunction of TMC channels in inner ear hair cells. *Cold Spring Harbor perspectives in medicine*. 2019;9(10):a033506.

Corns LF, Johnson SL, Kros CJ, Marcotti W. Calcium entry into stereocilia drives adaptation of the mechanoelectrical transducer current of mammalian cochlear hair cells. *Proceedings of the National Academy of Sciences of the United States of America*. 2014;111(41):14918-14923.

Corns LF, Johnson SL, Kros CJ, Marcotti W. Tmc1 point mutation affects Ca^{2+} sensitivity and block by dihydrostreptomycin of the mechanoelectrical transducer current of mouse outer hair cells. *The Journal of neuroscience*. 2016;36(2):336-349.

Corns LF, Johnson SL, Roberts T, et al. Mechanotransduction is required for establishing and maintaining mature inner hair cells and regulating efferent innervation. *Nature communications*. 2018;9(1):4015-15.

Cox BC, Liu Z, Lagarde MMM, Zuo J. Conditional gene expression in the mouse inner ear using Cre-loxP. *J. Assoc. Res. Otolaryngol.* 2012;13(3):295-322.

Crawford AC, Kennedy HJ, Fettiplace R. Force generation by mammalian hair bundles supports a role in cochlear amplification. *Nature*. 2005;433(7028):880-883.

Cruz HG, Lüscher C. Applications of two-photon microscopy in the neurosciences. *Front. Biosci.* 2005;10:2263-78.

Cunningham CL, Wu Z, Jafari A, Zhao B, Schrode K, Harkins-Perry S, Lauer A, Müller U. The murine catecholamine methyltransferase mTOMT is essential for mechanotransduction by cochlear hair cells. *Elife.* 2017;6:e24318.

d'Aldin C, Puel JL, Leducq R, Crambes O, Eybalin M, Pujol R. Effects of a dopaminergic agonist in the guinea pig cochlea. *Hear. Res.* 1995;90(1-2):202-11.

Dannhof BJ, Roth B, Bruns V. Length of hair cells as a measure of frequency representation in the mammalian inner ear? *Naturwissenschaften* 1991;78(12):570-3.

Deol MS, Robins MW. The spinner mouse. *The Journal of heredity*. 1962;53(3):133-136.

Di Guilmi MN, Boero LE, Castagna VC, et al. Strengthening of the efferent olivocochlear system leads to synaptic dysfunction and tonotopy disruption of a central auditory nucleus. *The Journal of neuroscience*. 2019;39(36):7037-7048.

Dieter A, Klein E, Keppeler D, Jablonski L, Harczos T et al. μLED-based optical cochlear implants for spectrally selective activation of the auditory nerve. *EMBO Mol. Med.* 2020;12(8):e12387.

Dombrowski T, Rankovic V, Moser T. Toward the optical cochlear implant. *Cold Spring Harb. Perspect. Med.* 2019;9(8):a033225.

Dou H, Vazquez A, Namkung Y, et al. Null mutation of α1D Ca^{2+} channel gene results in deafness but no vestibular defect in mice. *JARO*. 2004;5(2):215-226.

Driver EC, Pryor SP, Hill P, et al. Hedgehog signaling regulates sensory cell formation and auditory function in mice and humans. *The Journal of neuroscience*. 2008;28(29):7350-7358.

Duggan AW, Hendry IA, Morton CR, Hutchinson WD, Zhao ZQ. Cutaneous stimuli releasing immunoreactive substance P in the dorsal horn of the cat. *Brean Res.* 1988;451(1-2):261-73.

Dumont RA, Lins U, Filoteo AG, Penniston JT, Kachar B, Gillespie PG. Plasma membrane Ca^{2+}-ATPase isoform 2a is the PMCA of hair bundles. *Journal of Neuroscience*. 2001;21(14):5066-5078.

Dáibhid Ó Maoiléidigh, A. J. Hudspeth. Effects of cochlear loading on the motility of active outer hair cells. *Proceedings of the National Academy of Sciences - PNAS*. 2013;110(14):5474-5479.

Dulon D, Sugasawa M, Blanchet C, Erostegui C. Direct measurements of Ca(2+)-activated K+ currents in inner hair cells of the guinea-pig cochlea using photolabile Ca2+ chelators. *Pflugers Arch.* 1995;430(3):365-73.

Eatock RA, Corey DP, Hudspeth AJ. Adaptation of mechanoelectrical transduction in hair cells of the bullfrog's sacculus. *Journal of Neuroscience*. 1987;7(9):2821-2836.

Eckhard A, Gleiser C, Rask-Andersen H, et al. Co-localisation of K(ir)4.1 and AQP4 in rat and human cochleae reveals a gap in water channel expression at the transduction sites of endocochlear K(+) recycling routes. *Cell and tissue research*. 2012;350(1):27-43.

Effertz T, Becker L, Peng AW, Ricci AJ. Phosphoinositol-4,5-bisphosphate regulates auditory hair-cell mechanotransduction-channel pore properties and fast adaptation. *The Journal of neuroscience*. 2017;37(48):11632-11646.

Ehret G, Fischer R. Neuronal activity and tonotopy in the auditory system visualized by c-fos gene expression. *Brain. Res.* 1991;567:350-4.

Ehret G. Peripherial anatomy and physiology II. In: Willott, J.F. (Ed.), The Auditory Psychobiology of the Mouse. Charles C. Thomas, Springfield , pp 169-200.

Elgoyhen AB, Johnson DS, Boulter J, Vetter DE, Heinemann S. A9: An acetylcholine receptor with novel pharmacological properties expressed in rat cochlear hair cells. *Cell (Cambridge)*. 1994;79(4):705-715.

Elliott MR, Chekeni FB, Trampont PC, et al. Nucleotides released by apoptotic cells act as a find-me signal for phagocytic clearance. *Nature*. 2009;461(7261):282-286.

Emadi G, Richter CP, Dallos P. Stiffness of the gerbil basilar membrane: Radial and longitudinal variations. *Journal of Neurophysiology*. 2004;91(1):474-488.

Erostegui C, Norris CH, Bobbin RP. In vitro pharmacologic characterization of a cholinergic receptor on outer hair cells. *Hear. Res.* 1994;74(1-2):135-47.

Evans MG, Kiln J, Pinch D. No evidence for functional GABA receptors in outer hair cells isolated from the apical half of the guineapig cochlea. *Hear. Res.* 1996;101(1-2):1-6.

Fechner FP, Nadol JR, Burgess BJ, Brown MC. Innervation of supporting cells in the apical turns of the guinea pig cochlea is from type II afferent fibers. *J. Comp. Neurol.* 2001;429(2):289-98.

Fettiplace R. Is TMC1 the hair cell mechanotransduction channel? *Biophysical Journal.* 2016; 111(1):3-9.

Fettiplace R, Nam JH. Tonotopy in calcium homeostasis and vulnerability of cochlear hair cells. *Hear. Res.* 2019; 376:11-21.

Fex J, Altschuler RA. Neurotransmitter-related immunocytochemistry of the organ of corti. *Hearing Research*. 1986;22(1):249-263.

Ficarella R, Leva FD, Bortolozzi M, Ortolano S, Donaudy F, et al. A functional study of plasma-membrane calcium-pump isoform 2 mutants causing digenic deafness. *Proc. Natl. Acad. Sci. U S A.* 2007;104(5):1516-21.

Flock Å, Bretscher Am Weber K. Immunohistochemical localization of several cytoskeletal proteins in inner ear sensory and supporting cells. *Hearing Research* 1982;7(1):75-89.

Flores EM, Duggan A, Madathany T, Hogan A, et al. A non-canonical pathway from cochlea to brain signals tissue-damaging noise. *Curr. Biol.* 2015;25(5):606-12.

Flores-Otero J, Davis R. Synaptic proteins are tonotopically graded in postnatal and adult type I and type II spiral ganglion neurons. *J. Comp. Neurol.* 2011;519(8):1455-75.

Forge A. Outer hair cell loss and supporting cell expansion following chronic gentamicin treatment. *Hearing Research*. 1985;19(2):171-182.

Fredelius L, Rask-Andersen H. The role of macrophages in the disposal of degeneration products within the organ of Corti after acoustic overstimulation. *Acta Otolaryngol.* 1990;109(1-2):76-82.

Froud KE, Wong ACY, Cederholm JME, et al. Type II spiral ganglion afferent neurons drive medial olivocochlear reflex suppression of the cochlear amplifier. *Nature communications*. 2015;6(1):7115.

Frye MD, Yang W, Zhang C, Xiong B, Hu BH. Dynamic activation of basilar membrane macrophages in response to chronic sensory cell degeneration in aging mouse cochleae. *Hearing research*. 2017;344:125-134.

Frye MD, Ryan AF, Kurabi A. Inflammation associated with noise-induced hearing loss. *J. Acoust. Soc. Am*. 2019;146(5):4020.

Fuchs PA, Lehar M, Hiel H. Ultrastructure of cisternal synapse on outer hair cells of the mouse cochlea. *J. Comp. Neurol.* 2014;522(3):717-29.

Fuchs PA, Lauer AM. Efferent inhibition of the cochlea. *Cold Spring Harb. Perspect. Med.* 2019;(5):a033530.

Fujioka M, Kanzaki S, Okano HJ, Masuda M, Ogawa K, Okano H. Proinflammatory cytokines expression in noise-induced damaged cochlea. *Journal of neuroscience research*. 2006;83(4):575-583.

Furman AC, Kujawa SG, Liberman MC. Noise-induced cochlear neuropathy is selective for fibers with low spontaneous rates. *J Neurophysiol.* 2013;110(3):577-86.

Furness DN, Lehre KP. Immunocytochemical localization of a high-affinity glutamate-aspartate transporter, GLAST, in the rat and guinea-pig cochlea. *The European journal of neuroscience*. 1997;9(9):1961-1969.

Galambos R, Davis H. The response of single auditory-nerve fibers to acoustic stimulation. *Journal of Neurophysiology* 1943;6(1):39-57.

Gale JE, Piazza V, Ciubotaru CD, Mammano F. A mechanism for sensing noise damage in the inner ear. *Curr. Biol.* 2004;14(6):526-9.

Ghimire SR, Deans MR. *Frizzled3* and *Frizzled6* cooperate with *Vangl2* to direct cochlear innervation by type II spiral ganglion neurons. *J. Neurosci.* 2019;39(41):8013-8023.

Giese APJ, Tang Y, Sinha GP, et al. CIB2 interacts with TMC1 and TMC2 and is essential for mechanotransduction in auditory hair cells. *Nature communications*. 2017;8(1):43.

Gillespie PG, Hudspeth AJ. Adenine nucleoside diphosphates block adaptation of mechanoelectrical transduction in hair cells. *Proceedings of the National Academy of Sciences - PNAS*. 1993;90(7):2710.

Glowatzki E, Fuchs PA. Cholinergic synaptic inhibition of inner hair cells in the neonatal mammalian cochlea. *Science.* 200;288(5475):2366-8.

Glowatzki E, Fuchs PA. Transmitter release at the hair cell ribbon synapse. *Nat Neurosci.* 2002;5(2):147-54.

Glowatzki E, Cheng N, Hiel H, et al. The glutamate-aspartate transporter GLAST mediates glutamate uptake at inner hair cell afferent synapses in the mammalian cochlea. *The Journal of neuroscience*. 2006;26(29):7659-7664.

Goutman JD. Mechanisms of synaptic depression at the hair cell ribbon synapse that support auditory nerve function. *Proceedings of the National Academy of Sciences of the United States of America*. 2017;114(36):9719-9724

Goutman JD, Glowatzki E. Time course and calcium dependence of transmitter release at a single ribbon synapse. *Proceedings of the National Academy of Sciences of the United States of America*. 2007;104(41):16341-16346

Grant L, Yi E, Glowatzki E. Two modes of release shape the postsynaptic response at the inner hair cell ribbon synapse. *Journal of Neuroscience*. 2010;30(12):4210-4220.

Graydon CW, Cho S, Li G, Kachar B, von Gersdorff H. Sharp Ca^{2+} nanodomains beneath the ribbon promote highly synchronous multivesicular release at hair cell synapses. *The Journal of neuroscience*. 2011;31(46):16637-16650.

Gregory FD, Pangršič T, Calin-Jageman IE, Moser T, Lee A. Harmonin enhances voltage-dependent facilitation of Cav1.3 channels and synchronous exocytosis in mouse inner hair cells. *The Journal of Physiology*. 2013;591(13):3253-3269.

Guan Y, Liu Q, Tang Z, Raja SN, Anderson DJ, Dong X. Mas-related G-protein–coupled receptors inhibit pathological pain in mice. *Proceedings of the National Academy of Sciences of the United States of America*. 2010;107(36):15933-15938.

Guinan JJ, Warr WB, Norris BE. Differential olivocochlear projections from lateral versus medial zones of the superior olivary complex. *J. Comp. Neurol.* 1983;221(3):358-70.

Hackett TA, Rinaldi Barkat T, O'Brien BMJ, Hensch TK, Polley DB. Linking topography to tonotopy in the mouse auditory thalamocortical circuit. *The Journal of neuroscience*. 2011;31(8):2983-2995.

Hackney CM, Osen KK, Ottersen OP, Storm-Mathisen J, Manjaly G. Immunocytochemical evidence that glutamate is a neurotransmitter in the

cochlear nerve: a quantitative study in the guinea-pig anteroventral cochlear nucleus. *Eur. J. Neurosci*. 1996;8(1):79-91.

Hackney CM, Mahendrasingam S, Penn A, Fettiplace R. The concentrations of calcium buffering proteins in mammalian cochlear hair cells. *Journal of Neuroscience*. 2005;25(34):7867-7875.

Hacohen N, Assad JA, Smith WJ, Corey DP. Regulation of tension on hair-cell transduction channels: Displacement and calcium dependence. *Journal of Neuroscience*. 1989;9(11):3988-3997.

Haelens A, Wuyts A, Proost P, Struyf S, Opdenakker G, van Damme J. Leukocyte migration and activation by murine chemokines. *Immunobiology*. 1996;195(4):499-521.

Haenggeli C, Pongstaporn T, Doucet JR, Ryugo DK. Projections from the spinal trigeminal nucleus to the cochlear nucleus in the rat. *Journal of Comparative Neurology*. 2005;484(2):191-205.

Hams N, Padmanarayana M, Qiu W, Johnson CP. Otoferlin is a multivalent calcium-sensitive scaffold linking SNAREs and calcium channels. *Proceedings of the National Academy of Sciences of the United States of America*. 2017;114(30):8023-8028.

Hansen MR, Vijapurkar U, Koland JG, Green SH. Reciprocal signaling between spiral ganglion neurons and schwann cells involves neuregulin and neurotrophins. *Hearing Research*. 2001;161(1):87-98.

He DZZ, Evans BN, Dallos P. First appearance and development of electromotility in neonatal gerbil outer hair cells. *Hearing Research*. 1994;78(1):77-90.

He L, Gulyanon S, Mihovilovic Skanata M, et al. Direction selectivity in drosophila proprioceptors requires the mechanosensory channel tmc. *Current biology*. 2019;29(6):945-956.e3.

Hibino H, Nin F, Tsuzuki C, Kurachi Y. How is the highly positive endocochlear potential formed? the specific architecture of the stria vascularis and the roles of the ion-transport apparatus. *Pflugers Arch - Eur J Physiol*. 2009;459(4):521-533.

Hilgert N, Smith RJH, Van Camp G. Forty-six genes causing nonsyndromic hearing impairment: Which ones should be analyzed in DNA diagnostics? *Mutation research. Reviews in mutation research*. 2009;681(2-3):189-196.

Hirose K, Discolo CM, Keasler JR, Ransohoff R. Mononuclear phagocytes migrate into the murine cochlea after acoustic trauma. *The Journal of comparative neurology*. 2005;489(2):180-194.

Hirose K, Rutherford MA, Warchol ME. Two cell populations participate in clearance of damaged hair cells from the sensory epithelia of the inner ear. *Hearing research*. 2017;352:70-81.

Horváth T, Polony G, Fekete Á, Aller M, Halmos G, Lendvai B, Heinrich A, Sperlágh B, Vizi ES, Zelles T. ATP-evoked intracellular Ca^{2+} signalling of different

supporting cells in the hearing mouse hemicochlea. *Neurochem Res.* 2016:41(1-2):364-75.

Housley GD, Luo L, Ryan AF. Localization of mRNA encoding the P2X2 receptor subunit of the adenosine 5′-triphosphate-gated ion channel in the adult and developing rat inner ear by in situ hybridization. *Journal of Comparative Neurology*. 1998;393(4):403-414.

Housley GD, Morton-Jones R, Vlajkovic SM, et al. ATP-gated ion channels mediate adaptation to elevated sound levels. *Proceedings of the National Academy of Sciences - PNAS*. 2013;110(18):7494-7499.

Hu G, Huang K, Hu Y, et al. Single-cell RNA-seq reveals distinct injury responses in different types of DRG sensory neurons. *Scientific reports*. 2016;6(1):31851.

Huang L, Huang L, Ryan A, et al. Developmentally regulated expression of the P2X3 receptor in the mouse cochlea. *Histochem Cell Biol*. 2006;125(6):681-692.

Huang L, Thorne PR, Vlajkovic SM, Housley GD. Differential expression of P2Y receptors in the rat cochlea during development. *Purinergic signalling*. 2010;6(2):231-248.

Inoue M, Shimohira I, Yoshida A, Zimmerm Takeshima H, Sakurada T, Ueda H. Dose-related opposite modulation by nociceptin/orphanin FQ of substance P nociception in the nociceptors and spinal cord. *The Journal of pharmacology and experimental therapeutics*. 1999;291(1):308-313.

Jagger DJ, Housley GD. Membrane properties of type II spiral ganglion neurones identified in a neonatal rat cochlear slice. *The Journal of Physiology*. 2003;552(2):525-533.

Jean P, Lopez de la Morena D, Michanski S, et al The synaptic ribbon is critical for sound encoding at high rates and with temporal precision. *Elife*. 2018;7:e29275.

Jeng J, Ceriani F, Hendry A, et al. Hair cell maturation is differentially regulated along the tonotopic axis of the mammalian cochlea. *The Journal of Physiology*. 2020;598(1):151-170.

Jensen TS, Finnerup NB. Allodynia and hyperalgesia in neuropathic pain: clinical manifestations and mechanisms. *Lancet Neurol*. 2014:13(9):924-35.

Jia S, Dallos P, He DZZ. Mechanoelectric transduction of adult inner hair cells. *The Journal of neuroscience*. 2007;27(5):1006-1014.

Jia S, Yang S, Guo W, He DZZ. Fate of mammalian cochlear hair cells and stereocilia after loss of the stereocilia. *Journal of Neuroscience*. 2009;29(48):15277-15285.

Jiang H, Sha S, Forge A, Schacht J. Caspase-independent pathways of hair cell death induced by kanamycin in vivo. *Cell death and differentiation*. 2006;13(1):20-30.

Jiang M, Li H, Johnson A, et al. Inflammation up-regulates cochlear expression of TRPV1 to potentiate drug-induced hearing loss. *Science advances*. 2019;5(7)

Jing Z, Rutherford MA, Takago H, et al. Disruption of the presynaptic cytomatrix protein bassoon degrades ribbon anchorage, multiquantal release, and sound encoding at the hair cell afferent synapse. *The Journal of neuroscience*. 2013;33(10):4456-4467.

Johnson KR, Erway LC, Cook SA, Willott JF, Zheng QY. A major gene affecting age-related hearing loss in C57BL/6J mice. *Hear. Res.* 1997;114(1-2):83092.

Johnson SL, Marcotti W, Kros CJ. Increase in efficiency and reduction in ca 2+ dependence of exocytosis during development of mouse inner hair cells. *The Journal of physiology*. 2005;563(1):177-191.

Johnson SL, Adelman JP, Marcotti W. Genetic deletion of SK2 channels in mouse inner hair cells prevents the developmental linearization in the Ca^{2+} dependence of exocytosis. *The Journal of physiology*. 2007;583(2):631.

Johnson SL, Forge A, Knipper M, Munkner S, Marcotti W. Tonotopic variation in the calcium dependence of neurotransmitter release and vesicle pool replenishment at mammalian auditory ribbon synapses. *Journal of Neuroscience*. 2008;28(30):7670-7678.

Johnson SL, Beurg, M, Marcotti W, Fettiplace R. Prestin-driven cochlear amplification is not limited by the outer hair cell membrane time constant. *Neuron.* 2011;70(6):1143-54.

Johnson SL, Wedemeyer C, Vetter DE, et al. Cholinergic efferent synaptic transmission regulates the maturation of auditory hair cell ribbon synapses. *Open biology*. 2013;3(11):130163.

Johnson SL, Kuhn S, Franz C, et al. Presynaptic maturation in auditory hair cells requires a critical period of sensory-independent spiking activity. *Proceedings of the National Academy of Sciences - PNAS*. 2013;110(21):8720-8725.

Johnson SL, Ceriani F, Houston O, Polishchuk R, Polishchuk E, Crispino G, Zorzi V, Mammano F, Marcotti W. Connexin-mediated signaling in nonsensory cells is crucial for the development of sensory inner hair cells in the mouse cochlea. *J Neurosci.* 2017a;37(2):258-268.

Johnson SL, Olt J, Cho S, von Gersdorff H, Marcotti W. The coupling between ca 2+ channels and the exocytotic ca 2+ sensor at hair cell ribbon synapses varies tonotopically along the mature cochlea. *The Journal of neuroscience*. 2017b;37(9):2471-2484.

Johnson SL, Safieddine S, Mustapha M, Marcotti W. Hair cell afferent synapses: function and dysfunction. *Cold Spring Harb. Perspect. Med.* 2019;9(12):a033175

Jouret G, Poirsier C, Spodenkiewicz M, et al. Genetics of usher syndrome: New insights from a meta-analysis. *Otology & Neurotology*. 2019;40(1):121-129.

Kachar B, Parakkal M, Kurc M, Zhao Y, Gillespie PG. High-resolution structure of hair-cell tip links. *Proc. Natl. Acad. Sci. U S A.* 2000;97(24):13336-41.

Kalies S, Kuetemeyer K, Heisterkamp A. Mechanisms of high-order photobleaching and its relationship to intracellular ablation. *Biomed. Opt. Express.* 2011;2(4):805-16.

Kandler K, Clause A, Noh J. Tonotopic reorganization of developing brainstem circuits. *Nat. Neurosci.* 2009;12(6):711-7.

Kanagawa E, Sugahara K, Hirose Y, Mikuriya T, Shimogori H, Yamashita H. Effects of substance P during the recovery of hearing function after noise-induced hearing loss. *Brain Research*. 2014;1582:187-196.

Katz E, Elgoyhen AB, Gomez-Casati ME, et al. Developmental regulation of nicotinic synapses on cochlear inner hair cells. *Journal of Neuroscience*. 2004;24(36):7814-7820.

Kaur T, Zamani D, Tong L, et al. Fractalkine signaling regulates macrophage recruitment into the cochlea and promotes the survival of spiral ganglion neurons after selective hair cell lesion. *The Journal of neuroscience*. 2015;35(45):15050-15061. 15.2015.

Kaur T, Ohlemiller KK, Warchol ME. Genetic disruption of fractalkine signaling leads to enhanced loss of cochlear afferents following ototoxic or acoustic injury. *Journal of Comparative Neurology*. 2018;526(5):824-835.

Kawasaki Y, Kohno T, Zhuang Z, et al. Ionotropic and metabotropic receptors, protein kinase A, protein kinase C, and src contribute to C-fiber-induced ERK activation and cAMP response element-binding protein phosphorylation in dorsal horn neurons, leading to central sensitization. *Journal of Neuroscience*. 2004;24(38):8310-8321.

Kazmierczak P, Sakaguchi H, Tokita J, Wilson-Kubalek EM, Milligan RA, Müller U, Kachar B. Cadherin 23 and protocadherin 15 interact to form tip-link filaments in sensory hair cells. *Nature*. 2007;449(7158):87-91.

Kearney G, Zorilla de San Martín J, Vattino LG, Elgoyhen AB, Wedemeyer C, Katz E. Developmental synaptic changes at the transient olivocochlear-inner hair cell synapse. *J. Neurosci.* 2019;39(18):3360:3375.

Kelsell DP, Dunlop J, Stevens HP, Lench NJ, Liang JN, Parry G, Mueller RF, Leigh IM. Connexin 26 mutations in hereditary non-syndromic sensorineural deafness. *Letters to Nature* 1997;387:80-83.

Kemperman MH, Bom SJH, Lemaire FX, Verhagen WIM, Huygen PLM, Cremers CWRJ. DFNA9/COCH and its phenotype. *Adv. Otorhinolaryngol.* 2002;61:66-72.

Kennedy HJ, Crawford AC, Evans MG, Fettiplace R. Fast adaptation of mechanoelectrical transducer channels in mammalian cochlear hair cells. *Nature Neuroscience.* 2003;6(8):832-836.

Kennedy HJ, Crawford AC, Fettiplace R. Force generation by mammalian hair bundles supports a role in cochlear amplification. *Nature.* 2005;433(7028):880-3.

Kestell GR, Anderson RL, Clarke JN, Haberberger RV, Gibbins IL. Primary afferent neurons containing calcitonin gene-related peptide but not substance P in forepaw skin, dorsal root ganglia, and spinal cord of mice. *J. Comp. Neurol.* 2015;523(17):2555-69.

Khimich D, Nouvian R, Pujol R, et al. Hair cell synaptic ribbons are essential for synchronous auditory signalling. *Nature* 2005; 434, 889-894

Kiang NY, Rho JM, Northrop CC, Liberman MC, Ryugo DK. Hair-cell innervation by spiral ganglion cells in adult cats. *Science*. 1982;217(4555):175-177.

Kikuchi T, Adams JC, Miyabe Y, So E, Kobayashi T. Potassium ion recycling pathway via gap junction systems in the mammalian cochlea and its interruption in hereditary nonsyndromic deafness. *Med Electron Microsc.* 2000;33(2):51-6.

Kim CF, Moalem-Taylor G. Detailed characterization of neuro-immune responses following neuropathic injury in mice. *Brain Research*. 2011;1405:95-108.

Kim S, Taylor-Clark T. Development of a P2X2 reporter mouse model. *The FASEB Journal*. 2019;33(S1):546.6.

Knirsch M, Brandt N, Braig C, et al. Persistence of Cav1.3 Ca^{2+} channels in mature outer hair cells supports outer hair cell afferent signaling. *Journal of Neuroscience*. 2007;27(24):6442-6451.

Köles L, Szepesy J, Berekméri E, Zelles T. Purinergic Ssgnaling and Cochlear Injury-targeting the immune system? *Int. J. Mol. Sci.* 2019;20(12):2979.

Kros CJ, Rüsch A, Richardson GP. Mechano-electrical transducer currents in hair cells of the cultured neonatal mouse cochlea. *Proceedings. Biological sciences*. 1992;249(1325):185-193.

Kros CJ, Rupersberg JP. Rüsch A, Richardson GP. Expression of a potassium current in inner hair cells during development of hearing in mice. *Nature.* 1998. ;394(6690):281-4.

Kros CJ, Marcotti W, van Netten SM, et al. Reduced climbing and increased slipping adaptation in cochlear hair cells of mice with Myo7a mutations. *Nature neuroscience*. 2001;5(1):41-47.

Kros CJ, Eckrich T, Roberts TP, et al. Position-dependent patterning of spontaneous action potentials in immature cochlear inner hair cells. *Nature Neuroscience*. 2011;14(6):711-717.

Kubisch C, Schroeder BC, Friedrich T, et al. KCNQ4, a novel potassium channel expressed in sensory outer hair cells, is mutated in dominant deafness. *Cell*. 1999;96(3):437-446.

Kujawa SG, Liberman MC. Adding insult to injury: Cochlear nerve degeneration after "temporary" noise-induced hearing loss. *Journal of Neuroscience*. 2009;29(45):14077-14085.

Kurima K, Peters LM, Yang Y, et al. Dominant and recessive deafness caused by mutations of a novel gene, TMC1, required for cochlear hair-cell function. *Nature genetics*. 2002;30(3):277-284.

Kurpius D, Nolley EP, Dailey ME. Purines induce directed migration and rapid homing of microglia to injured pyramidal neurons in developing hippocampus. *Glia.* 2007;55(8):873-84.

Lahne M, Gale JE. Damage-induced activation of ERK1/2 in cochlear supporting cells is a hair cell death-promoting signal that depends on extracellular ATP and calcium. *J. Neurosci.* 2008;28(19):4918-28.

Lang H, Schulte B, Schmiedt R. Ouabain induces apoptotic cell death in type I spiral ganglion neurons, but not type II neurons. *JARO*. 2005;6(1):63-74.

Langguth B, Kreuzer PM, Kleinjung T, De Ridder D. Tinnitus: causes and clinical management. *Lancet Neurol.* 2013;12(9):920-930.

Lauer AM, Fuchs PA, Ryugo DK, Francis HW. Efferent synapses return to inner hair cells in the aging cochlea. *Neurobiology of Aging*. 2012;33(12):2892-2902.

Lauer AM, May BJ. The medial olivocochlear system attenuates the developmental impact of early noise exposure. *J. Assoc. Res. Otolaryngol.* 2011;12(3):329-43.

Lee Y. A morphogenetic wave of p27Kip1 transcription directs cell cycle exit during organ of corti development. *Development (Cambridge)*. 2006;133(15):2817-2826.

Leem JW, Willis WD, Chung JM. Cutaneous sensory receptors in the rat foot. *Journal of Neurophysiology*. 1993;69(5):1684-1699.

Li D, Ren Y, Xu X, Zou X, Fang L, Lin Q. Sensitization of primary afferent nociceptors induced by intradermal capsaicin involves the peripheral release of calcitonin gene-related peptide driven by dorsal root reflexes. *Journal of Pain*. 2008;9(12):1155-1168.

Li G, Keen E, Andor-Ardo D, Hudspeth AJ, von Gersdorff H. The unitary event underlying multiquantal EPSCs at a hair cell's ribbon synapse. *The Journal of neuroscience*. 2009;29(23):7558-7568.

Li J, Chen Y, Zeng S, et al. Contralateral suppression of DPOAEs in mice after ouabain treatment. *Neural plasticity*. 2018;2018:1-8.

Li L, Rutlin M, Abraira V, et al. The functional organization of cutaneous low-threshold mechanosensory neurons. *Cell (Cambridge)*. 2011;147(7):1615-1627.

Liberman LD, Liberman MC. Postnatal maturation of auditory-nerve heterogeneity, as seen in spatial gradients of synapse morphology in the inner hair cell area. *Hearing Research*. 2016;339:12-22.

Liberman LD, Liberman MC. Cochlear efferent innervation is sparse in humans and decreases with age. *The Journal of neuroscience*. 2019;39(48):9560-9569.

Liberman MC, Kiang NY. Acoustic trauma in cats. Cochlear pathology and auditory-nerve activity. *Acta Otolaryngol. Suppl.* 1978;358:1-63.

Liberman MC. The cochlear frequency map for the cat: labeling auditory-nerve fibers of known characteristic frequency. *J. Acoust. Soc. Am.* 1982;72(5):1441-9.

Liberman MC, Oliver ME. Morphometry of intracellularly labeled neurons of the auditory nerve: Correlations with functional properties. *Journal of Comparative Neurology*. 1984;223(2):163-176.

Liberman MC, Brown MC. Physiology and anatomy of single olivocochlear neurons in the cat. *Hearing Research*. 1986;24(1):17-36.

Liberman MC. Noise-induced and age-related hearing loss: New perspectives and potential therapies. *F1000 research*. 2017;6:927.

Lima SQ, Hromádka T, Znamenskiy P, Zador AM, PINP: a new method of tagging neuronal populations for identification during in vivo electrophysiological recording. *PloS One.* 2009;4(7):e6099.

Lina IA, Lauer AM. Rapid measurement of auditory filter shape in mice using the auditory brainstem response and notched noise. *Hear. Res.* 2013;293:73-9

Lioudyno M, Hiel H, Kong J, et al. A "synaptoplasmic cistern" mediates rapid inhibition of cochlear hair cells. *Journal of Neuroscience*. 2004;24(49):11160-11164.

Liu C, Glowatzki E, Fuchs PA. Unmyelinated type II afferent neurons report cochlear damage. *Proc. Natl. Acad. Sci. U S A.* 2015;112(47):14723-7.

Liu W, Davis R. Calretinin and calbindin distribution patterns specify subpopulations of type I and type II spiral ganglion neurons in postnatal murine cochlea. *J. Comp. Neurol.* 2014;522(10):2299-318.

Longo-Guess CM, Gagnon LH, Cook SA, et al. A missense mutation in the previously undescribed gene tmhs underlies deafness in hurry-scurry (hscy) mice. *Proceedings of the National Academy of Sciences of the United States of America*. 2005;102(22):7894-7899.

Madisen L, Mao T, Koch H, et al. A toolbox of cre-dependent optogenetic transgenic mice for light-induced activation and silencing. *Nature neuroscience*. 2012;15(5):793-802.

Mahendrasingam S, Fettiplace R, Alagramam KN, Cross E, Furness DN. Spatiotemporal changes in the distribution of LHFPL5 in mice cochlear hair

bundles during development and in the absence of PCH15. *PloS One.* 2017;12(10):e0185285.

Maison SF, Liu XP, Eatock RA, Sibley DR, Grandy DK, Liberman MC. Dopaminergic signaling in the cochlea: receptor expression patterns and deletion phentoypes. *J. Neurosci.* 2012;32(1):344-55.

Maison S, Liberman LD, Liberman MC. Type II cochlear ganglion neurons do not drive the olivocochlear reflex: Re-examination of the cochlear phenotype in peripherin knock-out mice. *eNeuro*. 2016;3(4):ENEURO.0207-16.2016.

Mammano F, Bortolozzi M, Ortolano S, Anselmi F. Ca^{2+} signaling in the inner ear. *Physiology (Bethesda).* 2007; 22:131-44.

Mann ZF, Kelley MW. Development of tonotopy in the auditory periphery. *Hear. Res.* 2011;276(1-2):2-15.

Marcotti W, Kros CJ. Developmental expression of the potassium current I K,n contributes to maturation of mouse outer hair cells. *The Journal of physiology*. 1999;520(3):653-660.

Marcotti W, Johnson SL, Rüsch A, Kros CJ. Sodium and calcium currents shape action potentials in immature mouse inner hair cells. *The Journal of Physiology*. 2003;552(3):743-761.

Marcotti W, Johnson SL, Kros CJ. A transiently expressed SK current sustains and modulates action potential activity in immature mouse inner hair cells. *The Journal of physiology*. 2004;560(3):691-708.

Marcotti W, Erven A, Johnson SL, Steel KP, Kros CJ. Tmc1is necessary for normal functional maturation and survival of inner and outer hair cells in the mouse cochlea. *The Journal of physiology*. 2006;574(3):677-698.

Marcotti W. Functional assembly of mammalian cochlear hair cells. *Exp. Physiol.* 2012;97(4):438-51.

Marcotti W, Corns LF, Goodyear RJ, et al. The acquisition of mechano-electrical transducer current adaptation in auditory hair cells requires myosin VI. *The Journal of physiology*. 2016;594(13):3667-3681.

Marcus DC, Wu T, Wangemann P, Kofuji P. KCNJ10(Kir4.1) potassium channel knockout abolishes endocochlear potential. *Am. J. Physiol. Cell. Physiol.* 2002;282(2):C403-7.

Markowitz AL, Kalluri R. Gradients in the biophysical properties of neonatal auditory neurons align with synaptic contact position and the intensity coding map of inner hair cells. *eLife*. 2020;9.

Marks K, Siegel J. Differentiating middle ear and medial olivocochlear effects on transient-evoked otoacoustic emissions. *JARO*. 2017;18(4):529-542.

Martinez-Monedero R, Liu C, Weisz C, Vyas P, Fuchs PA, Glowatzki E. GluA2-containing AMPA receptors distinguish ribbon-associated from ribbonless afferent contacts on rat cochlear hair cells. *eNeuro*. 2016;3(2):ENEURO.0078-16.2016.

Mathur P, Yang J. Usher syndrome: Hearing loss, retinal degeneration and associated abnormalities. *Biochimica et biophysica acta. Molecular basis of disease*. 2015;1852(3):406-420.

Matsui T, Svensson CI, Hirata Y, Mizobata K, Hua X, Yaksh TL. Release of prostaglandin E2 and nitric oxide from spinal microglia is dependent on activation of p38 mitogen-activated protein kinase. *Anesthesia and analgesia*. 2010;111(2):554-560.

May BJ, Lauer AM, Roos MJ. Impairments of the medial olivocochlear system increase the risk of noise-induced auditory neuropathy in laboratory mice. *Otology & neurotology*. 2011;32(9):1568-1578.

Meaud J, Grosh K. Coupling active hair bundle mechanics, fast adaptation, and somatic motility in a cochlear model. *Biophysical Journal*. 2011;100(11):2576-2585.

Mendell LM, Wall PD. Responses of single dorsal cord cells to peripheral cutaneous unmyelinated fibres. *Nature*. 195(206):97-99.

Michna M, Knirsch M, Hoda J, et al. Cav1.3 (α1D) Ca^{2+} currents in neonatal outer hair cells of mice. *The Journal of Physiology*. 2003;553(3):747-758.

Middlebrooks JC, Dykes RW, Merzenich MM. Binaural response-specific bands in primary auditory cortex (AI) of the cat: topographic organization orthogonal to isofrequency contours. *Brain Res.* 1980;181(1):31-48.

Mistrik P, Ashmore J. The role of potassium recirculation in cochlear amplification. *Current opinion in otolaryngology & head and neck surgery*. 2009;17(5):394-399.

Monzack EL, Cunningham LL. Lead roles for supporting actors: Critical functions of inner ear supporting cells. *Hearing Research*. 2013;303:20-29.

177

Monzack EL, May LA, Roy S, Gale JE, Cunningham LL. Live imaging the phagocytic activity of inner ear supporting cells in response to hair cell death. *Cell death and differentiation*. 2015;22(12):1995-2005.

Morgan YV, Ryugo DK, Brown MC. Central trajectories of type II (thin) fibers of the auditory nerve in cats. *Hear. Res.* 1994;79(1-2):74-82.

Muñoz DJB, Thorne PR, Housley GD, Billett TE. Adenosine 5′-triphosphate (ATP) concentrations in the endolymph and perilymph of the guinea-pig cochlea. *Hearing Research*. 1995;90(1):119-125.

Murthy SE, Loud MC, Daou I, et al. The mechanosensitive ion channel Piezo2 mediates sensitivity to mechanical pain in mice. *Science translational medicine*. 2018;10(462).

Nayagam BA, Muniak MA, Ryugo DK. The spiral ganglion: connecting the peripheral and central auditory systems. *Hear. Res.* 2011;278(1-2):2-20.

Neeliyath A. Ramakrishnan, Marian J. Drescher, Dennis G. Drescher. Direct interaction of otoferlin with syntaxin 1A, SNAP-25, and the L-type voltage-gated calcium channel CaV1.3. *Journal of Biological Chemistry*. 2009;284(3):1364-1372

Nemzou N RM, Bulankina AV, Khimich D, Giese A, Moser T. Synaptic organization in cochlear inner hair cells deficient for the CaV1.3 (α1D) subunit of L-type Ca^{2+} channels. *Neuroscience*. 2006;141(4):1849-1860.

Nikolic P, Housley GD, Luo L, Ryan AF, Thorne PR. Transient expression of P2X 1 receptor subunits of ATP-gated ion channels in the developing rat cochlea. *Developmental Brain Research*. 2001;126(2):173-182.

Nilius B, Flockerzi V. *Mammalian transient receptor potential (TRP) cation channels.* Vol 222. 2014th ed. Berlin, Heidelberg: Springer; 2014.

Nin F, Hibino H, Doi K, Suzuki T, Hisa Y, Kurachi Y. The endocochlear potential depends on two K+ diffusion potentials and an electrical barrier in the stria vascularis of the inner ear. *Proc. Natl. Acad. Sci. U S A.* 2008;105(5):1751-6.

Noguchi K, Senba E, Morita Y, Sato M, Tohyama M. Co-expression of α-CGRP and β-CGRP mRNAs in the rat dorsal root ganglion cells. *Neuroscience Letters.* 1990;108(1):1-5.

Nouvian R, Neef J, Bulankina AV, et al. Exocytosis at the hair cell ribbon synapse apparently operates without neuronal SNARE proteins. *Nature neuroscience.* 2011;14(4):411-413.

Oishi Y, Manabe I. Macrophages in inflammation, repair and regeneration. *Int. Immunol.* 2018;30(11):511-528.

O'Keeffe MG, Thorne PR, Housley GD, Robson SC, Vlajkovic SM. Developmentally regulated expression of ectonucleotidases NTPDase5 and NTPDase6 and UDP-responsive P2Y receptors in the rat cochlea. *Histochemistry and cell biology.* 2010;133(4):425-436.

Oertel D, Young ED. What's a cerebellar circuit doing in the auditory system? *Trends in neurosciences (Regular ed.).* 2004;27(2):104-110.

Oestreicher E, Arnold W, Ehrenberger K, Felix D. Dopamine regulates the glutamatergic inner hair cell activity in guinea pigs. *Hear. Res.* 1997;107(1-2):46-52.

Offner FF, Dallos P, Cheatham MA. Positive endocochlear potential: Mechanism of production by marginal cells of stria vascularis. *Hearing Research*. 1987;29(2):117-124.

Ohlemiller KK. Recent findings and emerging questions in cochlear noise injury. *Hearing Research*. 2008;245(1):5-17.

Oliver D, Fakler B. Expression density and functional characteristics of the outer hair cell motor protein are regulated during postnatal development in rat. *The Journal of Physiology*. 1999;519(3):791-800.

Oliver D, Klöcker N, Schuck J, Baukrowitz T, Ruppersberg JP, Fakler B. Gating of Ca^{2+}-activated K+ channels controls fast inhibitory synaptic transmission at auditory outer hair cells. *Neuron*. 2000;26(3):595-601.

Osswald M, Winkler F. Inisghts into cell-to-cell and cell-to-blood-vessel communications in the brain: in vivo multiphoton microscopy. *Cell Tissue Res.* 2013;352(1):149-59.

Pan B, Géléoc G, Asai Y, et al. TMC1 and TMC2 are components of the mechanotransduction channel in hair cells of the mammalian inner ear. *Neuron (Cambridge, Mass.)*. 2013;79(3):504-515.

Pan B, Akyuz N, Liu X, et al. TMC1 forms the pore of mechanosensory transduction channels in vertebrate inner ear hair cells. *Neuron (Cambridge, Mass.)*. 2018;99(4):736-753.e6.

Patil MJ, Hovhannisyan AH, Akopian AN. Characteristics of sensory neuronal groups in CGRP-cre-ER reporter mice: Comparison to Nav1.8-cre, TRPV1-cre and TRPV1-GFP mouse lines. *PloS one*. 2018;13(6):e0198601.

Patuzzi R. Ion flow in stria vascularis and the production and regulation of cochlear endolymph and the endolymphatic potential. *Hear Res.* 2011;277(1-2):4-19.

Peng AW, Effertz T, Ricci AJ. Adaptation of mammalian auditory hair cell mechanotransduction is independent of calcium entry. *The Journal of neuroscience*. 2016;36(10):2945-2956.

Peng AW, Gnanasambandam R, Sachs F, Ricci AJ. Adaptation independent modulation of auditory hair cell mechanotransduction channel open probability implicates a role for the lipid bilayer. *The Journal of neuroscience*. 2016;36(10):2945-2956.

Perkins RE, Morest DK. A study of cochlear innervation patterns in cats and rats with the Golgi method and Nomarkski optics. *J. Comp. Neurol.* 1975;163(2):129-58.

Petitpré C, Wu H, Sharma A, Tokarska A, Fontanet P, et al. Neuronal heterogeneity and stereotyped connectivity in the auditory afferent system. *Nat. Commun.* 2018;9(1):3961.

Piazza V, Ciubotaru CD, Gale JE, Mammano F. Purinergic signalling and intercellular Ca^{2+} wave propagation in the organ of Corti. *Cell Calcium.* 2007;31(1):77-86.

Pickles JO, Comis SD, Osborne MP. Cross-links between stereocilia in the guinea pig organ of corti, and their possible relation to sensory transduction. *Hearing research*. 1984;15(2):103-112.

Pienkowski M, Tyler RS, Roncancio ER, Jun HJ, Brozoski T, et al. A review of hyperacusis and future direction: part II. Measurement, mechanisms, and treatment. *Am. J. Audiol.* 2014;23(4):420-36.

Platzer J, Engel J, Schrott-Fischer A, Stephan K, Bova S, Chen H, Zheng H, Striessnig J. Congenital deafness and sinoatrial node dysfunction in mice lacking class D L-type Ca^{2+}channels. *Cell*. 2000;102(1):89-97.

Prajapati-DiNubila M, Benito-Gonzalez A, Golden EJ, Zhang S, Doetzlhofer A. A counter gradient of Activin A and follistatin instructs the timing of hair cell differentiation in the murine cochlea. *Elife.* 2019;8:e47613.

Proost P, Wuyts A, van Damme J. The role of chemokines in inflammation. *Int. J. Clin. Lab. Res.* 1996;26(4):211-23.

Puel JL, Ruel J, d'Aldin CG, Pujol R. Excitotoxicity and repeair of cochlear synapses after noise-trauma induced hearing loss. *Neuroreport.* 1998;9(9):2109-14.

Pujol R, Carlier E. Cochlear synaptogenesis after sectioning the efferent bundle. *Brain Res.* 1982;255(1):151-4.

Raphael Y, Altschuler RA. Scar formation after drug-induced cochlear insult. *Hearing Research*. 1991;51(2):173-183.

Raphael Y, Altschuler RA. Structure and innervation of the cochlea. *Brain Research Bulletin*. 2003;60(5):397-422.

Ray P, Torck A, Quigley L, et al. Comparative transcriptome profiling of the human and mouse dorsal root ganglia: An RNA-seq-based resource for pain and sensory neuroscience research. *Pain (Amsterdam)*. 2018;159(7):1325-1345.

Reichenbach T, Husdpeth AJ. The physics of hearing: fluid mechanics and the active process of the inner ear. *Rep Prog Phys.* 2014;77(7):076601.

Ren Y, Xou X, Fang L, Lin Q. Involvement of peripheral purinoceptors in sympathetic modulation of capsaicin-induced sensitization of primary afferent fibers. *J. Neurophysiol.* 2006;96(5):22-7-16.

Ricci AJ. The transduction channel filter in auditory hair cells. *The Journal of neuroscience*. 2005;25(34):7831-7839.

Rice FL, Fundin BT, Arvidsson J, Aldskogius H, Johansson O. Comprehensive immunofluorescence and lectin binding analysis of vibrissal follicle sinus complex innervation in the mystacial pad of the rat. *Journal of Comparative Neurology*. 1997;385(2):149-184.

Richter CA, Amin S, Linden J, Dixon J, Dixon MJ, Tucker AS. Defects in middle ear cavitation cause conductive hearing loss in the Tcof1 mutant mouse. *Human molecular genetics*. 2010;19(8):1551-1560.

Richter C, Edge R, He DZZ, Dallos P. Development of the gerbil inner ear observed in the hemicochlea. *JARO*. 2000;1(3):195-210.

Robertson D. Horseradish peroxidase injection of physiologically characterized afferent and efferent neurons in the guinea pig spiral ganglion. *Hear. Res.* 1984;15(2):113-21.

Robertson D, Gummer M. Physiological and morphological characterization of efferent neurons in the guinea pig cochlea. 1985;20(1);63-77.

Robertson D, Sellick PM, Patuzzi R. The continuing search for outer hair cell afferents in the guinea pig spiral ganglion. *Hearing Research*. 1999;136(1):151-158.

Rohmann KN, Wersinger E, Braude JP, Pyott SJ, Fuchs PA. Activation of BK and SK channels by efferent synapses on outer hair cells in high-frequency regions of the rodent cochlea. *The Journal of neuroscience*. 2015;35(5):1821-1830.

Romand MR, Romand R. The ultrastructure of spiral ganglion cells in the mouse. *Acta Otolaryngol.* 1987;104(1-2):29-39.

Roth B, Bruns V. Postnatal development of the rat organ of corti. II. hair cell receptors and their supporting elements. *Anatomy and embryology*. 1992;185(6):571-581.

Roux I, Safieddine S, Nouvian, et al., Otoferlin, defective in a human deafness form, is essential for exocytosis at the auditory ribbon synapse. *Cell*. 2006;127(2):277-289.

Roux I, Hosie S, Johnson SL, et al. Myosin VI is required for the proper maturation and function of inner hair cell ribbon synapses. *Human molecular genetics*. 2009;18(23):4615-4628.

Roux I, Wersinger E, McIntosh JM, Fuchs PA, Glowatzki E. Onset of cholinergic efferent synaptic function in sensory hair cells of the rat cochlea. *The Journal of neuroscience*. 2011;31(42):15092-15101.

Ruben RJ. Development of the inner ear of the mouse: a radioautographic study of terminal mitoses. *Acta Otolaryngol.* 1967;Supple 220:1-44.

Ruel J, Emery S, Nouvian R, et al. Impairment of SLC17A8 encoding vesicular glutamate transporter-3, VGLUT3, underlies nonsyndromic deafness DFNA25 and inner hair cell dysfunction in null mice. *American journal of human genetics*. 2008;83(2):278-292.

Ruel J, Nouvian R, d'Aldin CG, Pujol R, Eybalin M, Puel JL. Dopamine inhibition of auditory nerve activity in the adult mammalian cochlea. *Eur. J. Neurosci*. 2001;14(6):977-86.

Ruel J, Wang J, Demémes D, Gobaille S, Puel JL, Rebillard G. Dopamine transporter is essential for the maintenance of spontaneous activity of auditory nerve neurons and their responsiveness to sound stimulation. *J. Neurochem*. 2006;97(1):190-200.

Russell IJ, Kössl M. The voltage responses of hair cells in the basal turn of the guinea-pig cochlea. *The Journal of Physiology*. 1991;435(1):493-511.

Ryan AF, Woolf NK, Bone RC. Ultrastructural correlates of selective outer hair cell destruction following kanamycin intoxication in the chinchilla. *Hearing Research*. 1980;3(4):335-351.

Ryugo DK, Dodds LW, Benson TE, Kiang NYS. Unmyelinated axons of the auditory nerve in cats. *Journal of Comparative Neurology*. 1991;308(2):209-223.

Sakagami M, Fukazawa K, Matsunaga T, et al. Cellular localization of rat I sk protein in the stria vascularis by immunohistochemical observation. *Hearing Research*. 1991;56(1):168-172.

Salt AN, Melichar I, Thalmann R. Mechanisms of endocochlear potential generation by stria vascularis. *Laryngoscope.* 1987;97(8pt 1):984-91.

Samantha A, Hughes TET, Moiseenkova-Bell VY. Transient receptor potential (TRP) channels. *Subcell. Biochem* 2018; 87:141-165.

Scalia F, Arango V. Topographic organization of the projections of the retina to the pretectal region in the rat. *Journal of Comparative Neurology.* 1979;186(2):271-292.

Schacht J, Talaska AE, Rybak LP. Cisplatin and aminoglycoside antibiotics: hearing loss and its prevention. *Anat. Rec. (Hoboken).* 2012;295(11):1837-50.

Schmiedt RA, Okamura HO, Lang H, Schulte BA. Ouabain application to the round window of the gerbil cochlea: a model of auditory neuropathy and apoptosis. *J. Assoc. Res. Otolaryngol.* 2002;3(3):223-33.

Schmitz F, Königstorker, Südhof. RIBEYE, a component of synaptic ribbons: a protein's journey through evolution provides insight into synaptic ribbon function. *Neuron.* 2000;28(3):857-872.

Schulte BA, Adams JC. Distribution of immunoreactive Na+,K+-ATPase in gerbil cochlea. *J. Histochem. Cytochem.* 1989;37(2):127-34.

Schulte BA, Steel KP. Expression of alpha and beta subunit isoforms of Na,K-ATPase in the mouse inner ear and changes with mutation at the Wv or Sld loci. *Hear. Res.* 1994;78(1):65-76.

Seal RP, Akil O, Yi E, Weber CM, Grant L, Yoo J, Clause A, Kandler K, Noebels JL, Glowatzki E, Lustig LR, Edwards RH. Sensorineural deafness and

seizures in mice lacking vesicular glutamate transporter 3. *Neuron.* 2008;57(2):263-75.

Sher AE. The embryonic and postnatal development of the inner ear of the mouse. *Acta Otolaryngol. Suppl.* 1971;285:1-77.

Sherill HE, Jean P, Drive EC, Sanders TR, Ftizgerald TS, Moser T, Kelley MW. Pou4f1 defines a subgroup of type I spiral ganglion neurons and is necessary for normal inner hair cell presynaptic Ca^{2+} signaling. *J Neurosci.* 2019;39(27):5284-5298.

Shotwell SL, Jacobs R, Hudspeth AJ. Directional sensitivity of individual vertebrate hair cells to controlled deflection of their hair bundles. *Annals of the New York Academy of Sciences*. 1981;374(1):1-10.

Shrestha BR, Chia C, Wu L, Kujawa SG, Liberman MC, Goodrich LV. Sensory neuron diversity in the inner ear is shaped by activity. *Cell.* 2018;174(5):1229-1246.

Simmons DD, Liberman MC. Afferent innervation of outer hair cells in adult cats: I. Light microscopic analysis of fibers labeled with horseradish peroxidase. *J. Comp. Neurol.* 1988;270(1):132-44

Simmons DD. Development of the inner ear efferent system across vertebrate species. *J. Neurobiol.* 2002;53(2):228-50.

Sirko P, Gale JE, Ashmore JF. Intercellular Ca^{2+} signalling in the adult mouse cochlea. *J Physiol.* 2019;597(1):3030-317.

Smith AK, O'Hara CL, Stucky CL. Mechanical sensitization of cutaneous sensory fibers in the spared nerve injury mouse model. *Molecular Pain*. 2013;9(1):61.

Smith CA. Innervation of the cochlea of the guinea pig by use of the golgi stain. *Annals of Otology, Rhinology & Laryngology*. 1975;84(4):443-458.

Sobkowicz HM, Rose JE, Scott GL, Levenick CV. Distribution of synaptic ribbons in the developing organ of Corti. *J. Neurocytol.* 1986;15(6):693-714.

Soliman AC, Yu JSC, Coderre TJ. mGlu and NMDA receptor contributions to capsaicin-induced thermal and mechanical hypersensitivity. *Neuropharmacology*. 2005;48(3):325-332.

Son EJ, Ma JH, Ankamreddy H, Shin JO, Choi JY, Wu DK, Bok J. Conserved role of Sonic Hedgehog in tonotopic organization of the avian basilar papilla and mammalian cochlea. *Proc. Natl. Acad. Sci. U S A.* 2015;112(12):3746-51.

Spicer SS, Schulte BA. Novel structures in marginal and intermediate cells presumably relate to functions of apical versus basal strial strata. *Hearing Research*. 2005;200(1):87-101.

Spiden SL, Bortolozzi M, Di Leva F, et al. The novel mouse mutation oblivion inactivates the PMCA2 pump and causes progressive hearing loss. *PLoS genetics*. 2008;4(10):e1000238.

Spoendlin H. Innervation patterns in the organ of Corti of the cat. *Acta Otolaryngol.* 1969;67(2):239-54.

Spoendlin H. Degeneration behavior of the cochlear nerve. *Archiv fr klinische und experimentelle Ohren-, Nasen-, und Kehlkopfheilkunde* 1971;200,275-291.

Spoendlin Neuroanatomy of the cochlea. *Facts and Models in Hearing* 1973 pp18-32.

Stamataki S, Francis HW, Lehar M, May BJ, Ryugo DK. Synaptic alterations at inner hair cells precede spiral ganglion cell loss in aging C57BL/6J mice. *Hear. Res.* 2006;221(1-2):104-18.

Stankovic K, Rio C, Xia A, et al. Survival of adult spiral ganglion neurons requires erbB receptor signaling in the inner ear. *Journal of Neuroscience*. 2004;24(40):8651-8661.

Stauffer EA, Holt JR. Sensory transduction and adaptation in inner and outer hair cells of the mouse auditory system. *Journal of Neurophysiology*. 2007;98(6):3360-3369.

Steel KP, Friedman TB, Avraham KB, et al. Beethoven, a mouse model for dominant, progressive hearing loss DFNA36. *Nature Genetics*. 2002;30(3):257-258.

Stellwagen D, Schatz CJ. An instructive role for retinal waves in the development of retinogeniculate connectivity. *Neuron.* 2002;33(3):357-67.

Sterling P, Matthews G. Structure and function of ribbon synapses. *Trends in neurosciences (Regular ed.).* 2005;28(1):20-29.

Street VA, McKee-Johnson JW, Fonseca RC, Tempel BL, Noben-Trauth K. Mutation in a plasma membrane Ca^{2+}-ATPase gene cause deafness in deafwaddler mice. *Nat. Genet.* 1998;19(4):390-4.

Sun S, Babola T, Pregernig G, So KS, Nguyen M et al. Hair cell mechanotransduction regulates spontaneous activity and spiral ganglion subtype specification in the auditory system. *Cell*. 2018;174(5):1247-1263.

Svoboda K, Denk Wm Kleinfeld D, Tank DW. In vivo dendritic calcium dynamics in neocortical pyramidal neurons. *Neuron.* 1997;385(6612):161-5.

Svoboda K, Yasuda R. Principles of two-photon excitation microscopy and its applications to neuroscience. *Neuron.* 2006;50(6):823-39,

Takago H, Oshima-Takago T, Moser T. Disruption of otoferlin alters the mode of exocytosis at the mouse inner hair cell ribbon synapse. *Frontiers in molecular neuroscience*. 2018;11:492.

Tan WJT, Thorne PR, Vlajkovic SM. Characterisation of cochlear inflammation in mice following acute and chronic noise exposure. *Histochem Cell Biol*. 2016;146(2):219-230.

Taub DD, Proost P, Murphy WJ, et al. Monocyte chemotactic protein-1 (MCP-1), -2, and -3 are chemotactic for human T lymphocytes. *The Journal of clinical investigation*. 1995;95(3):1370-1376.

Teudt IU, Richter CP. Baslilar membrane and tectorial membrane stiffness in the CBA/CaJ mouse. *J. Assoc. Res. Otolaryngol.* 2014;15(5):675-94.

Thiers FA, Nadol JB, Liberman MC. Reciprocal synapses between outer hair cells and their afferent terminals: evidence for a local neural network in the mammalian cochlea. *J. Assoc. Res. Otolar*yngol. 2008;9(4)477-89.

Thomsen E. The ultrastructure of the spiral ganglion in the guinea pig. *Acto Otolaryngol.* 1966;Suppl 224:442.

Tian L, Hires SA, Looger LL. Imaging neuronal activity with genetically encoded calcium indicators. *Cold Spring Harbor protocols*. 2012;2012(6):647.

Tilney LG, Egelman E, DeRosier DJ. Actin in the inner ear: The remarkable structure of the stereocilium. *Nature*. 1980;287(5780):291-296.

Tonndorf J. The analogy between tinnitus and pain: a suggestion for a physiological basis of chronic tinnitus. *Hear. Res.* 1987;28(2-3):271-5.

Tritsch NX, Eunyoung Y, Gale JE, Glowatzki E, Bergles DE. The origin of spontaneous activity in the developing auditory system. *Nature.* 2007;450, 50-55.

Tritsch NX, Zhang Y, Ellis-Davies G, Bergles DE. ATP-induced morphological changes in supporting cells of the developing cochlea. *Purinergic signalling*. 2010;6(2):155-166.

Tyler RS, Pienkowski M, Roncancio ER, Jun HJ, Brozoski T, et al. A review of hyperacusis and future direction: part I. Definitions and manifestations. *Am. J. Audiol.* 2014;23(4):402-19.

Valero MD, Hancock KE, Liberman MC. The middle ear muscle reflex in the diagnosis of cochlear neuropathy. *Hearing Research*. 2016;332:29-38.

Vikman KS, Rycroft BK, Christie MJ. Switch to Ca^{2+}-permeable AMPA and reduced NR2B NMDA receptor-mediated neurotransmission at dorsal horn

nociceptive synapses during inflammatory pain in the rat. *The Journal of physiology*. 2008;586(2):515.

Vincent PFY, Bouleau Y, Safieddine S, Petit C, Dulon D. Exocytotic machineries of vestibular type I and cochlear ribbon synapses display similar intrinsic otoferlin-dependent Ca^{2+} sensitivity but a different coupling to Ca^{2+} channels. *The Journal of neuroscience*. 2014;34(33):10853-10869.

Vincent PFY, Bouleau Y, Petit C, Dulon D. A synaptic F-actin network controls otoferlin-dependent exocytosis in auditory inner hair cells. *eLife*. 2015;4:e10988.

Vogl C, Cooper BH, Neef J, et al. Unconventional molecular regulation of synaptic vesicle replenishment in cochlear inner hair cells. *Journal of cell science*. 2015;128(4):638-644.

Vreugde S, Erven A, Kros CJ, Marcotti W, et al. Beethoven, a mouse model for dominant, progressive hearing loss DFNA36. *Nat. Genet.* 2002;30(3):257-8.

Vyas P, Wu JS, Zimmerman A, Fuchs PA, Glowatzki E. Tyrosine Hydroxylase expression in type II cochlear afferents in mice. *JARO.* 2017;18(1):139-151.

Vyas P, Wu JS, Jimenez A, Glowatzki E, Fuchs PA. Characterization of transgenic mouse lines for labeling type I and type II afferent neurons in the cochlea. *Scientific reports*. 2019;9(1):5549.

Wagner EL, Shin JB. Mechanisms of hair cell damage and repair. *Trends Neurosci.* 2019;42(6):414-424.

Wang H, Lin C, Cheung R, et al. Spontaneous activity of cochlear hair cells triggered by fluid secretion mechanism in adjacent support cells. *Cell*. 2015;163(6):1348-1359.

Wang J, Raybould N, Luo L, et al. Noise induces up-regulation of P2X2 receptor subunit of ATP-gated ion channels in the rat cochlea. *NeuroReport*. 2003;14(6):817-823.

Wang Z, Jung JS, Inbar TC, Rangoussis KM, Faaborg-Andersen C, Coate TM. The purinergic receptor P2rx3 is required for spiral ganglion neuron branch refinement during development. eNeuro 16 July 2020, 7 (4) ENEURO.0179-20.2020

Weisz CJC, Glowatzki E, Fuchs PA. The postsynaptic function of type II cochlear afferents. *Nature* 2009;461(7267):1126-9.

Weisz CJC, Lehar M, Hiel H, Glowatzki E, Fuchs PA. Synaptic transfer from outer hair cells to type II afferent fibers in the rat cochlea. *The Journal of neuroscience*. 2012;32(28):9528-9536.

Weisz CJC, Glowatzki E, Fuchs PA. Excitability of type II cochlear afferents. *J Neurosci.* 2014;34(6):2365-73.

Wersinger E, McLean WJ, Fuchs PA, Pyott SJ. BK channels mediate cholinergic inhibition of high frequency cochlear hair cells. *PloS one*. 2010;5(11):e13836.

Woller SA, Eddinger KA, Corr M, Yaksh TL. An overview of pathways encoding nociception. *Clinical and experimental rheumatology*. 2018;36(1):172.

Wong AB, Rutherford MA, Gabrielaitis M, et al. Developmental refinement of hair cell synapses tightens the coupling of Ca^{2+} influx to exocytosis. *The EMBO Journal*. 2014;33(3):247-264.

Wood MB, Mull K, Nowak NJ, Goldring A, Lehar M, Fuchs PA. Acoustic trauma increases ribbon number and size in outer hair cells of the mouse cochlea. *JARO* Article in press.

Wu JS, Young ED, Glowatzki E. Maturation of spontaneous firing properties after hearing onset in rat auditory nerve fibers: Spontaneous rates, refractoriness, and interfiber correlations. *The Journal of neuroscience*. 2016;36(41):10584-10597.

Wu JS, Vyas P, Glowatzki E, Fuchs PA. Opposing expression gradients of calcitonin-related polypeptide alpha (Calca/Cgrpα) and tyrosine hydroxylase (Th) in type II afferent neurons of the mouse cochlea. *J. Comp. Neurol.* 2018;526(3):425-438.

Wu JS, Yi E, Manca M, Javaid H, Lauer AM, Glowatzki E. Sound exposure dynamically induces dopamine synthesis in cholinergic LOC efferents for feedback to auditory nerve fibers. *eLife*. 2020;9.

Wu PZ, Liberman LD, Bennett K, de Gruttola V, O'Malley JT, Liberman MC. Primary neural degeneration in the human cochlea: Evidence for hidden hearing loss in the aging ear. *Neuroscience*. 2019;407:8-20.

Xiong W, Grillet N, Elledge H, et al. TMHS is an integral component of the mechanotransduction machinery of cochlear hair cells. *Cell*. 2012;151(6):1283-1295.

Yamoah EN, Gillespie PG. Phosphate analogs block adaptation in hair cells by inhibiting adaptation-motor force production. *Neuron*. 1996;17(3):523-533.

Yan D, Zhu Y, Walsh T, et al. Mutation of the ATP-gated P2X2 receptor leads to progressive hearing loss and increased susceptibility to noise. *Proceedings of the National Academy of Sciences - PNAS*. 2013;110(6):2228-2233.

Yang PW, Henderson D, Hua Hu B, Nicotera TM. Quantitative analysis of apoptotic and necrotic outer hair cells after exposure to different levels of continuous noise. *Hearing Research*. 2004;196(1):69-76.

Young ED, Nelken I, Conley RA. Somatosensory effects on neurons in dorsal cochlear nucleus. *J. Neurophsyiol.* 1995;73(2):743-65.

Zachary SP, Fuchs PA. Re-emergent inhibition of cochlear inner hair cells in a mouse model of hearing loss. *J Neurosci*. 2015;35(26):9701-9706.

Zachary SP, Nowak NJ, Vyas P, Bonanni L, Fuchs PA. Voltage-gated calcium influx modifies cholinergic inhibition of inner hair cells in the immature rat cochlea. *J. Neurosci.* 2018;38(25):5677-5687.

Zhang LI, Poo M. Electrical activity and development of neural circuits. *Nature neuroscience*. 2001;4(S11):1207-1214.

Zhang KD, Coate TM. Recent advances in the development and function of type II spiral ganglion neurons in the mammalian inner ear. *Semin. Cell Dev. Biol.* 2017;65:80-87.

Zhao B, Wu Z, Grillet N, et al. TMIE is an essential component of the mechanotransduction machinery of cochlear hair cells. *Neuron (Cambridge, Mass.)*. 2014;84(5):954-967.

Zheng J, Shen W, He DZZ, Long KB, Madison LD, Dallos P. Prestin is the motor protein of cochlear outer hair cells. *Nature (London)*. 2000;405(6783):149-155.

Zheng J, Du GG, Anderson CT, et al. Analysis of the oligomeric structure of the motor protein prestin. *Journal of Biological Chemistry*. 2006;281(29):19916-19924.

Zhu Y, Zhao H. ATP activates P2X receptors to mediate gap junctional coupling in the cochlea. *Biochemical and biophysical research communications*. 2012;426(4):528-532.

Zilberstein Y, Liberman MC, Corfas G. Inner hair cells are not required for survival of spiral ganglion neurons in the adult cochlea. *The Journal of neuroscience*. 2012;32(2):405-410.

Zimmerman A, Bai L, Ginty DD. The gentle touch receptors of mammalian skin. *Science (American Association for the Advancement of Science)*. 2014;346(6212):950-954.

Zorilla de San Martín J, Pyott S, Ballestero J, Katz E. Ca(2+) and Ca(2+)-activated K(+) channels that support and modulate transmitter release at the olivocochlear efferent-inner hair cell synapse. *J Neurosci.* 2010l30(36):12157-67.

Curriculum Vitae

Nathaniel Nowak
929 N Wolfe St. Unit #1111, Baltimore, MD, USA
nnowak2@jhmi.edu
(949) 357-6005

Education

2015-Present Johns Hopkins University, School of Medicine
            Neuroscience Graduate Program

2010- 2014   University of California, Los Angeles, B.S.
              Major: Neuroscience
              GPA: 3.939
              Major GPA: 3.945
              Global GPA: 4.00

2006-2010   Laguna Hills High School, Laguna Hills, CA, diploma
             GPA 4.83

Research Experience

March 2016-Present *Doctoral Candidate*, Lab of Dr. Paul Fuchs
Studied the effects of transient efferent innervation of inner hair cells resulting in a second author paper. Coded a statistical model to estimate the effects of noise exposure on type II spiral ganglion neuron action potential generation. Thesis work on the development of type II spiral ganglion neuron activity, especially in response to cochlear damage, by developing a novel dissection approach to allow for calcium imaging for the first time in this system.

June 2014- June 2015 *Full Regular Member,* Elegant Mind Club
        Student-led research laboratory under the tutelage of Dr. Katsushi Arisaka, Department of Physics and Astronomy at UCLA; with the express goal of studying the behavior and underlying neural mechanisms in the model organism *C. elegans*. Personal experience thus far includes handling samples, performing phototaxis behavioral assays, processing videos with After Effects, and analyzing data with Matlab.

January 2013-May 2014 *Undergraduate Research Assistant*, Lab of Dr. Desmond Smith, Department of Molecular and Medical Pharmacology at UCLA
        Assisted in carrying out research duties for two projects: the first of which studied the interaction of genetics and Parkinson's Disease in a mouse model and the second of which studied the effect of cancer drugs on genetic expression in hamster hybrid cell lines. Presented the former project at Neuroscience Poster Day in May 2014.

Teaching Experience
August 2017 Research Coordinator at Biology of the Inner Ear at the Marine Biological Laboratories at Woods Hole, MA
Taught students of the Biology of the Inner Ear Course how to perform whole cell patch clamp recordings from cells within the cochlea. Also assisted in setting up the laboratory space, preparing for experimental technique demonstrations, and addressing the needs of the students.

January 2016-May 2016 Teaching Assistant for Neuroscience and Cognition II course at Johns Hopkins University School of Medicine
Acted as a resource for students in need of clarifications about the taught materials, prepared study aids for the students before examinations, and assisted in grading examinations.

Spring 2013 Project Brainstorm, UCLA
Designed a lesson plan for a chosen neuroscience related topic and corresponding supporting activities to teach to students attending Los Angeles area public schools. Additionally, participate in further educational activities and events such as Brain Awareness Week.

Extracurricular Experience
2016-Present JHU Neuroscience Recruitment Committee
Planning and organizing the events of the Johns Hopkins Neuroscience Graduate Program's recruitment efforts including scheduling, travel logistics, and interacting with potential new graduate students. Following the events of recruitment gathered with others on the committee to discuss improvements to the process and to access candidate's viability.

2015-Present Project Bridge
Member of the 2019 SfN Next generation award winning outreach arm of the John Hopkins Neuroscience Program. Project Bridge aims to connect with and educate members of the larger Baltimore community about neuroscience. Went to farmer's markets to engage community members. Helped establish and helmed a booth at Brainfest, a daylong annual event hosted at a elementary school in Baltimore to present neuroscience information.

2012-March 2014 *Member,* Interaxon
Went to inner city schools to teach students about topics related to neuroscience with entertaining, interactive, and educational presentations. Volunteer at neuroscience related events such as the Brain Bee and Brain Awareness Week.

2011-March 2014 S*enior Member*, Neuroscience Undergraduate Society (NUS)
Helped neuroscience majors in areas such as class planning, career options, research and volunteer opportunities by interacting with upperclassman neuroscience majors, guidance counselors, and professors. Planned events

related to academics for our members such as Lab Placement Fair, symposiums, etc.

Awards and Honors
2014: Latin Honors: Summa Cum Laude

2011-2014 Golden Key Honor Society
   National Society of Collegiate Scholars (NSCS)
   Alpha Lambda Delta & Phi Eta Sigma National Honor Societies (ALPDES)
   William Homan Scholarship, Life Sciences ($3000)

2010-2014 Dean's Honor List

2010   Robert C. Bryd Scholarship ($1500)
   Salutatorian, Laguna Hills High School
   AP Scholar with Distinction
   California Scholarship Federation Member
   German National Honor Society (Delta Epsilon Phi)
   Tri-M Music Honor Society

Poster Presentations
March 2020 Johns Hopkins Neuroscience Graduate Program Recruitment

Tissue damage evoke calcium signals in type II cochlear afferents

Nathaniel Nowak, Megan B. Wood, and Paul Albert Fuchs

October 2019 Society for Neuroscience

ATP sensitivity in mouse type II spiral ganglion neurons over the course of development

Nathaniel Nowak, Megan B. Wood, and Paul Albert Fuchs

September 2019 Johns Hopkins Neuroscience Program Retreat

ATP sensitivity in mouse type II spiral ganglion neurons over the course of development

Nathaniel Nowak, Megan B. Wood, and Paul Albert Fuchs

February 2019 Association for Research in Otolaryngology, MidWinter Meeting

ATP sensitivity in mouse type II spiral ganglion neurons over the course of development

Nathaniel Nowak, Megan B. Wood, and Paul Albert Fuchs

September 2018 Johns Hopkins Neuroscience Program Retreat

Voltage-gated calcium influx modifies cholinergic inhibition of inner hair cells in the immature rat cochlea

Stephen Zachary, Nathaniel Nowak, Pankhuri Vyas, Luke Bonanni, and Paul Albert Fuchs

Podium Presentations

October 2019 Chalk Talk for Johns Hopkins Center for Hearing and Balance

Taking advantage of new genetic tools to study type II cochlear afferents

Nathaniel Nowak, Megan B. Wood, and Paul Albert Fuchs

November 2017 Johns Hopkins Neuroscience Program Lab Lunch

Calcium Crosstalk in Immature Inner Hair Cells

Nathaniel Nowak, Stephen Zachary, and Paul Albert Fuchs

Publications
Voltage-gated calcium influx modifies cholinergic inhibition of inner hair cells in the immature rat cochlea
Stephen Zachary, Nathaniel Nowak, Pankhuri Vyas, Luke Bonanni, and Paul Albert Fuchs
Journal of Neuroscience 22 May 2018
https://doi.org/10.1523/JNEUROSCI.0230-18.2019

Publications in Review
Acoustic trauma increases ribbon number and size in outer hair cells of the mouse cochlea
Megan B Wood, Keira Mull, Nathaniel Nowak, Adam Goldring, Mohamed Lehar, and Paul A Fuchs
Submitted to Journal of the Association for Research in Otolaryngology on 10 June 2020

Specialized Skills
　　　　Computer: R, Matlab, After Effects, Adobe Illustrator, Microsoft Excel, Word, and Powerpoint
　　　　Laboratory Techniques: volumetric, spectrophotometric, and potentiometric analysis; use and preparation of buffers and pH meters; synthesis and analysis of compounds; purification by extraction, chromatography, recrystallization, and sublimation; characterization by mass spectroscopy, UV, NMR, and IR spectroscopy, optical activity, electrochemistry, pH titration; ammonium sulfate fractionation, affinity chromatography, protein and enzyme

assays, polyacrylamide gel electrophoresis, gel exclusion chromatography, and enzyme kinetic analysis; experience dissecting and analyzing brain sections; DNA isolation & amplification (PCR); handling and performing behavioral assays on mice, mouse colony maintenance; intraperitoneal injections; cell culture maintenance; sample preparation of *C. elegans*, phototaxis assay for *C. elegans*; *D. melanogaster* brain microdissection; rodent cochlear microdissection; whole-cell patch clamp electrophysiology; immunohistochemistry; confocal and two-photon microscopy; brain clearing techniques; statistical modeling; semicircular canal injections.